LEVEL II

DNA 4923F

ASPECTS OF LATE-TIME STRIATION BEHAVIOR AND SATELLITE COMMUNICATION EFFECTS

JAYCOR
1401 Camino Del Mar
Del Mar, California 92014

1 February 1979

Final Report for Period 22 December 1976—31 January 1979

CONTRACT No. DNA 001-76-C-0186

THIS WORK SPONSORED BY THE DEFENSE NUCLEAR AGENCY
UNDER RDT&E RMSS CODE B322078464 S99QAXHC04114 H2590D.

Prepared for
Director
DEFENSE NUCLEAR AGENCY
Washington, D. C. 20305

Destroy this report when it is no longer needed. Do not return to sender.

PLEASE NOTIFY THE DEFENSE NUCLEAR AGENCY, ATTN: STTI, WASHINGTON, D.C. 20305, IF YOUR ADDRESS IS INCORRECT, IF YOU WISH TO BE DELETED FROM THE DISTRIBUTION LIST, OR IF THE ADDRESSEE IS NO LONGER EMPLOYED BY YOUR ORGANIZATION.

UNCLASSIFIED

SECURITY CLASSIFICATION OF THIS PAGE *(When Data Entered)*

REPORT DOCUMENTATION PAGE	READ INSTRUCTIONS BEFORE COMPLETING FORM
1. REPORT NUMBER: DNA 4923F	2. GOVT ACCESSION NO.: AD-A085577
3. RECIPIENT'S CATALOG NUMBER:	
4. TITLE *(and Subtitle)*: ASPECTS OF LATE-TIME STRIATION BEHAVIOR AND SATELLITE COMMUNICATION EFFECTS	5. TYPE OF REPORT & PERIOD COVERED: Final Report for Period 22 Dec 76—31 Jan 79
	6. PERFORMING ORG. REPORT NUMBER: J78-2005-TR
7. AUTHOR(s): S. Robert Goldman, Jacob L. Sperling	8. CONTRACT OR GRANT NUMBER(s): DNA 001-76-C-0186
9. PERFORMING ORGANIZATION NAME AND ADDRESS: JAYCOR, 1401 Camino Del Mar, Del Mar, California 92014	10. PROGRAM ELEMENT, PROJECT, TASK AREA & WORK UNIT NUMBERS: Subtask S99QAXHC041-14
11. CONTROLLING OFFICE NAME AND ADDRESS: Director, Defense Nuclear Agency, Washington, D.C. 20305	12. REPORT DATE: 1 February 1979
	13. NUMBER OF PAGES: 126
14. MONITORING AGENCY NAME & ADDRESS *(if different from Controlling Office)*	15. SECURITY CLASS *(of this report)*: UNCLASSIFIED
	15a. DECLASSIFICATION/DOWNGRADING SCHEDULE

16. DISTRIBUTION STATEMENT *(of this Report)*

Approved for public release; distribution unlimited.

17. DISTRIBUTION STATEMENT *(of the abstract entered in Block 20, if different from Report)*

18. SUPPLEMENTARY NOTES

This work sponsored by the Defense Nuclear Agency under RDT&E RMSS Code B322078464 S99QAXHC04114 H2590D.

19. KEY WORDS *(Continue on reverse side if necessary and identify by block number)*

Late-time Striation Behavior
Satellite Communication Effects
Plasma Wave Turbulence
Striation Diffusion
Drift-Dissipative Modes

20. ABSTRACT *(Continue on reverse side if necessary and identify by block number)*

This report is a study of aspects of plasma wave turbulence relevant to late-time striation behavior and satellite communication effects. These include:

1. Basic theory of particle diffusion due to quasi-neutral plasma modes.

2. Forms for the diffusion coefficients of linear and nonlinear mode properties.

DD FORM 1 JAN 73 1473 EDITION OF 1 NOV 65 IS OBSOLETE

UNCLASSIFIED

SECURITY CLASSIFICATION OF THIS PAGE *(When Data Entered)*

20. ABSTRACT (Continued)

3. Relevance to E x B gradient-drift modes in the absence of other modes.

4. Diffusion due to drift-dissipative turbulence.

5. Characterization of the diffusion coefficient from drift-dissipative modes in computer simulations.

6. Observational aspects of drift-dissipative waves relevant to in-situ measurement and scintillation.

7. Discussion of some selected experimental situations and phenomena such as the BUARO release, STRESS, and Three-Meter Backscatter.

8. Survey of additional density-gradient instabilities possibly relevant to anomalous diffusion under HANE conditions.

The study suggests that modes other than the E x B mode can contribute to striation dynamics at high altitudes. Possible experimental tests of the relationship of plasma turbulence and striation evolution are described.

PREFACE

We acknowledge extensive stimulating discussions on the BUARO release with Dr. M. B. Pongratz and a number of very helpful conversations on the STRESS probe rocket data with Dr. K. D. Baker. Figures 25 and 27 respectively are presented with the kind permission of these authors. The computer program for finding diffusion coefficient and rate as a function of ambient ionospheric conditions was written and implemented by John Wondra and Carol Meister of JAYCOR.

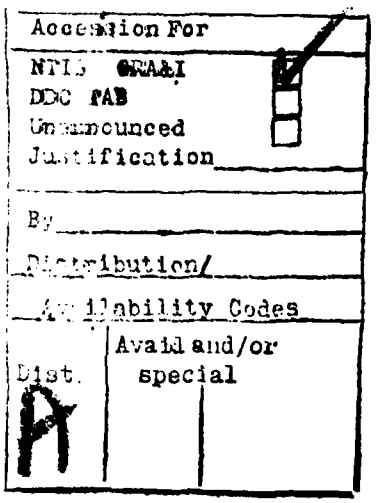

CONTENTS

ILLUSTRATIONS

Page

Page

TABLES

1. INTRODUCTION

In this report, we study aspects of the role of plasma turbulence in late-time striation behavior and satellite communication effects.

Sections 2 through 4 are general and conceptual. We begin in Section 2 by deriving a basic picture of particle diffusion due to quasi-neutral plasma modes. In Section 3, we relate the form of the diffusion coefficient to linear and non-linear plasma theory. The results for the form of the diffusion coefficient are shown in Eqs. (4), (7) and (8). In Section 4, we discuss as it might apply to E x B modes in the absence of other modes gaining insight into some of the limitations of the concept, as well as possibly into bifurcation.

In Sections 5 through 8, aspects specifically related to drift-dissipative modes are presented. In Section 5, we discuss diffusion due to drift-dissipative modes (DDM) showing that the contribution at a given altitude along a field line should not be shorted out by the behavior at other altitudes, and that DDM diffusion should act to limit striation bifurcation. Perpendicular diffusion coefficients and rates of perpendicular diffusion due to DDM along in the absence of background convection and other diffusive mechanisms are presented as functions of background parameters. It is shown here (and in Appendix B) that effects due to an electric field, E_x, in the direction of the background striation density gradient and perpendicular to B limit the growth and diffusion as long as the velocity cE_x/B is larger than an appropriately averaged ion diamagnetic drift velocity = $(v^*_i)_{av}$. In Section 6, diffusion coefficients from drift-dissipative modes are characterized for use in computer simulations. In Section 7, observational aspects of drift waves in the ionosphere are considered, and in Section 8, specific experimental situations are treated. These latter include aspects of the BUARO release, STRESS, and three-meter backscatter.

In Section 9, conclusions and experimental suggestions are presented.

2. BASIC PICTURE OF TURBULENT DIFFUSION FOR QUASI-NEUTRAL MODES

The basic picture of turbulent diffusion for quasi-neutral modes in a plasma can be gotten by assuming that both ions and electrons behave according to the Vlasov equation with particle collisions neglected. This would appear to be valid as long as the diffusion due to turbulence dominates the diffusion due to ordinary collisions.

We consider modes which vary on a relatively fast time scale compared to the turbulent diffusion. The magnetic field B is chosen to be in the z-direction and the background density gradient is in the x-direction. Then the Vlasov equation for each species can be written

$$\frac{\partial f}{\partial t} + \vec{v}\cdot\frac{\partial f}{\partial \vec{r}} + \frac{q_s}{m_s}\vec{v}\times\vec{B}\cdot\frac{\partial f}{\partial \vec{v}} + \frac{q_s}{m_s}\vec{E}\cdot\frac{\partial f}{\partial \vec{v}} = 0 \qquad (1)$$

with f the particle distribution function in r, v and t space; q_s = species charge, m_s = species mass; E = electric field; and subscript e = electrons, subscript i = ions.

On writing

$$f = f_o + f_1$$

(with f_o the slowly varying background distribution, and f_1 the distribution associated with the turbulent modes) and averaging Eq. (1) for a time long compared to the time scale for variation of the turbulent modes one obtains

$$\frac{\partial f_o}{\partial t} + \vec{v}\cdot\frac{\partial f_o}{\partial \vec{r}} + \frac{q_s}{m_s}\frac{\vec{v}\times\vec{B}}{c}\frac{\partial f_o}{\partial v} + \frac{q_s}{m_s}\vec{E}\cdot\frac{\partial f_o}{\partial v} + \frac{q_s}{m_s}\left\langle\vec{E}_1\cdot\frac{\partial f_1}{\partial v}\right\rangle = 0 \qquad (2)$$

where $\langle\ \rangle$ denotes the time average as well as a summation over modes. Multiplying through by v and integrating over velocity space yields

$$\frac{\partial}{\partial t}(n\vec{v}) + \nabla\cdot(n\vec{v}\vec{v} + \psi) + \int\frac{q_s}{m_s}\vec{v}\frac{v\times B}{c}\cdot\frac{\partial f_o}{\partial v}\,dv + \int\frac{q_s}{m_s}vE\cdot\frac{\partial f_o}{\partial v}dv + \int\frac{q_s}{m_s}\left\langle E_1\cdot\frac{\partial f_1}{\partial v}\right\rangle dv = 0$$

where ψ is the particle random energy stress tensor.[1] After some simplification this becomes:

$$\frac{\partial}{\partial t}(n\vec{v}) + \nabla\cdot(n\vec{v}\vec{v} + \psi) - \frac{q_s B}{m_s c}(nv_y\hat{i}) + \frac{q_s B}{m_s c}(nv_x\hat{j}) - \frac{q_s}{m_s}\vec{E}n - \frac{q_s}{m_s}\left\langle \vec{E}_1 n_1 \right\rangle = 0 \quad . \quad (3)$$

where $\nabla \circ \psi \simeq \nabla p$, with p being the pressure, subscript "1" denoting a first-order quantity, n is the ionized number density and v is now the fluid velocity. If the background motion has a time scale τ, velocity v and length scale L, then one expects

$$\omega_{cs} = \frac{|q_s|B}{m_s c} >> \frac{1}{\tau} \quad , \quad \left|\frac{L}{\vec{v}}\right| \quad .$$

This allows one to neglect the terms in $\partial/\partial t(n\vec{v})$ and $\nabla\cdot(n\vec{v}\vec{v})$. Further we expect no background pressure gradient in the y-direction. Then on taking the y-component of Eq. (3) one has:

$$nv_x = \frac{c}{B}\langle E_{1y} n_1 \rangle + \frac{c}{B} E_y n \quad .$$

Convection in the x-direction is associated with the term $cE_y n/B$. It is clear that diffusion in the direction of the density gradient (x-direction) must be associated with the term $(c/B)\langle E_1 y\ n_1 \rangle$. This term is identical for ions and electrons provided the modes are quasi-neutral; hence diffusion occurs locally at a given point in three-dimensional space independent of ambi-polar electric fields or the short-circuiting effects which can arise with ordinary particle collisions[2] in the inhomogeneous ionosphere.

3. DETERMINATION OF THE FORM OF DIFFUSION

If plasma turbulence is in a quasi-stationary state, i.e., the mode amplitudes are changing slowly compared to the mode frequencies, the product $\langle E_{1y} n_1 \rangle$ is determined by a balance of linear and nonlinear growth and damping processes. In place of solving strongly nonlinearly coupled equations for mode amplitudes, estimates for $\langle E_{1y} n_1 \rangle$ can be obtained by using the relation between E_{1y} and n_1 for linear growth (i.e., at amplitudes below saturation) and using n_1 as estimated at saturation. Computer simulations of universal modes[3,3a] suggest this to be a reasonable procedure.

It is conceptually simpler to use electrons to establish the linear relation between E_{1y} and n_1 because finite Larmor radius effects are negligible provided $k\rho_e \ll 1$ where k is the model wave number perpendicular to B and ρ_e is the electron Larmor radius. If this is the case, the mean electron drift in the x-direction is cE_{1y}/B. If the mode has a growth rate γ and flow for electrons perpendicular to the magnetic field is incompressible, then the fractional growth per unit time is

$$\frac{-1}{n_1} \frac{cE_{1y}}{B} \frac{\partial n}{\partial x} = \gamma$$

(The minus sign is used since an unstable mode will lead to a flux of plasma opposite to the density gradient.) This results in

$$nv_x = \left\langle \frac{-\gamma n_1^2}{\partial n/\partial x} \right\rangle + \frac{c}{B} E_y n \quad . \tag{4}$$

Provided that n_1 is randomly varying, this form for the diffusion equation suggests that a close relationship between scintillation and diffusion exists since scintillation in the weak scattering limit is a linear function of the three dimensional power spectrum.[4] Of course, scintillation may also arise if n_1 is not randomly varying.

For strong turbulence,[5] with γ comparable to the wave oscillatory frequency ω, n_1 is limited by the condition that its perturbed density gradient in the direction of the mean density gradient (the x-direction) becomes of the order of the mean density gradient. Then one has

$$k_x n_1 \sim \frac{\partial n}{\partial x} \tag{5}$$

and

$$nv_x = \left\langle -\frac{\gamma}{k_x^2}\left(\frac{\partial n}{\partial x}\right)^2 \frac{1}{\partial n/\partial x}\right\rangle = -\left\langle \frac{\gamma}{k_x^2}\right\rangle \frac{\partial n}{\partial x} \ . \tag{6}$$

Here k_x is the component of the wavenumber vector $\vec{k}$, in the x-direction. Hence the diffusion coefficient perpendicular to the magnetic field, is

$$D_\perp = \langle \gamma/k_x^2 \rangle \ . \tag{7}$$

For weak turbulence, with $\gamma/\omega << 1$, if in addition there exists a surface of wave vectors k' in k-space such that

$$\omega_{\vec{k}} = \omega_{\vec{k}'} + \omega_{\vec{k}-\vec{k}'} \ ,$$

(with ω_k denoting frequency as a function of wave vector) it has been estimated[5] that the diffusion coefficient is

$$D_\perp = \langle \gamma^2/\omega k_x^2 \rangle \ .$$

4. DIFFUSION, E × B MODES, AND BIFURCATION

Application of the notion of turbulent diffusion to E × B modes[6] in the absence of other modes leads to an appreciation of the approximate nature of the concept especially as applied to ionospheric scintillation as well as to insight into the process of bifurcation.

Turbulent diffusion is a concept based on the separation of space scales between the background density gradient and the turbulent modes which serve to diffuse it. For E × B modes, wavelengths approaching $\langle(1/n)(dn/dx)\rangle^{-1}$ are unstable so that the separation of space scales does not generally apply. However one interesting and illuminating paradox involving E × B modes and turbulent diffusion can still occur.

We note that with E × B modes alone, the quantity

$$\int_{\text{all space}} n^2 \, dV \quad ,$$

with V indicating volume, must be conserved.[7] To see this we observe for electrons in the absence of finite Larmor radius effects.

$$\frac{\partial n}{\partial t} + \frac{cE \times B}{B^2} \cdot \nabla n = 0 \quad ,$$

or multiplying by n, using $\nabla\cdot(E \times B) = 0$ and integrating over all space

$$\frac{\partial}{\partial t} \int n^2 \, dV = 0 \quad .$$

However for relatively short wavelength E × B modes it is still possible to derive a diffusion coefficient since whenever

$$\gamma = \frac{cE_y}{B} \frac{1}{n} \frac{dn}{dx} \quad ,$$

and

$$k_x^2 = k_y \frac{1}{n} \frac{dn}{dx} \quad ,$$

one has

$$D \approx \sum_{\text{"short wavelengths"}} \frac{cE_y}{B|k_y|} \neq 0 \quad .$$

Then:

$$\frac{\partial n}{\partial t} + \frac{cE \times B}{B^2} \cdot \nabla n = \nabla \cdot (D_\perp \nabla n)$$

or

$$\frac{\partial}{\partial t} \int n^2 \, dV = - \int D_\perp \nabla n \cdot \nabla n \, dV < 0 \quad . \tag{8}$$

The resolution of the paradox lies in noting that the diffusion equation only applies to length scales greater than the (short) turbulent mode length scale. One expects that turbulence involving modes at shorter scale lengths should act to decrease

$$\int n^2 \, dV$$

when n is restricted to Fourier components at wavelengths greater than the turbulent wavelengths, precisely because $\int n^2 \, dV$ is rigorously conserved over all wavelengths for E × B turbulence.

For insight into bifurcation we consider a striation of thickness L′ with gradient scale length $L_\perp$ (both dimensions measured perpendicular to B.) [Typically in bifurcation one would expect a striation to break up into wavelengths of 2L′/3 (see Figure 1). Certainly the picture of turbulence superposed on a laminar background of much larger scale length is inappropriate.] For a plasma in the limit $\nu_{in} >> \tau^{-1}$, where ν_{in} is the ion-neutral collision frequency and τ is the time scale for plasma velocity variation, simulations[8] indicate that bifurcation is suppressed for

$$\frac{L_\perp v_o}{D_\perp} < 400 \quad , \tag{9a}$$

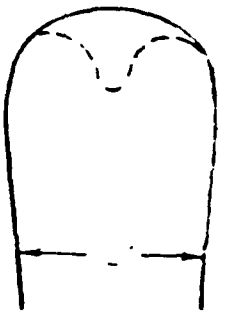

$\lambda = \frac{2L'}{3}$, $k_{bifurcation} = \frac{3-}{L'}$

Figure 1. Bifurcation as an instability on a striation tip.

with v_0 the neutral wind velocity. For the equations used in the NRL simulations modal growth rates, γ, can be estimated by

$$\gamma = \frac{\alpha v_0}{L_\perp} - D_\perp k^2 \quad .$$

with α expected to be less than unity. The result with $\alpha = 1$ is based on an "ideal" geometry with uniform ion neutral velocity v_0 in the x-direction anti-parallel to the background density gradient and perpendicular to the direction of spatially oscillatory variation of the E × B mode. For non-ideal cases one expects $\alpha < 1$. Further the eigenmode is assumed to have no variation in the x-direction (local approximation).

For stability with $k = 3\pi/L'$ this requires

$$\frac{L_\perp v_0}{D_\perp} < \frac{(3\pi)^2}{\alpha}\left(\frac{L_\perp}{L'}\right)^2 \quad . \tag{9b}$$

The similarity of this estimate to the computer results provides two results.

1. The Reynolds number criterion $L_\perp v_0/D_\perp < 400$ for bifurcation suppression may well be a direct reflection of the suppression of striation instability at sufficiently small values of $L_\perp v_0/D$. Although $L_\perp/L' < 1$ for the simulations[9] one would expect that a more realistic value of α ($\alpha < 1$) would work to increase the critical value of $L_\perp v_0/D$.
2. The presence of the factor $(L_\perp/L')$ on the right hand side of Eq. (9a) suggests that bifurcation in the numerical simulations could be a function of the extent of the grid (in the y-direction) perpendicular to the initial density gradient compared to the initial density scale length, e.g., the larger the extent of the grid in the y-direction the larger the possible values of L' and the smaller the value of $L_\perp v_0/D_\perp$ at which bifurcation is suppressed.

5. DIFFUSION WITH DRIFT-DISSIPATIVE MODES

We have previously treated some aspects of drift dissipative modes.[10] A new discussion of the basic physical mechanism involved in driving the mode is presented in Appendix A.

Drift dissipative modes are quasi-neutral. Hence electrons and ions diffuse identically across the magnetic field without an ambipolar electric field. This means that diffusion can take place at one altitude along a magnetic field line without "shorting out" or limiting from contributions at other altitudes.

The largest growth rates occur for $k_y\rho_i \approx 1$,[10] provided that ion-ion collisions, ν_{ii}, are sufficiently weak that $0.3\ \nu_{ii} \lesssim \nu_{in}$, the ion-neutral collision frequency. Further, in this case, one expects modes to be damped whenever the wave frequency is comparable to ν_{in}, i.e., with wave numbers such that

$$k_y\rho_i < L_\perp \nu_{in}/C_s \ ,$$

(with C_s the ion-sound speed $= \sqrt{T_e/m_i}$, and temperatures including Boltzmann's constant). Hence for a striation of thickness L' with $k_y \approx 3\pi/L'$ for bifurcation, short wavelength turbulence is expected for

$$L' >> 3\pi \frac{\rho_i C_s}{L_\perp \nu_{in}} \ .$$

This implies, as shown in Figure 2, that drift dissipative modes can act to diffuse striations on a large scale or averaged sense.

Since bifurcation is a large scale length phenomenon the diffusion due to drift-dissipative turbulence should be relevant in limiting it according to Eqs. (9) or (10). On letting $v_{ts} = \sqrt{T_s/m_s}$, using Eqs. (7) and (9a) with $\gamma \approx 0.1\ v_{ti}/L_\perp$, for "vigorous" growth and $k_x^{-2} = \rho_i L_\perp$ the criterion for bifurcation becomes

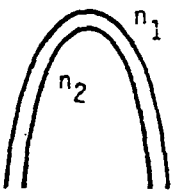

a. Original density contours n_1 and n_2

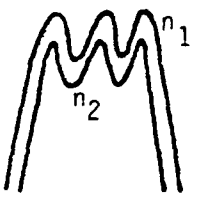

b. Density contours with turbulent diffusion

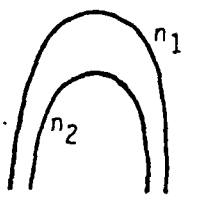

c. Averaged density contours, diffusion on a large scale.

Figure 2. Turbulent diffusion: (a) original density contours n_1 and n_2; (b) density contours with turbulent diffusion; and (c) averaged density contours, diffusion on a large scale.

$$L_\perp > 40 \frac{\rho_i v_{ti}}{v_o} \quad . \tag{11}$$

Since characteristically $v_{ti}/v_o \simeq 10$ and $\rho_i \simeq 5 \times 10^2$ cm, bifurcation is limited to

$$L_\perp > 2 \text{ km.}$$

provided "vigorous" drift dissipative turbulence is present. (Here v_o is the neutral wind velocity.) If vigorous drift dissipative turbulence does not break out until some scale length $L_\perp^* < 2.0$ km it is clear that bifurcation will continue down to $L_\perp^*$.

We have previously indicated rough estimates of growth rates and diffusion rates for drift-dissipative modes in the absence of electric fields in the direction of the background density gradient.[10] Modal growth rates taking into account finite ion Larmor radius effects and electron-ion collisional effects are derived in Appendix C. The results are approximately valid for

$$\frac{\omega_{ci}}{v_{ti}} > k_y > \frac{1}{L_\perp}$$

$$\min\left(\frac{\nu_e}{v_{te}}, \frac{\omega_D}{v_{ti}}\right) > k_z > \frac{2\pi}{L_z}$$

$$\nu_e > \omega \quad .$$

(Here L_z = length scale parallel to $\vec{B}$.)

Figures (3) to (7) and (13) to (16) show the diffusion coefficient as given by the strong turbulence result, Eq. (7), which is derived on the basis of Eq. (4) and expression (5). We note that the rough estimate for n_1 indicated in expression (5) is also derivable by consideration of a <u>wave scattering</u> of particles[11] which can lead to particle diffusion perpendicular to the magnetic field[12] and hence wave damping. The value of k_x^2 is taken to be $(\rho_i L)^{-1}$ in keeping with previous results.

The reciprocal of the time scale due to diffusion is estimated as $D_\perp/L_\perp^2$. These values are shown in Figures (8) to (12) and (17) to (20) as functions of background parameters. We caution that a given background density gradient with diffusion rate $D_\perp/L_\perp^2$ need not actually be diffusing. Due to the

interplay of convective and diffusive processes as indicated by Eq. (4) it is possible for a density gradient with diffusion present to be increasing with time rather than decreasing. As shown by barium cloud releases and simulations, convective processes alone frequently tend to increase density gradients and hence can be effectively anti-diffusive. Estimates for gradients at striation tips have been derived from the balancing of convective steepening and diffusion.[10]

Modal parameters associated with the diffusion are shown in Tables 1 through 5 for $n = 10^6$ cm^{-3} and neutral density ranging from neutral density = 10^6 cm^{-3} (Table 1) to neutral density = 10^{10} cm^{-3} (Table 5) in decades.

Values of $D_\perp$ and $D_\perp/L_\perp^2$ for barium clouds are shown respectively in Figures (21) and (22) and Figures (23) and (24). For these figures $\nu_{in} = 10^{-10}\ n_n$ and L_z = 25 km. There is no instability and hence no anomalous diffusion for $n_n > 10^{10}$ cm^{-3} at $n = 10^6$ cm^{-3} or for $n_n > 3.16 \times 10^9$ cm^{-3} at $n = 10^7$ cm^{-3}.

A major limit to the applicability of drift-dissipative mode turbulence has been the uncertainty of effects due to an electric field, E_x, in the direction of the density gradient perpendicular to the magnetic field. This should be a significant factor in the occurrence of drift dissipative modes because striations if driven by an ambient electric field tend to elongate in the direction perpendicular to the field. Hence along most of their perimeter the electric field is in the direction of the density gradient.

The problem is treated in Appendix B. In the limit $|v_e| >> (v_i^*)_{av}$ with $v_e = cE_x/B$ and $(v_i^*)_{av} = -T_i/(m_i\omega_{ci}\varkappa)$ with $\varkappa$ a typical scale length for the region of density gradient, the growth rate, γ, has an additional contribution

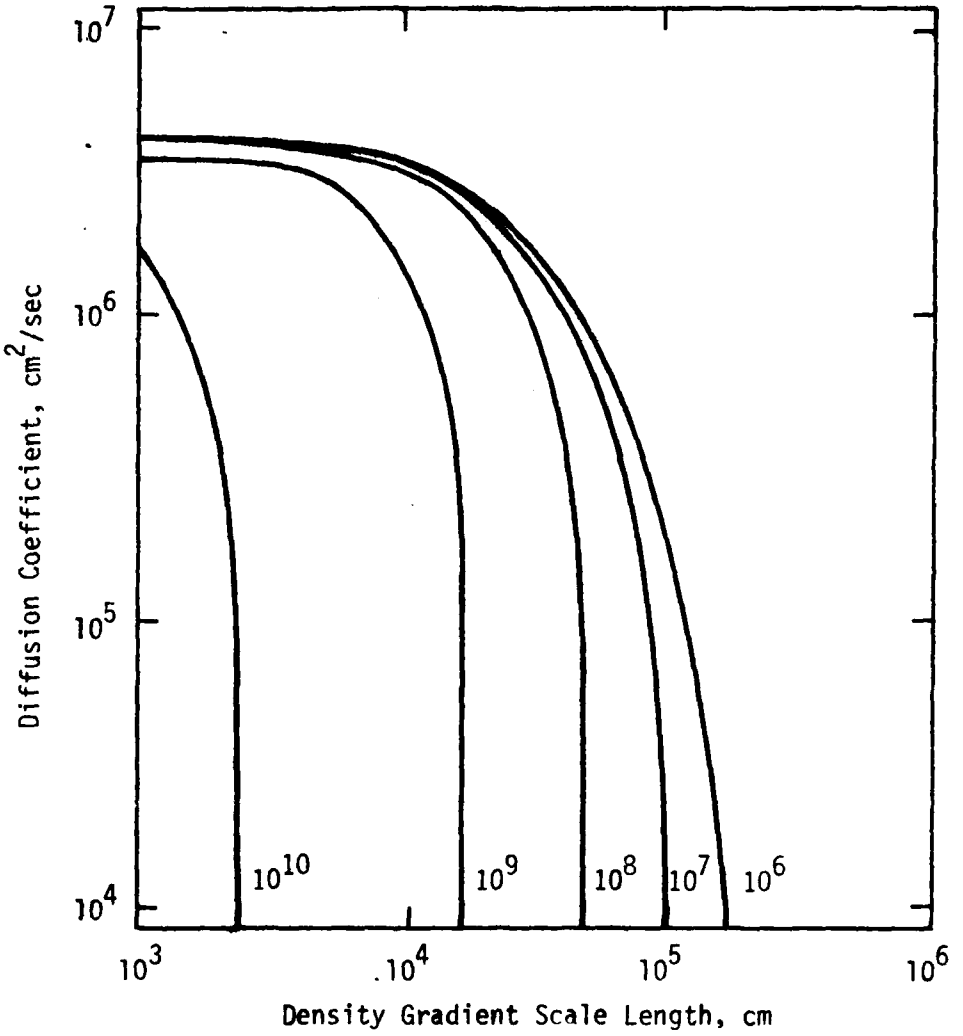

Figure 3. Plot of the diffusion coefficient (cm^2/sec) vs the density gradient scale length (cm) for various values of the neutral density (cm^{-3}) in a singly ionized and neutral oxygen plasma. $n = 10^4\ cm^{-3}$, $L_z = 10^7$ cm, B = 0.35 gauss, $T_e/T_i = 1$, and $\rho_i = 4.62 \times 10^2$ cm. The corresponding classical diffusion coefficient from interspecies coulomb collisions is $1.68 \times 10^2\ cm^2/sec$.

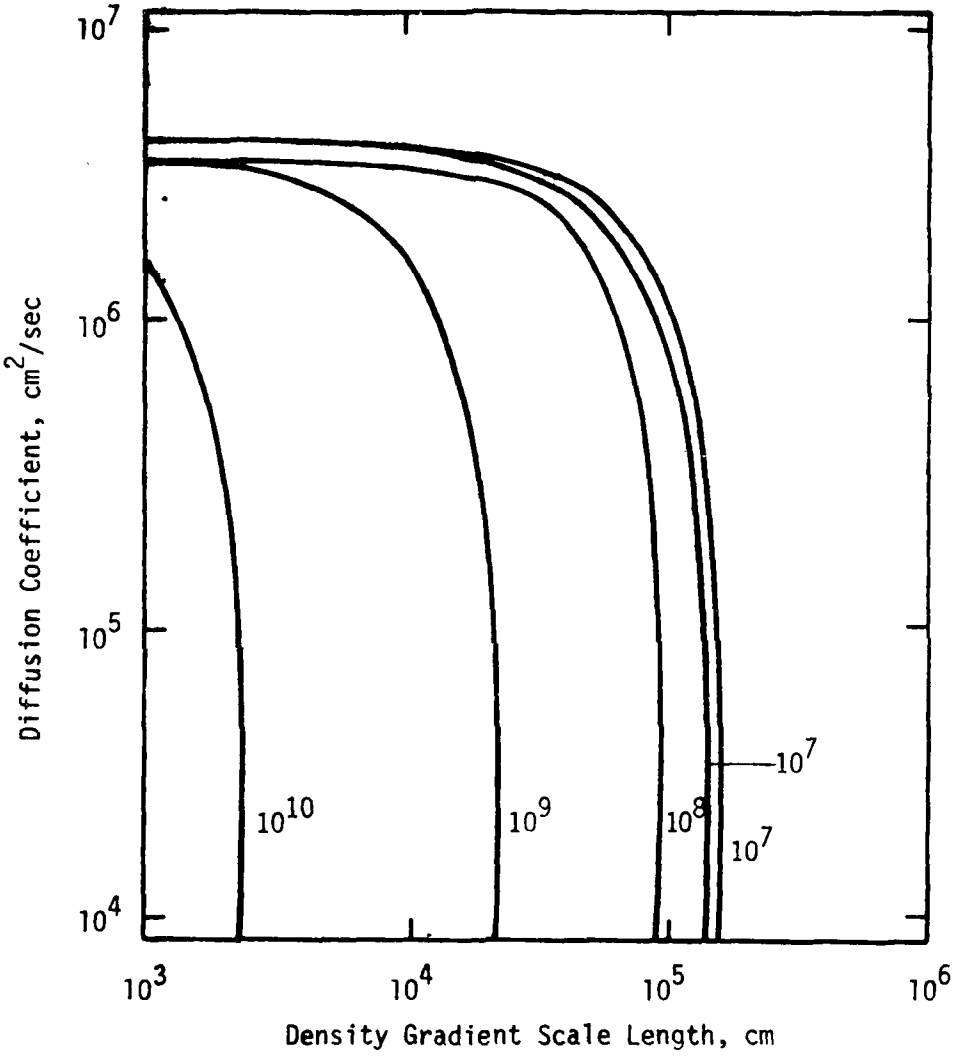

Figure 4. Plot of the diffusion coefficient (cm^2/sec) vs the density gradient scale length (cm) for various values of the neutral density (cm^{-3}) in a singly ionized and neutral oxygen plasma. $n = 10^5\ cm^{-3}$, $L_z = 10^7$ cm, B = 0.35 gauss, $T_e/T_i = 1$, and $\rho_i = 4.62 \times 10^2$ cm. The corresponding classical diffusion coefficient from interspecies coulomb collisions is $1.68 \times 10^3\ cm^2/sec$.

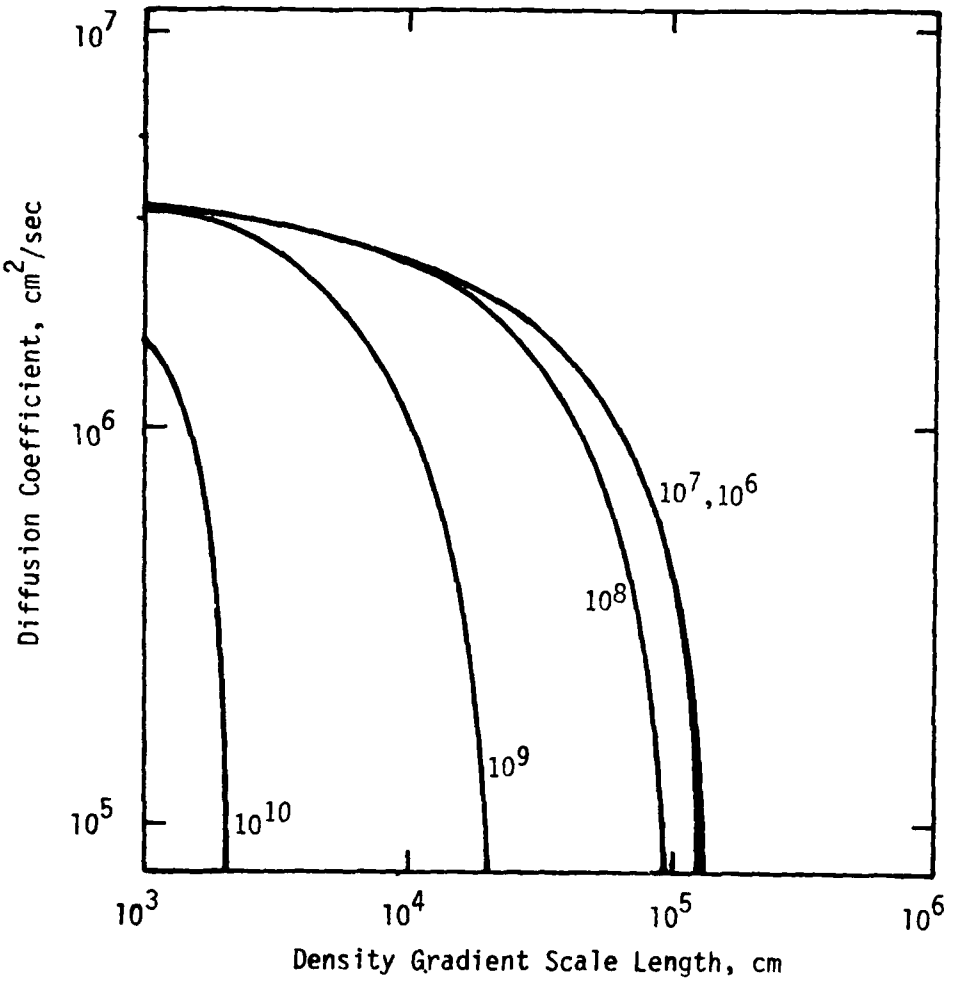

Figure 5. Plot of the diffusion coefficient (cm^2/sec) vs the density gradient scale length (cm) for various values of the neutral density (cm^{-3}) in a singly ionized and neutral oxygen plasma. $n = 10^6\ cm^{-3}$, $L_z = 10^7$ cm, B = 0.35 gauss, $T_e/T_i = 1$, and $\rho_i = 4.62 \times 10^2$ cm. The corresponding classical diffusion coefficient from interspecies coulomb collisions is $1.68 \times 10^4\ cm^2/sec$.

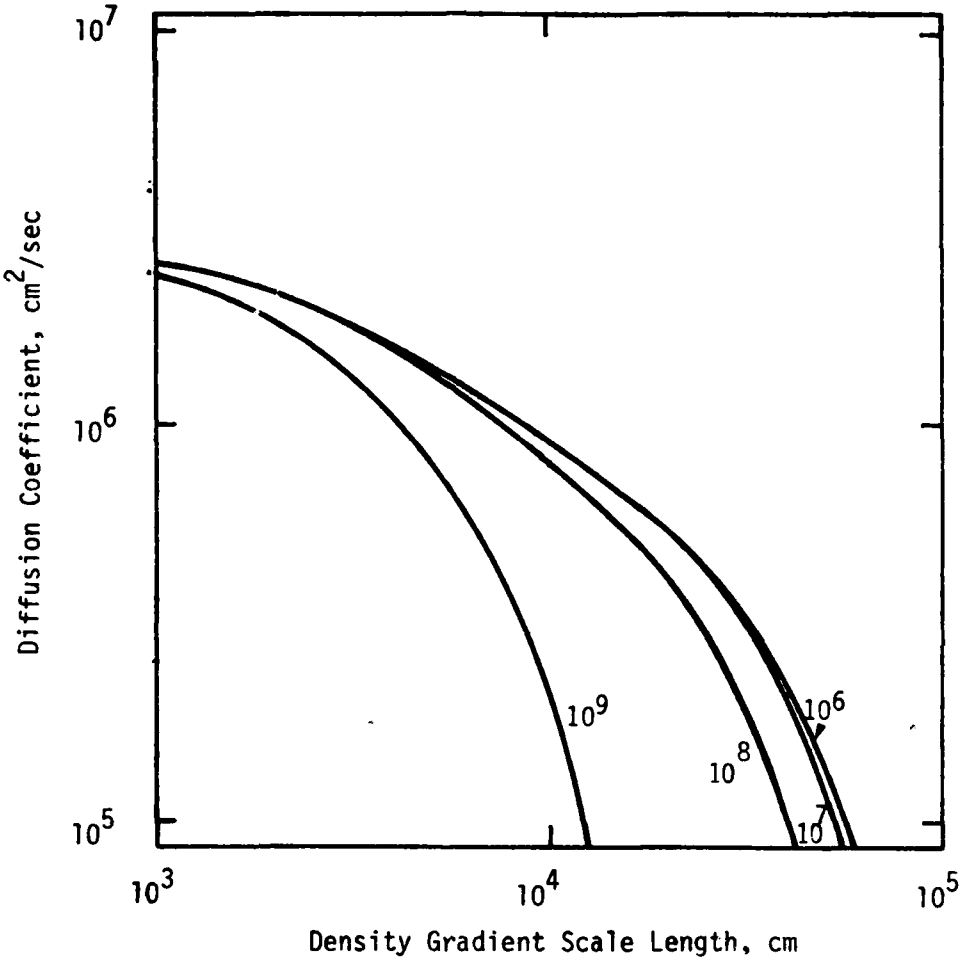

Figure 6. Plot of the diffusion coefficient (cm^2/sec) vs the density gradient scale length (cm) for various values of the neutral density (cm^{-3}) in a singly ionized and neutral oxygen plasma. $n = 10^7\ cm^{-3}$, $L_z = 10^7$ cm, B = 0.35 gauss, $T_e/T_i = 1$, and $\rho_i = 4.62 \times 10^2$ cm. The corresponding classical diffusion coefficient from interspecies coulomb collisions is $1.68 \times 10^5\ cm^2/sec$.

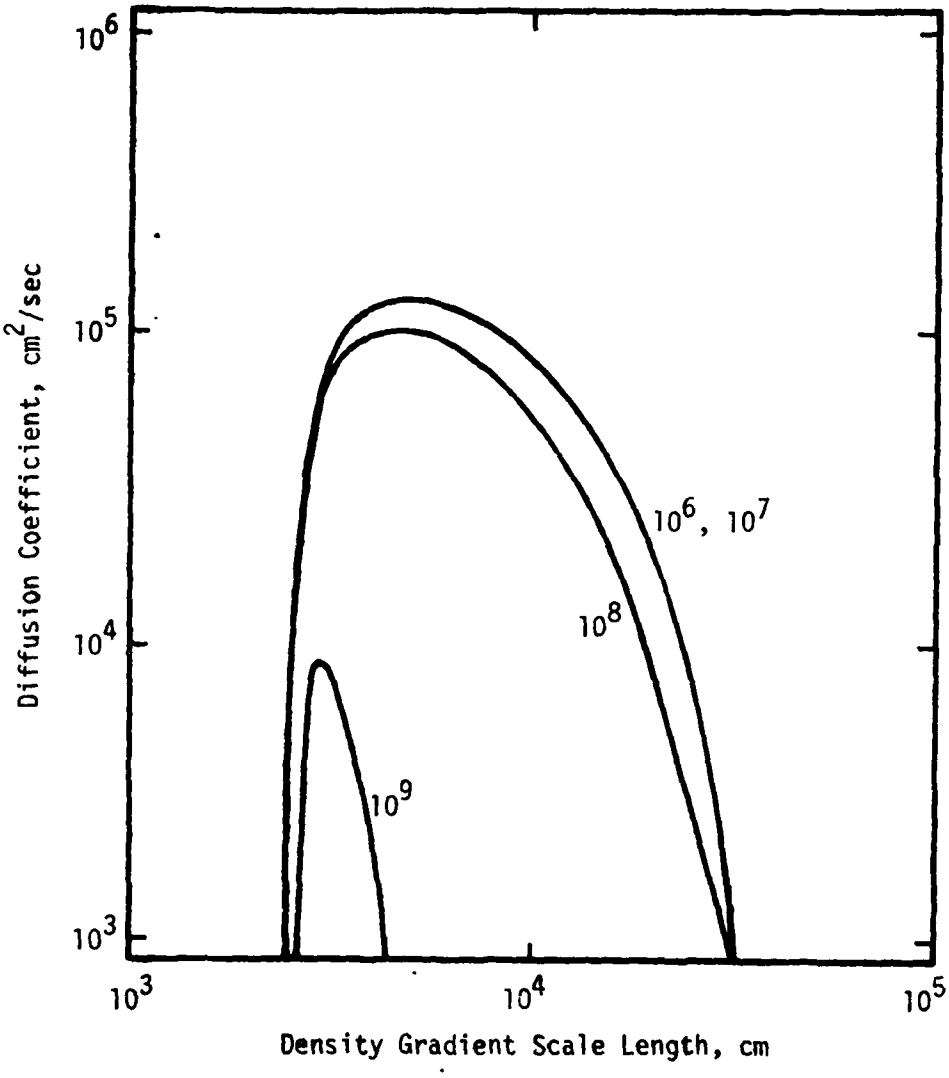

Figure 7. Plot of the diffusion coefficient (cm^2/sec) vs. the density gradient scale length (cm) for various values of the neutral density (cm^{-3}) in a singly ionized and neutral oxygen plasma. $n = 10^8\ cm^{-3}$, $L_z = 10^7$ cm, B = 0.35 gauss, $T_e/T_i = 1$, and $\rho_i = 4.62 \times 10^2$ cm. The corresponding classical diffusion coefficient from interspecies coulomb collisions is 1.68×10 cm^2/sec.

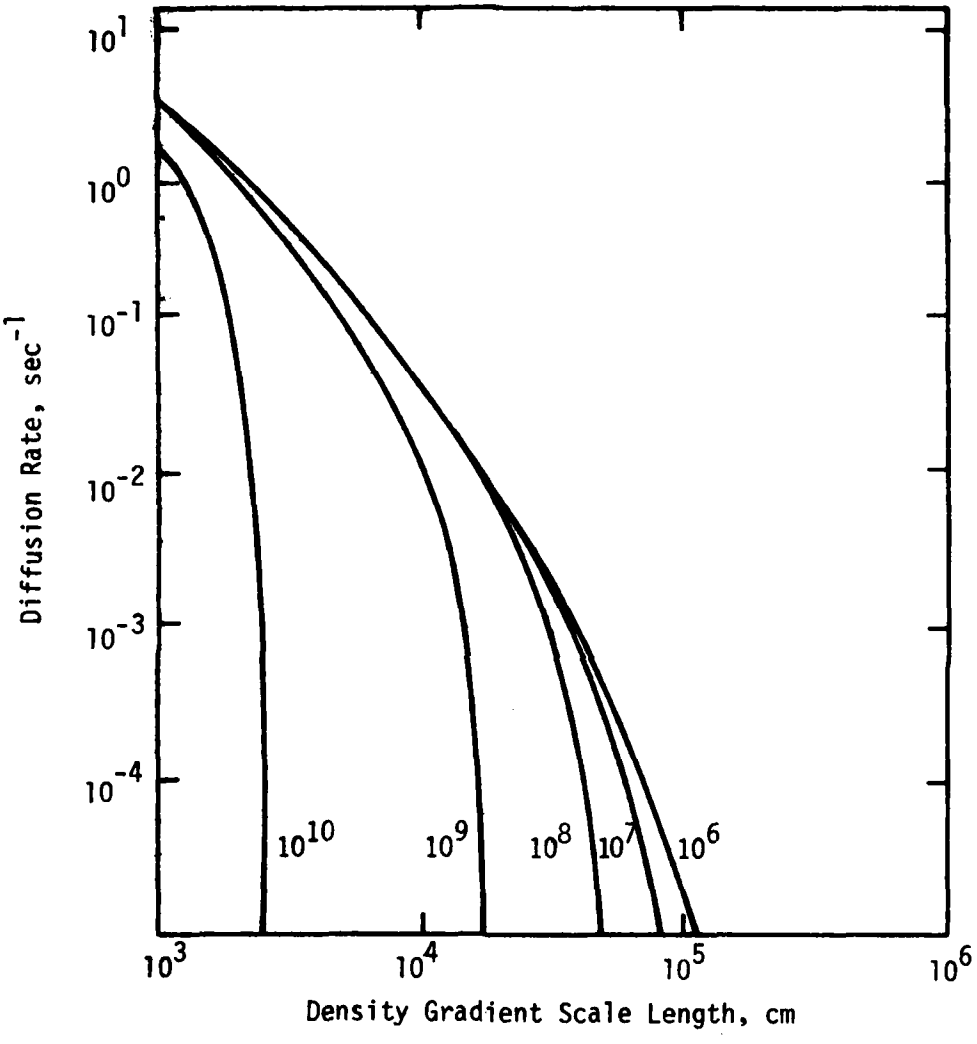

Figure 8. Plot of the diffusion rate (sec^{-1}) (the diffusion coefficient divided by L_D^2) vs the density gradient scale length (cm) for various values of the neutral density (cm^{-3}) in a singly ionized and neutral oxygen plasma. $n = 10^4$ cm^{-3}, $L_z = 10^7$ cm, B = 0.35 gauss, $T_e/T_i = 1$, and $\rho_i = 4.62 \times 10^2$ cm.

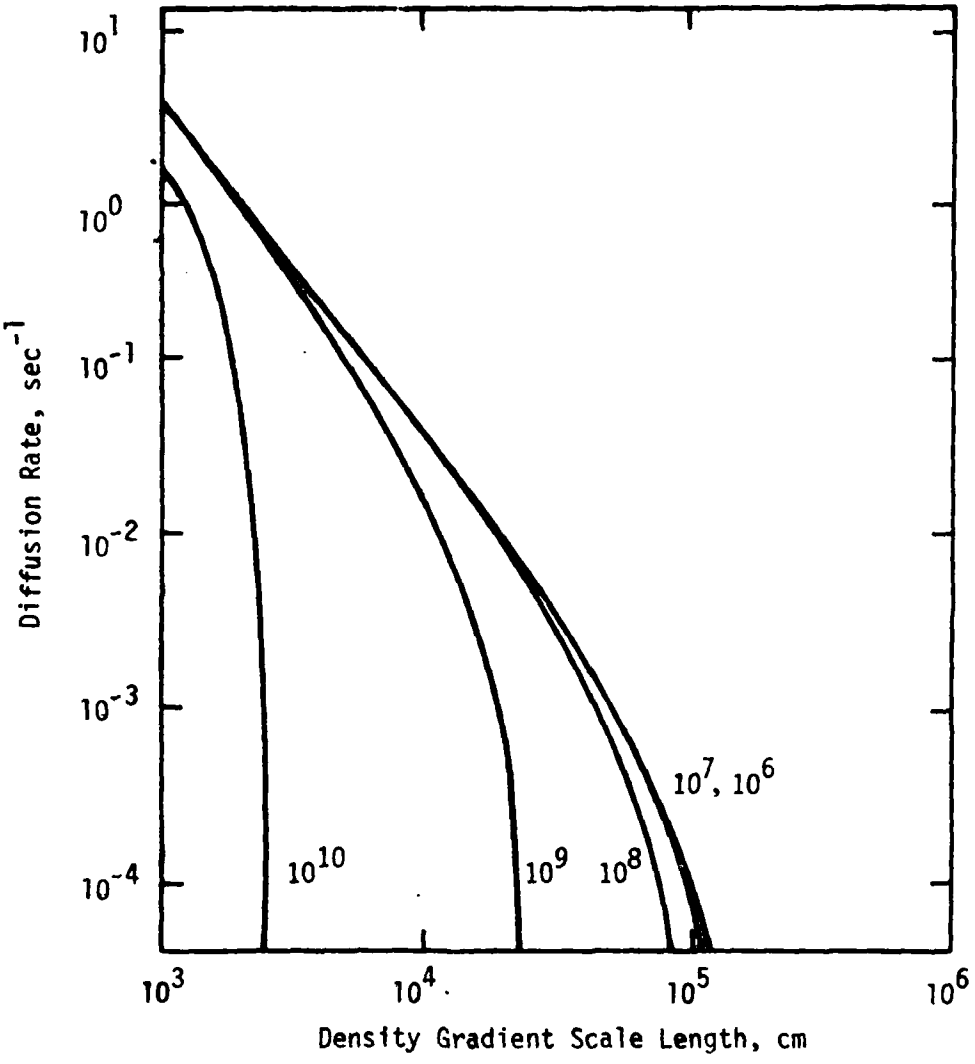

Figure 9. Plot of the diffusion rate (sec^{-1}) (the diffusion coefficient divided by L_D^2) vs the density gradient scale length (cm) for various values of the neutral density (cm^{-3}) in a singly ionized and neutral oxygen plasma. $n = 10^5$ cm^{-3}, $L_z = 10^7$ cm, $B = 0.35$ gauss, $T_e/T_i = 1$, and $\rho_i = 4.62 \times 10^2$ cm. The corresponding

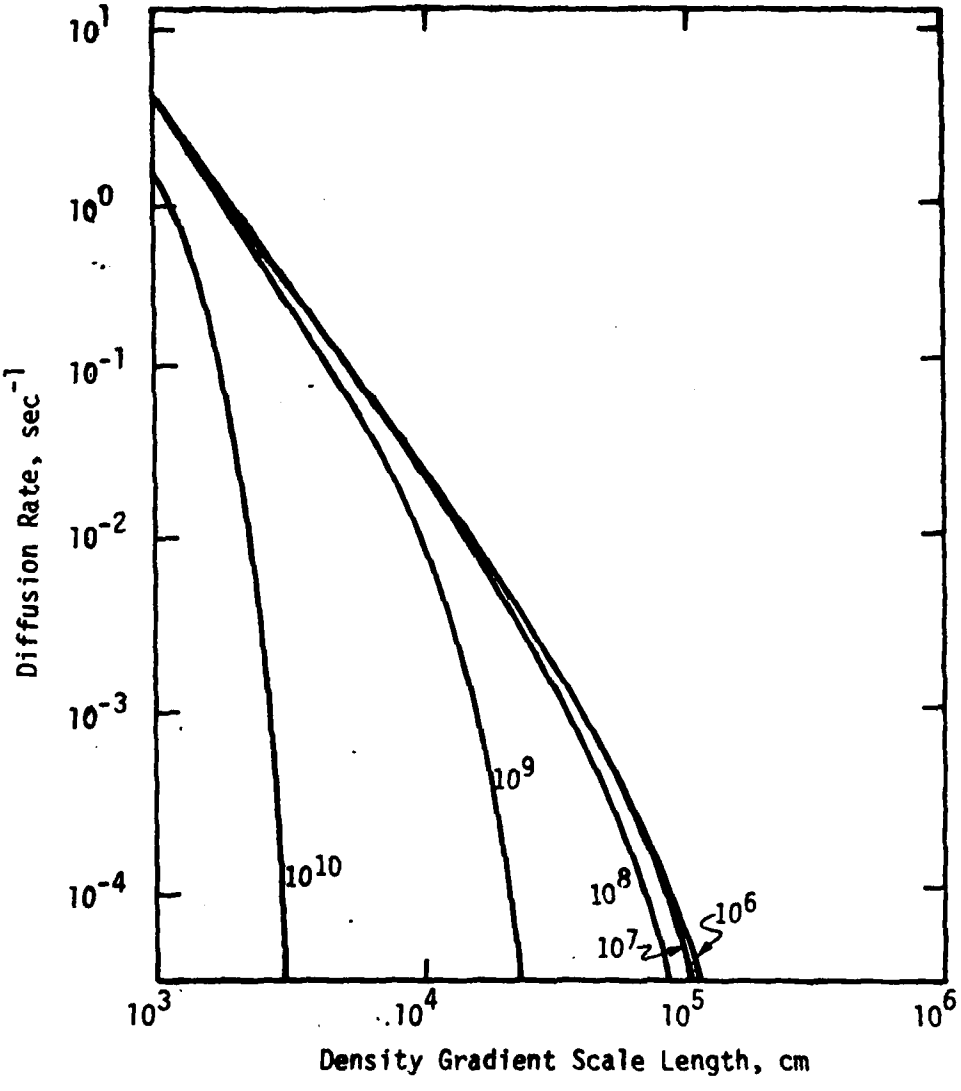

Figure 10. Plot of the diffusion rate (sec^{-1}) (the diffusion coefficient divided by L_n^2) vs the density gradient scale length (cm) for various values of the neutral density (cm^{-3}) in a singly ionized and neutral oxygen plasma. $n = 10^6$ cm^{-3}, $L_z = 10^7$ cm, B = 0.35 gauss, $T_e/T_i = 1$, and $\rho_i = 4.62 \times 10^2$ cm. The corresponding

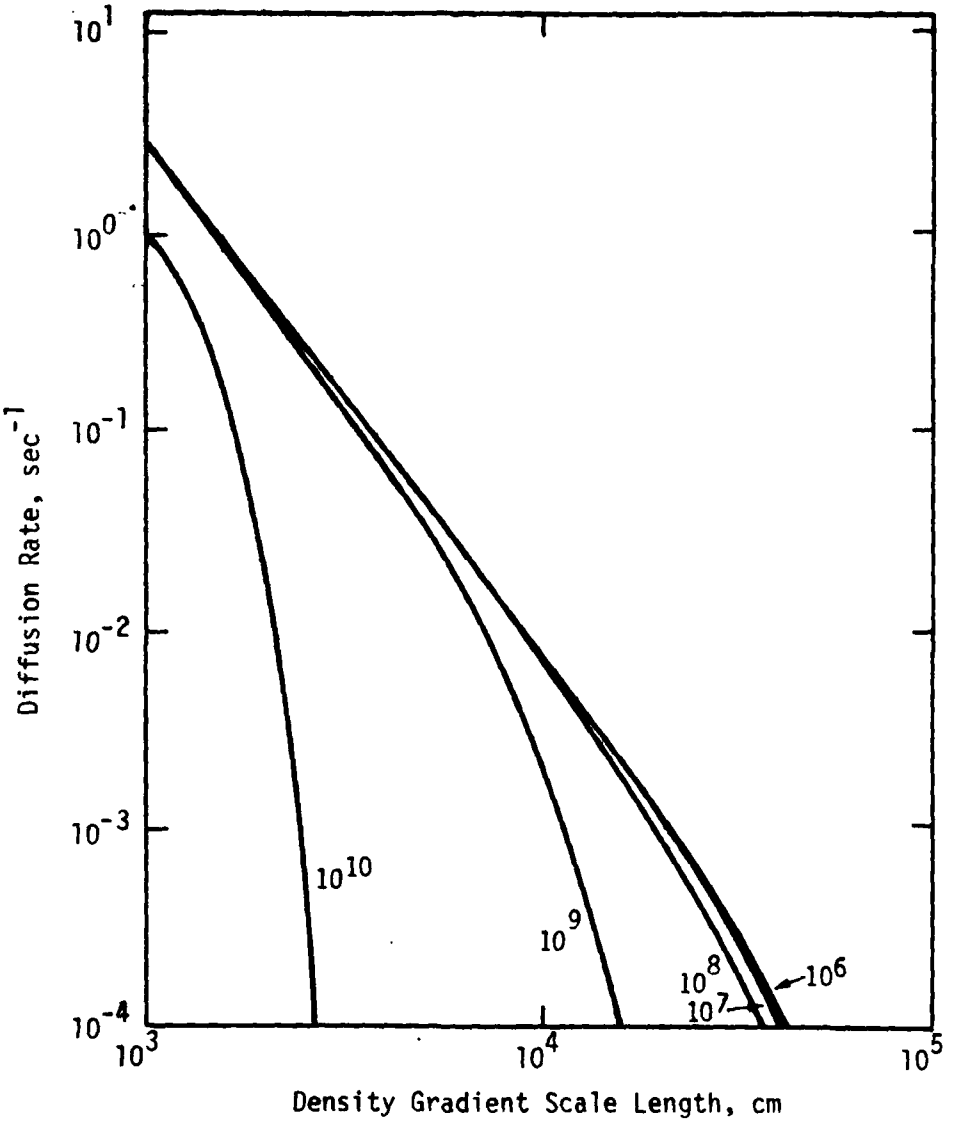

Figure 11. Plot of the diffusion rate (sec^{-1}) (the diffusion coefficient divided by L_p^2) vs the density gradient scale length (cm) for various values of the neutral density (cm^{-3}) in a singly ionized and neutral oxygen plasma. $n = 10^7$ cm^{-3}, $L_z = 10^7$ cm, B = 0.35 gauss, $T_e/T_i = 1$, and $\rho_i = 4.62 \times 10^2$ cm. The corresponding

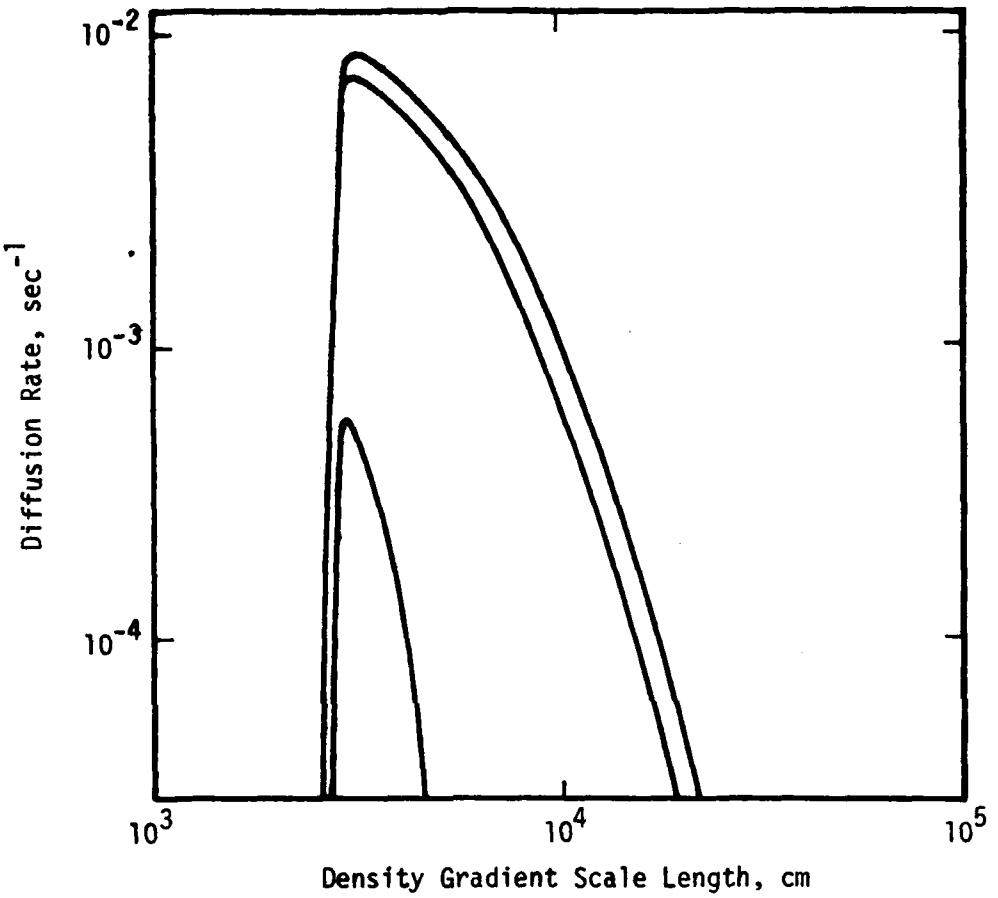

Figure 12. Plot of the diffusion rate (sec^{-1}) (the diffusion coefficient divided by L_p^2) vs. the density gradient scale length (cm) for various values of the neutral density (cm^{-3}) in a singly ionized and neutral oxygen plasma. $n = 10^8$ cm^{-3}, $L_z = 10^7$ cm, B = 0.35 gauss, $T_e/T_i = 1$, and $\rho_i = 4.62 \times 10^2$ cm.

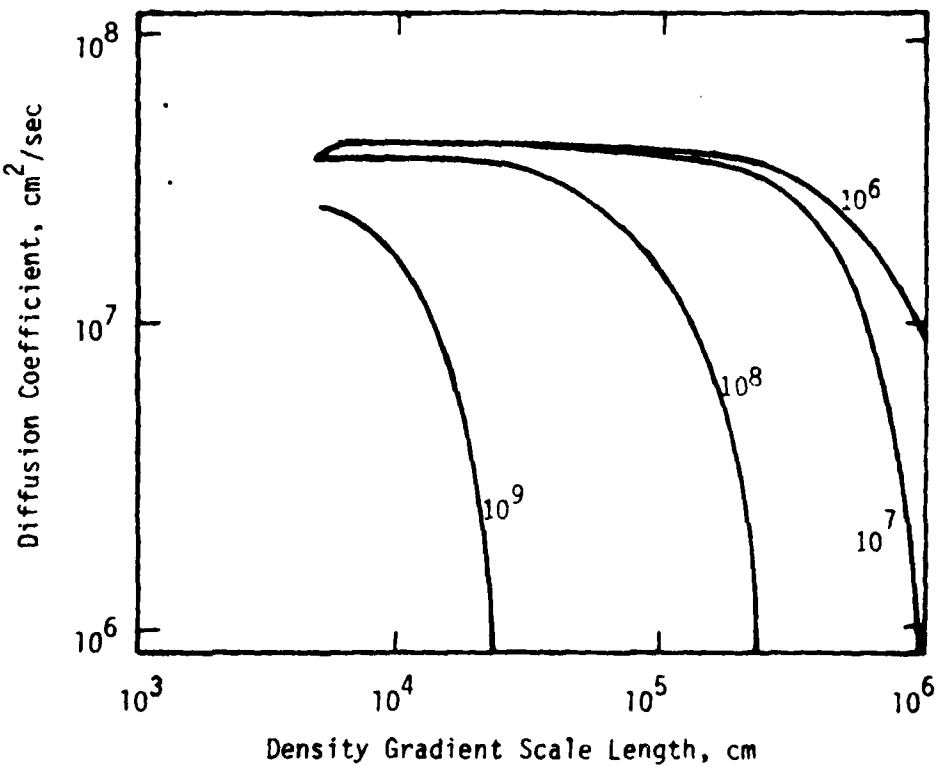

Figure 13. Plot of the diffusion coefficient (cm^2/sec) vs the density gradient scale length (cm) for various values of the neutral density (cm^{-3}) in a singly ionized and neutral oxygen plasma. $n = 10^4$ cm^{-3}, $L_z = 10^8$ cm, B = .035 gauss, $\rho_i = 4.62 \times 10^3$ cm. The corresponding classical diffusion coefficient from inter-species coulomb collisions is 1.68×10^4 cm^2/sec.

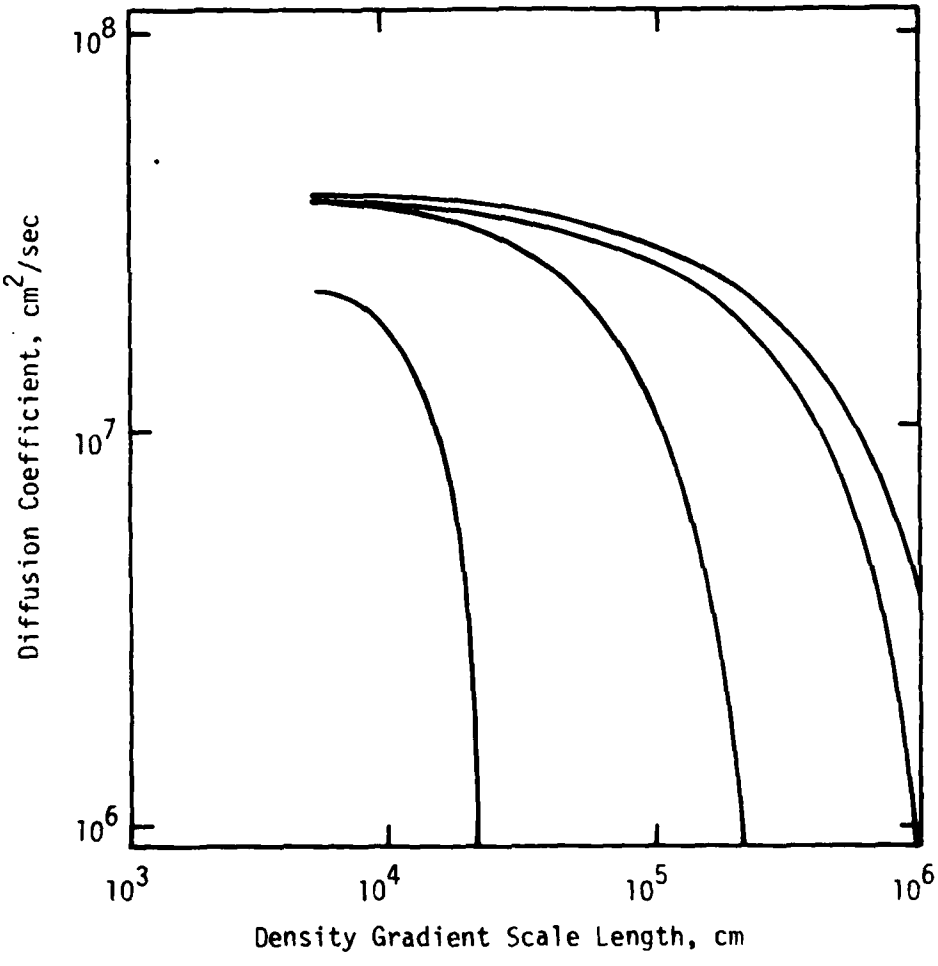

Figure 14. Plot of the diffusion coefficient (cm^2/sec) vs the density gradient scale length (cm) for various values of the neutral density (cm^{-3}) in a singly ionized and neutral oxygen plasma. $n = 10^5\ cm^{-3}$, $L_z = 10^8$ cm, B = .035 gauss, $\rho_i = 4.62 \times 10^3$ cm. The corresponding classical diffusion coefficient from inter-species coulomb collisions is $1.68 \times 10^{-5}\ cm^2/sec$.

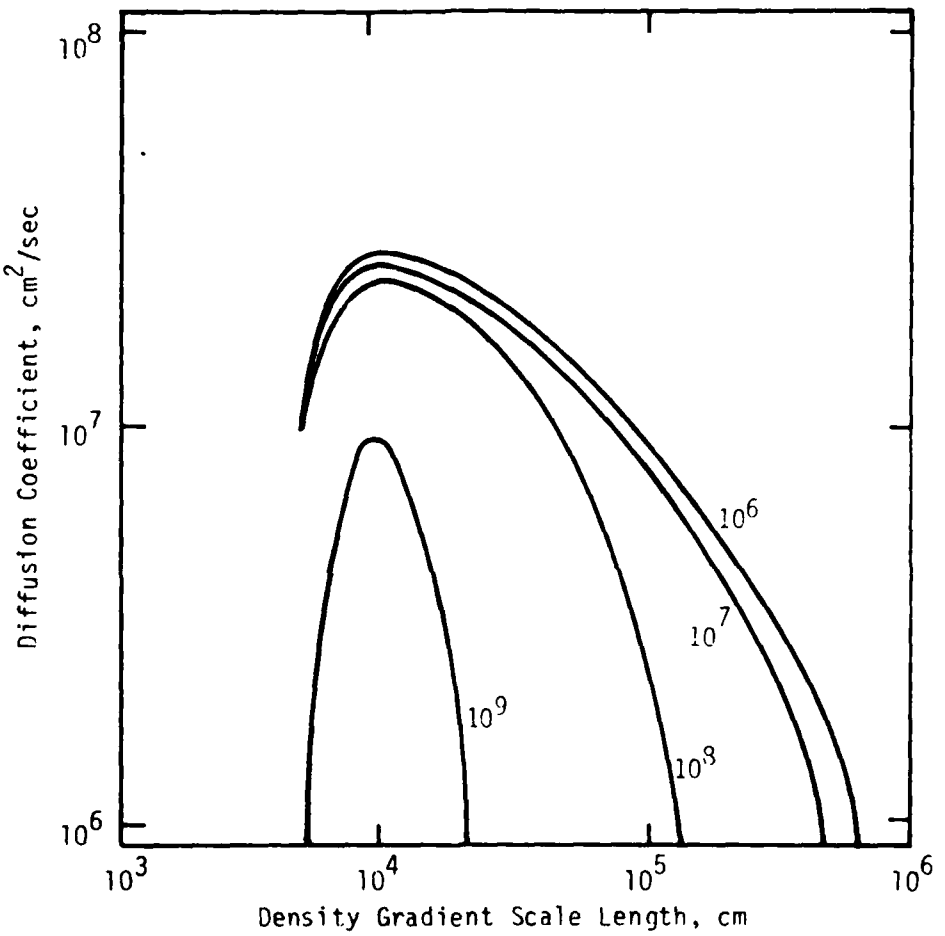

Figure 15. Plot of the diffusion coefficient (cm^2/sec) vs. the density gradient scale length (cm) for various values of the neutral density (cm^{-3}) in a singly ionized and neutral oxygen plasma. $n = 10^6\ cm^{-3}$, $L_z = 10^8$ cm, B = 0.035 gauss, $\rho_i = 4.62 \times 10^3$ cm. The corresponding classical diffusion coefficient from interspecies coulomb collisions is $1.68 \times 10^6\ cm^2/sec$.

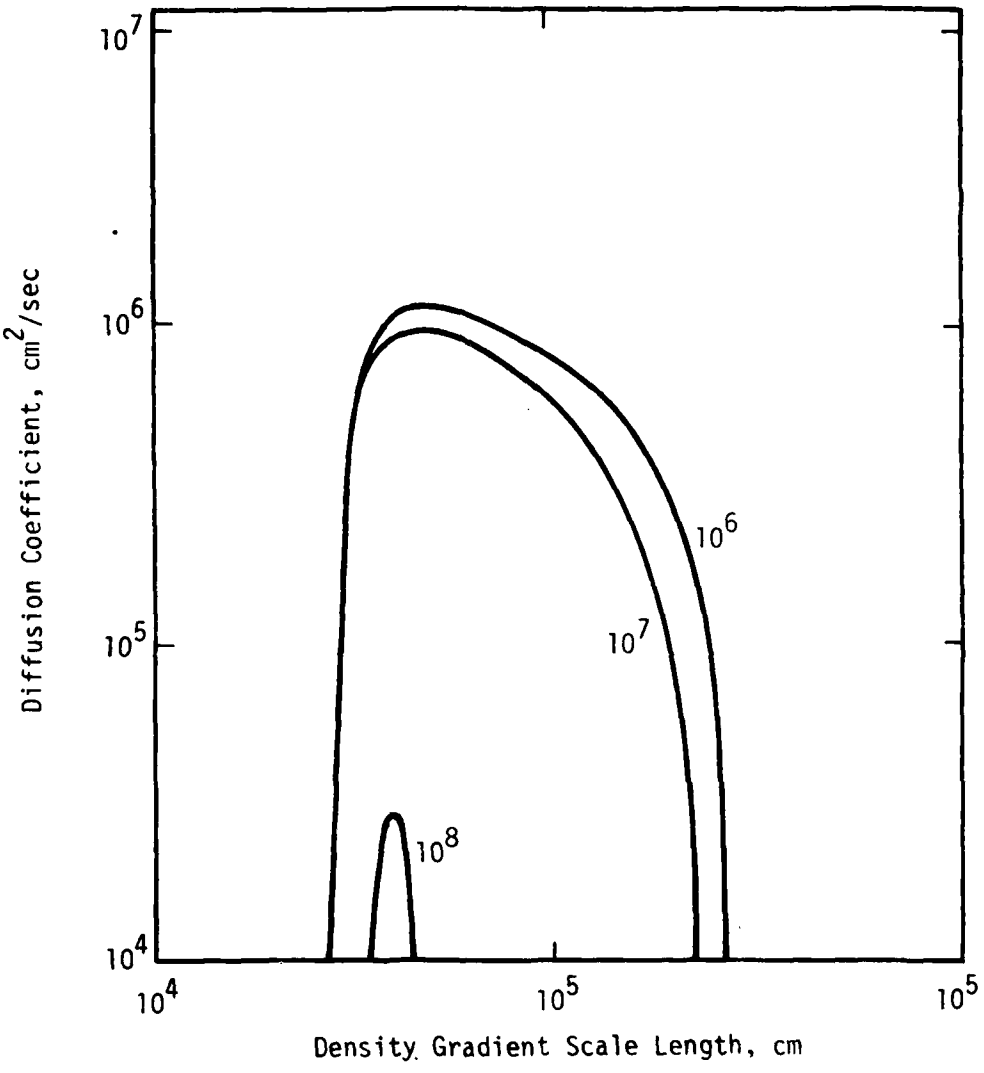

Figure 16. Plot of the diffusion coefficient (cm^2/sec) vs. the density gradient scale length (cm) for various values of the neutral density (cm^{-3}) in a singly ionized and neutral oxygen plasma. $n = 10^7$ cm^{-3}, $L_z = 10^8$ cm, B = 0.035 gauss, $\rho_i = 4.62 \times 10^3$ cm. The corresponding classical diffusion coefficient from interspecies coulomb collisions is 1.68×10^7 cm^2/sec.

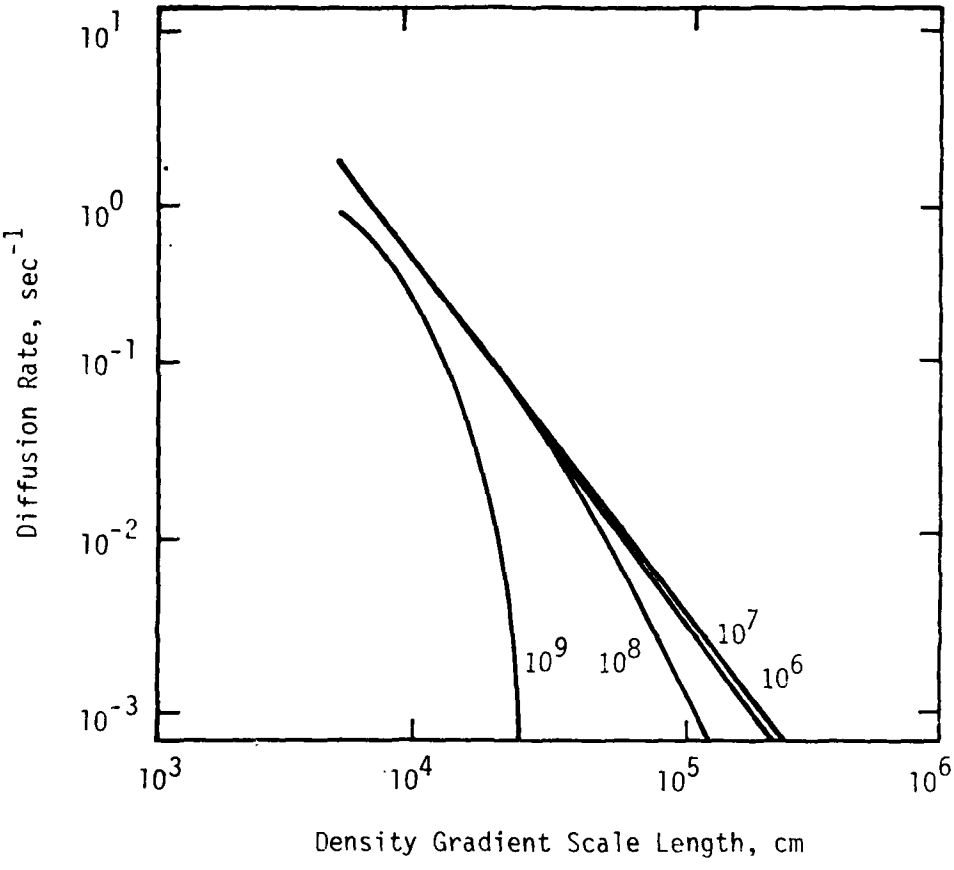

Figure 17. Plot of the diffusion rate (sec^{-1}) vs the density gradient scale length (cm) for various values of the neutral density (cm^{-3}) in a singly ionized and neutral oxygen plasma. $n = 10^{4}$ cm^{-3}, $L_z = 10^{8}$ cm, B = .035 gauss, $\rho_i = 4.62 \times 10^{3}$ cm.

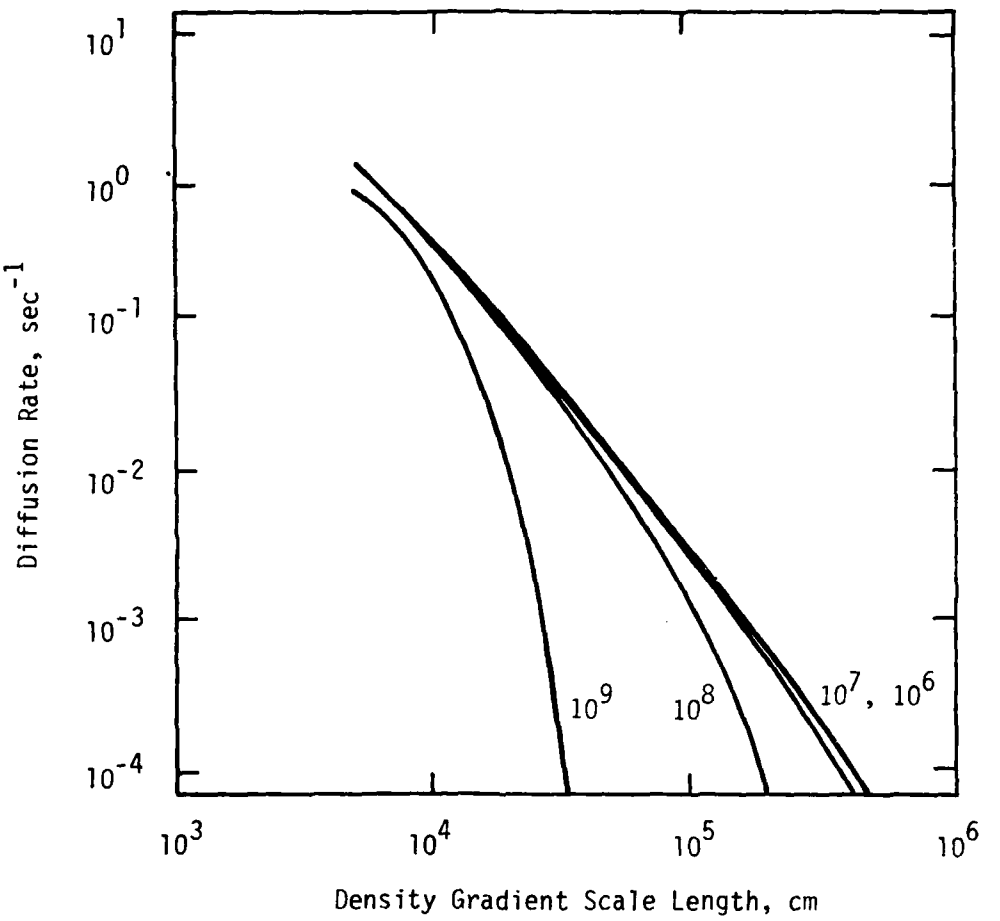

Figure 18. Plot of the diffusion rate (sec^{-1}) vs the density gradient scale length (cm) for various values of the neutral density (cm^{-3}) in a singly ionized and neutral oxygen plasma. $n = 10^{5}$ cm^{-3}, $L_z = 10^{8}$ cm, B = .035 gauss, $\rho_i = 4.62 \times 10^{3}$ cm.

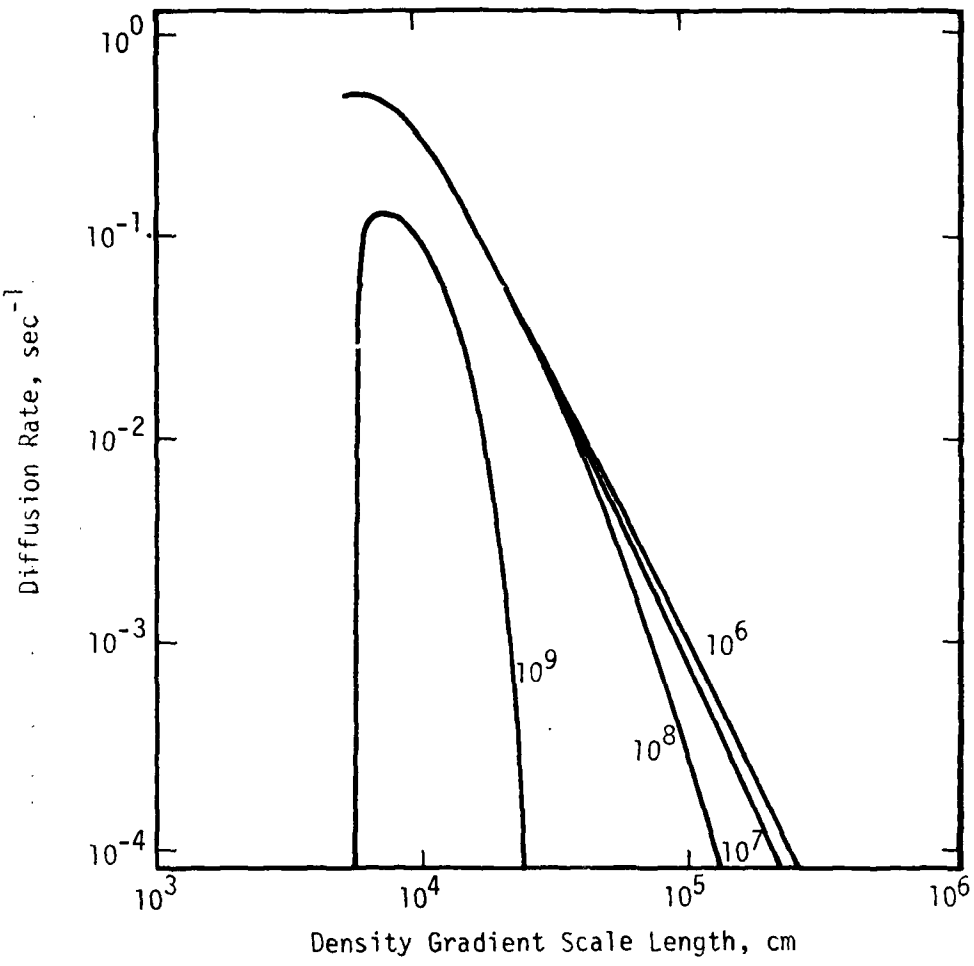

Figure 19. Plot of the diffusion rate (sec^{-1}) vs. the density gradient scale length (cm) for various values of the neutral density (cm^{-3}) in a singly ionized and neutral oxygen plasma. $n = 10^{6}$ cm^{-3}, $L_z = 10^{8}$ cm, B = 0.035 gauss, $\rho_i = 4.62 \times 10^{3}$ cm.

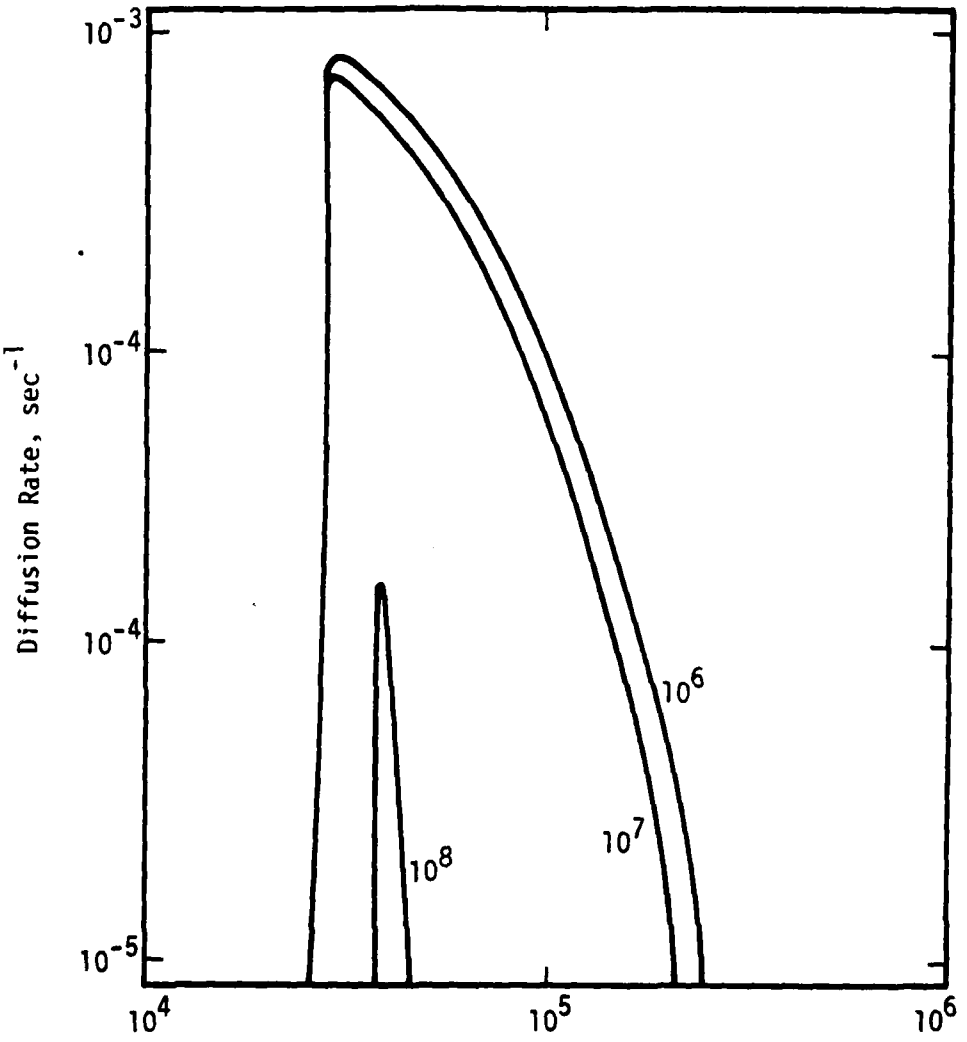

Figure 20. Plot of the diffusion rate (sec^{-1}) vs. the density gradient scale length (cm) for various values of the neutral density (cm^{-3}) in a singly ionized and neutral oxygen plasma. $n = 10^{7}$ cm^{-3}, $L_z = 10^{8}$ cm, B = 0.35 gauss, $\rho_i = 4.62 \times 10^{3}$ cm.

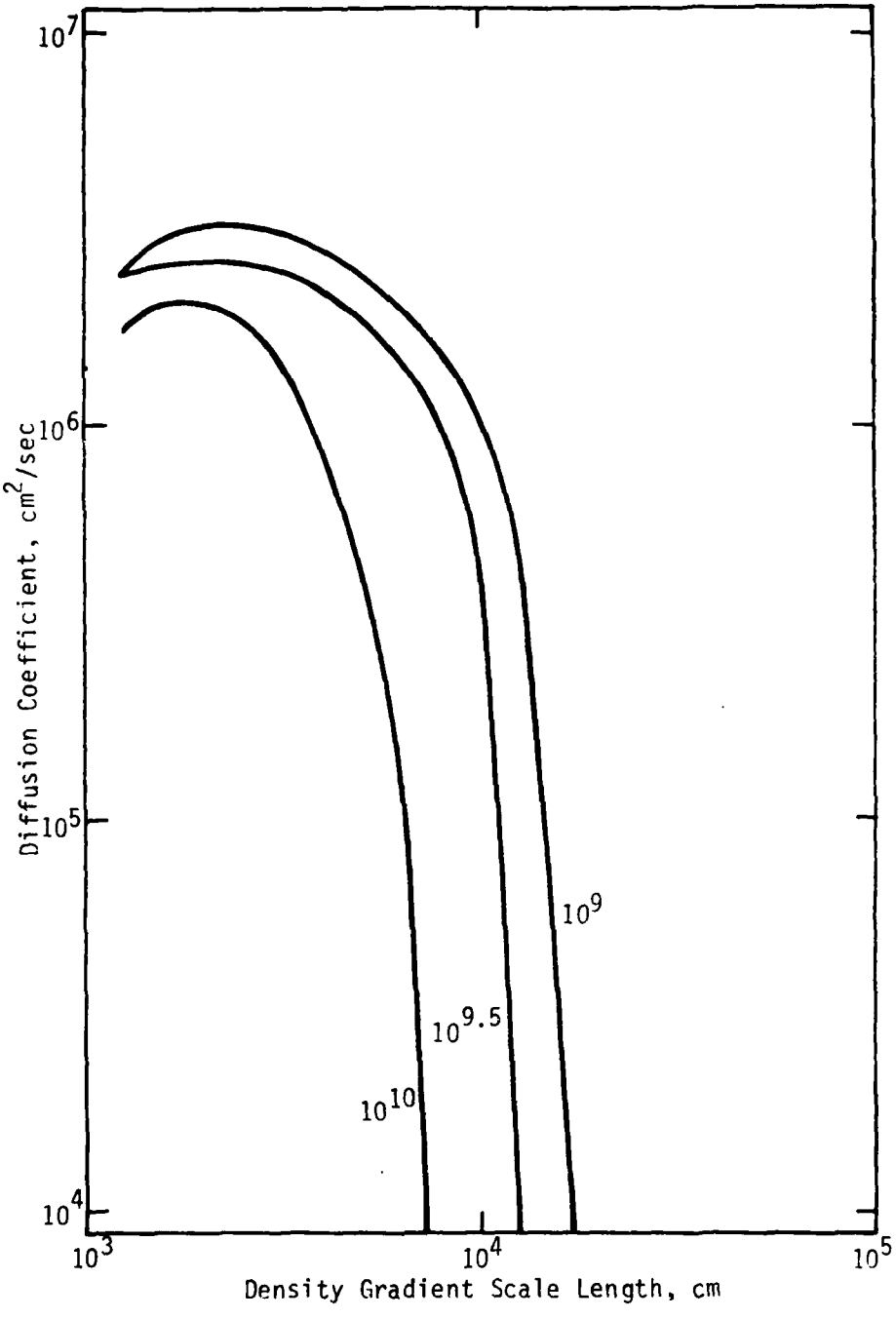

Figure 21. Plot of the diffusion coefficient (cm^2/sec) vs the density gradient scale length (cm) for various values of the neutral density (cm^{-3}) in a singly ionized and neutral barium plasma. $n = 10^6$ cm^{-3}, $L_z = 2.5 \times 10^6$ cm, B = 0.35 gauss, $T_e/T_i = 1$, and $\rho_i = 1.1 \times 10^{-3}$ cm. There is no anomalous diffusion at $n_o = 10^{10.5}$ cm^{-3} and above. The classical coulomb diffusion coefficient is 1.68×10^4 cm^2/sec.

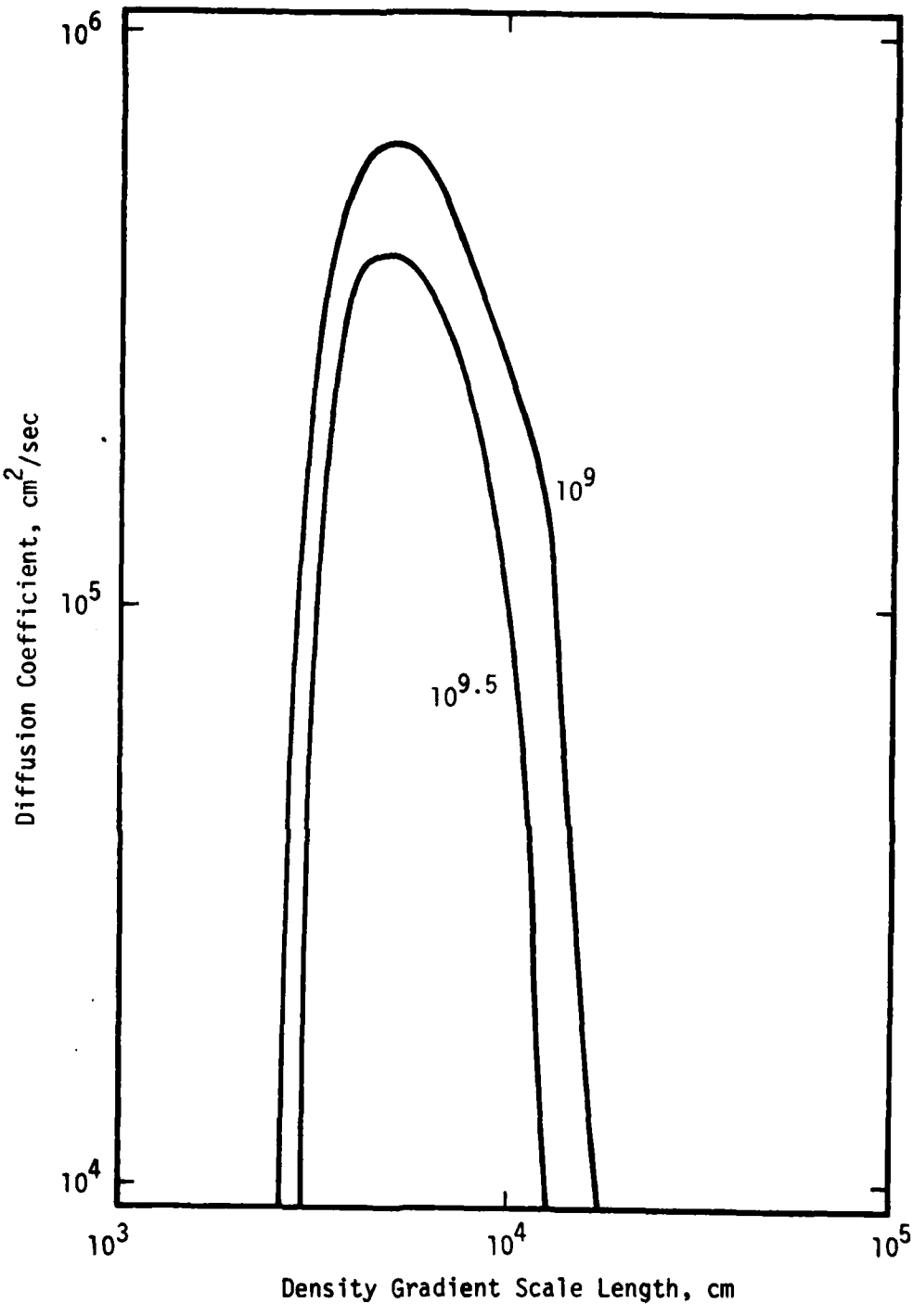

Figure 22. Plot of the diffusion coefficient (cm^2/sec) vs. the density gradient scale length (cm) for various values of the neutral density (cm^{-3}) in a singly ionized and neutral barium plasma. $n = 10^7$ cm^{-3}, $L_z = 2.5 \times 10^6$ cm, B = 0.35 gauss, $T_e/T_i = 1$, and $\rho_i = 1.1 \times 10^3$ cm. There is no anomalous diffusion at $n_n = 10^{10}$ cm^{-3} and above. The classical coulomb diffusion coefficient is 1.68×10^5 cm^2/sec.

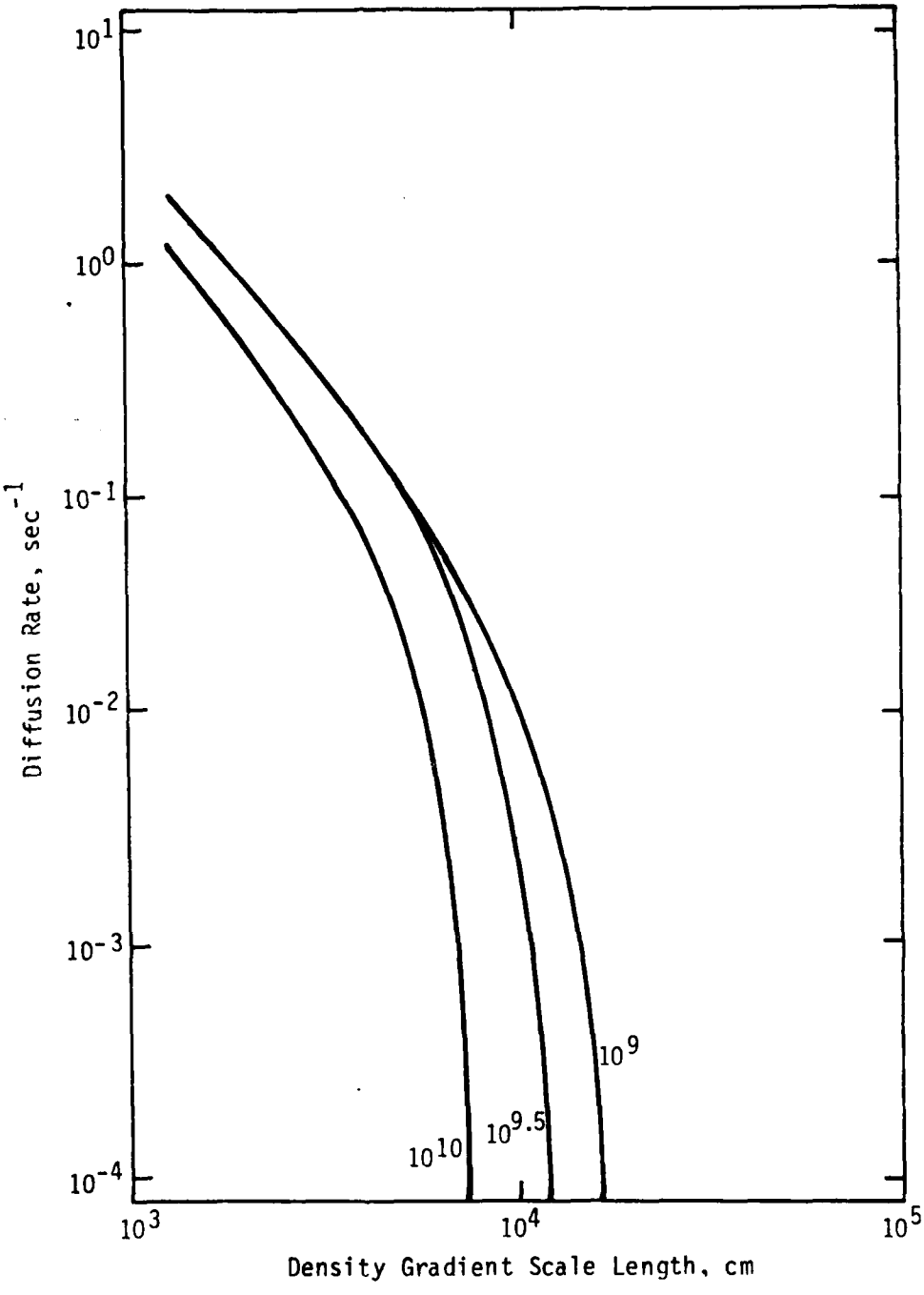

Figure 23. Plot of the diffusion rate (sec^{-1})(the diffusion coefficient divided by L_p^2) vs the density gradient scale length (cm) for various values of the neutral density (cm^{-3}) in a singly ionized and neutral barium plasma. $n = 10^6$ cm^{-3}, $L_z = 2.5 \times 10^6$ cm, B = 0.35 gauss, $T_e/T_i = 1$, and $\rho_i = 1.1 \times 10^3$ cm. There is no anomalous diffusion at $n_n = 10^{10.5}$ cm^{-3} and above.

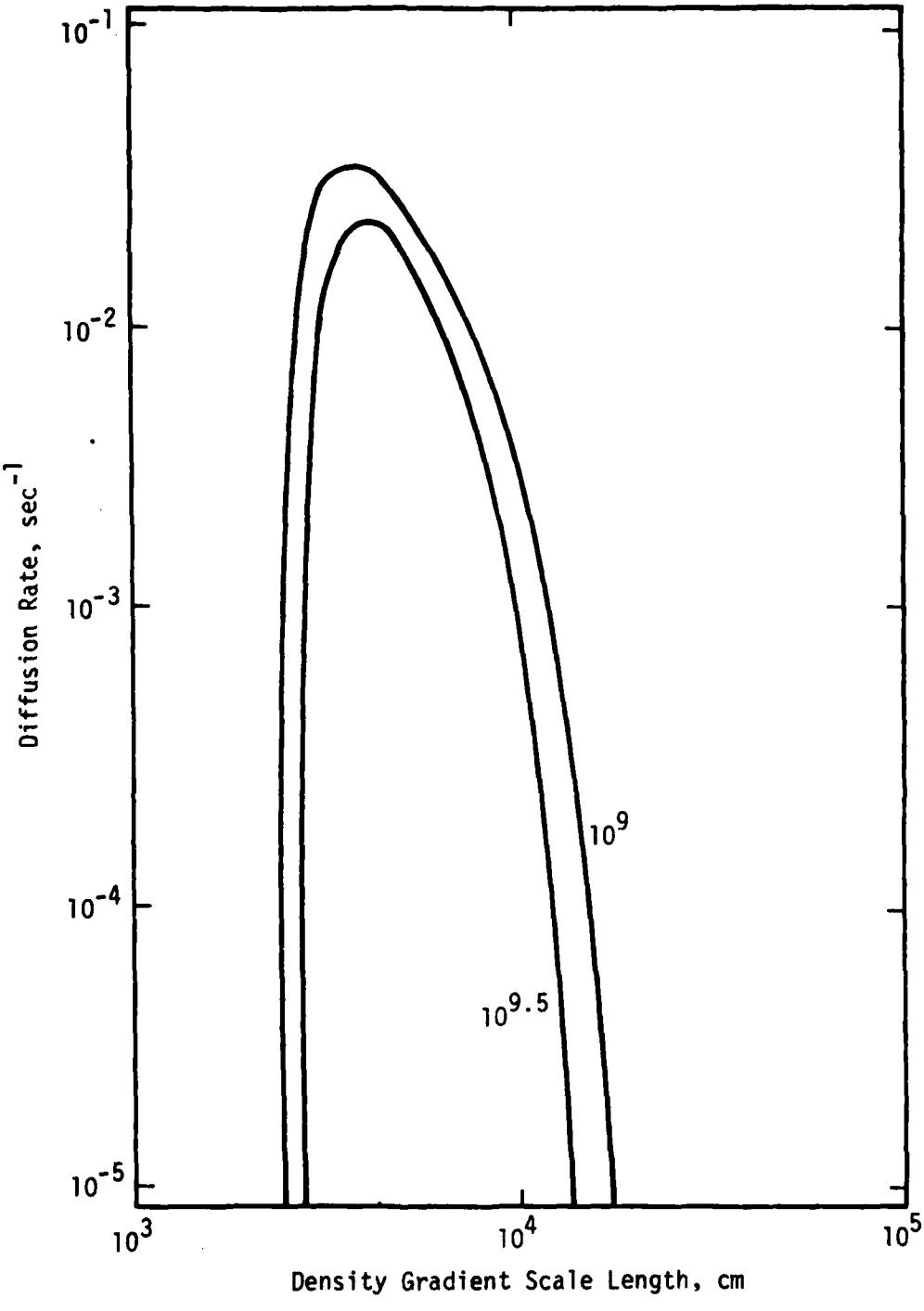

Figure 24. Plot of the diffusion rate (sec^{-1}) (the diffusion coefficient divided by $L_{\perp}^2$) vs. the density gradient scale length (cm) for various values of the neutral density (cm^{-3}) in a singly ionized and neutral barium plasma. $n = 10^7$ cm^{-3}, $L_z = 2.5 \times 10^6$ cm, B = 0.35 gauss, $T_e/T_i = 1$, and $\rho_i = 1.1 \times 10^3$ cm. There is no anomalous diffusion at $n_n = 10^{10}$ cm^{-3} and above.

Table 1. Modal parameters associated with diffusion for $n = 10^6$ cm^{-3} and neutral density = 10^6 cm^{-3}. The diffusion coefficients and rates (DIFRTM) for this table are plotted in Figures 5 and 10. The frequency, k_z and k_y values of the mode with largest diffusion contribution for given ambient parameters are given as FREQM, KZM, and KYM, respectively. The corresponding modal growth rate (γ) is (DIFRTM) x $(L_\perp/\rho_i)$, with $\rho_i = 4.62 \times 10^2$ cm.

L	DIFRTM	FREQM	KZM	KYM
1.000000E+03	3.814634E+00	-9.769753E+00	1.066358E-05	1.382213E-03
1.258925E+03	2.369956E+00	-9.496501E+00	1.066358E-05	1.338603E-03
1.584893E+03	1.464790E+00	-5.978324E+00	8.033977E-06	1.328175E-03
1.995262E+03	9.099748E-01	-5.479202E+00	8.033977E-06	1.350158E-03
2.511886E+03	5.609202E-01	-4.269953E+00	6.052827E-06	1.139464E-03
3.162278E+03	3.433089E-01	-3.682328E+01	6.052827E-06	1.201212E-03
3.981072E+03	2.090178E-01	-2.627965E+00	4.337902E-06	1.026121E-03
5.011872E+03	1.270536E-01	-2.014682E+00	4.118116E-06	1.121778E-03
6.309573E+03	7.607813E-02	-1.820443E+00	3.585815E-06	9.699496E-04
7.943282E+03	4.530903E-02	-1.218509E+00	2.483167E-06	8.386703E-04
1.000000E+04	2.692350E-02	-9.000448E-01	2.411565E-06	9.623929E-04
1.258925E+04	1.609415E-02	-8.273793E-01	2.149995E-06	8.422823E-04
1.584893E+04	9.401440E-03	-5.893355E-01	1.591634E-06	7.371620E-04
1.995262E+04	5.384977E-03	-4.381297E-01	1.224249E-06	6.451611E-04
2.511886E+04	3.037790E-03	-2.825324E-01	8.441201E-07	5.646424E-04
3.162278E+04	1.729756E-03	-2.886011E-01	1.129290E-06	6.968087E-04
3.981072E+04	9.774986E-04	-1.919144E-01	8.117573E-07	6.172797E-04
5.011872E+04	5.460831E-04	-1.401367E-01	6.283185E-07	5.468276E-04
6.309573E+04	2.817955E-04	-1.352709E-01	6.283185E-07	4.844164E-04
7.943282E+04	1.141932E-04	-1.159713E-01	6.283185E-07	4.291284E-04
1.000000E+05	4.312406E-05	-8.447109E-02	6.283185E-07	5.695165E-04
1.258925E+05	1.250024E-05	-7.567366E-02	6.283185E-07	5.106671E-04
1.584893E+05	0.	0.	0.	0.
1.995262E+05	0.	0.	0.	0.
2.511886E+05	0.	0.	0.	0.
3.162278E+05	0.	0.	0.	0.
3.981072E+05	0.	0.	0.	0.
5.011872E+05	0.	0.	0.	0.
6.309573E+05	0.	0.	0.	0.
7.943282E+05	0.	0.	0.	0.
1.000000E+06	0.	0.	0.	0.

Table 2. Modal parameters associated with diffusion for $n = 10^6$ cm^{-3} and neutral density = 10^7 cm^{-3}. The diffusion coefficients and rates (DIFRTM) for this table are plotted in Figures 5 and 10. The frequency, k_z and k_y values of the mode with largest diffusion contribution for given ambient parameters are given as FREQM, KZM, and KYM, respectively. The corresponding modal growth rate (γ) is (DIFRTM) x $(L_\perp/\rho_i)$, with $\rho_i = 4.62 \times 10^2$ cm.

L	DIFRTM	FREQM	KZM	KYM
1.000000E+03	3.812435E+00	-9.768440E+00	1.066408E-05	1.382213E-03
1.258925E+03	2.368332E+00	-9.495257E+00	1.066408E-05	1.338603E-03
1.584893E+03	1.463419E+00	-5.976889E+00	8.034318E-06	1.328175E-03
1.995262E+03	9.089246E-01	-5.477855E+00	8.034318E-06	1.350158E-03
2.511886E+03	5.601502E-01	-4.268416E+00	6.053055E-06	1.139464E-03
3.162278E+03	3.427019E-01	-3.680882E+00	6.053055E-06	1.201212E-03
3.981072E+03	2.085587E-01	-2.626207E+00	4.337902E-06	1.026121E-03
5.011872E+03	1.266694E-01	-2.012980E+00	4.118116E-06	1.121778E-03
6.309573E+03	7.581483E-02	-1.818750E+00	3.585815E-06	9.699496E-04
7.943282E+03	4.510241E-02	-1.216663E+00	2.483167E-06	8.386703E-04
1.000000E+04	2.674409E-02	-8.982056E-01	2.411565E-06	9.623929E-04
1.258925E+04	1.597287E-02	-8.255790E-01	2.149995E-06	8.422823E-04
1.584893E+04	9.309413E-03	-5.874334E-01	1.591634E-06	7.371620E-04
1.995262E+04	5.317152E-03	-4.361742E-01	1.224249E-06	6.451611E-04
2.511886E+04	2.982904E-03	-2.804537E-01	8.441201E-07	5.646424E-04
3.162278E+04	1.689643E-03	-2.866735E-01	1.129290E-06	6.968087E-04
3.981072E+04	9.461926E-04	-1.898572E-01	8.117573E-07	6.172797E-04
5.011872E+04	5.252151E-04	-1.588993E-01	7.010836E-07	5.468276E-04
6.309573E+04	2.691069E-04	-1.334874E-01	6.283185E-07	4.844164E-04
7.943282E+04	1.078633E-04	-1.145967E-01	6.283185E-07	4.291284E-04
1.000000E+05	3.577331E-05	-8.277380E-02	6.283185E-07	5.695165E-04
1.258925E+05	8.427287E-06	-7.437796E-02	6.283185E-07	5.106671E-04
1.584893E+05	0.	0.	0.	0.
1.995262E+05	0.	0.	0.	0.
2.511886E+05	0.	0.	0.	0.
3.162278E+05	0.	0.	0.	0.
3.981072E+05	0.	0.	0.	0.
5.011872E+05	0.	0.	0.	0.
6.309573E+05	0.	0.	0.	0.
7.943282E+05	0.	0.	0.	0.
1.000000E+06	0.	0.	0.	0.

Table 3. Modal parameters associated with diffusion for $n = 10^6$ cm^{-3} and neutral density = 10^8 cm^{-3}. The diffusion coefficients and rates (DIFRTM) for this table are plotted in Figures 5 and 10. The frequency, k_z and k_y values of the mode with largest diffusion contribution for given ambient parameters are given as FREQM, KZM, and KYM, respectively. The corresponding modal growth rate (γ) is (DIFRTM) x ($L_\perp/\rho_i$), with $\rho_i = 4.62 \times 10^{-2}$ cm.

L	DIFRTM	FREQM	KZM	KYM
1.000000E+03	3.790454E+00	-9.755299E+00	1.066911E-05	1.382213E-03
1.258925E+03	2.352100E+00	-9.482805E+00	1.066911E-05	1.338603E-03
1.584893E+03	1.449715E+00	-5.962516E+00	8.037728E-06	1.328175E-03
1.995262E+03	8.984281E+01	-5.464354E+00	8.037728E-06	1.350158E-03
2.511886E+03	5.524566E-01	-4.253012E+00	6.055340E-06	1.169434E-03
3.162278E+03	3.366383E-01	-3.666386E+00	6.055340E-06	1.201212E-03
3.981072E+03	2.039740E-01	-2.608569E+00	4.337902E-06	1.026121E-03
5.011872E+03	1.228337E-01	-1.995874E+00	4.118116E-06	1.121778E-03
6.309573E+03	7.318907E-02	-1.801739E+00	3.585815E-06	9.699496E-04
7.943282E+03	4.304561E-02	-1.198066E+00	2.483167E-06	8.386703E-04
1.000000E+04	2.495868E-02	-8.796328E-01	2.411565E-06	9.623929E-04
1.258925E+04	1.476939E-02	-8.074161E-01	2.149995E-06	8.422823E-04
1.584893E+04	8.400296E-03	-5.681944E-01	1.591634E-06	7.371620E-04
1.995262E+04	4.651611E-03	-4.163627E-01	1.224249E-06	6.451611E-04
2.511886E+04	2.504937E-03	-3.166900E-01	9.784000E-07	5.646424E-04
3.162278E+04	1.308483E-03	-2.124721E-01	7.144664E-07	4.941727E-04
3.981072E+04	6.767454E-04	-2.041036E-01	9.226763E-07	6.172797E-04
5.011872E+04	3.312950E-04	-1.390763E-01	7.010836E-07	5.468276E-04
6.309573E+04	1.525947E-04	-1.157783E-01	6.283185E-07	4.844164E-04
7.943282E+04	4.981477E-05	-1.012316E-01	6.283185E-07	4.291284E-04
1.000000E+04	4.219431E-06	-8.144010E-02	6.283185E-07	3.801506E-04
1.258925E+05	0.	0.	0.	0.
1.584893E+05	0.	0.	0.	0.
1.995262E+05	0.	0.	0.	0.
2.511886E+05	0.	0.	0.	0.
3.162278E+05	0.	0.	0.	0.
3.981072E+05	0.	0.	0.	0.
5.011872E+05	0.	0.	0.	0.
6.309573E+05	0.	0.	0.	0.
7.943282E+05	0.	0.	0.	0.
1.000000E+06	0.	0.	0.	0.

Table 4. Modal parameters associated with diffusion for $n = 10^6$ cm^{-3} and neutral density 10^9 cm^{-3}. The diffusion coefficients and rates (DIFRTM) for this table are plotted in Figures 5 and 10. The frequency, k_z and k_y values of the mode with largest diffusion contribution for given ambient parameters are given as FREQM, KZM, and KYM, respectively. The corresponding modal growth rate (γ) is (DIFRTM) x $(L_\perp/\rho_i)$, with $\rho_i = 4.62 \times 10^2$ cm.

L	DIFRTM	FREQM	KZM	KYM
1.000000E+03	3.571184E+00	-9.622375E+00	1.071929E-05	1.382213E-03
1.258925E+03	2.190344E+00	-9.356805E+00	1.071929E-05	1.338603E-03
1.584893E+03	1.313225E+00	-5.816218E+00	8.071748E-06	1.328175E-03
1.995262E+03	7.940079E-01	-5.326672E+00	8.071748E-06	1.350158E-03
2.511886E+03	4.761895E-01	-4.095235E+00	6.078115E-06	1.139464E-03
3.162278E+03	2.766258E-01	-3.517393E+00	6.078115E-06	1.201212E-03
3.981072E+03	1.588103E-01	-2.425808E+00	4.337902E-06	1.026121E-03
5.011872E+03	8.711108E-02	-2.145190E+00	3.760364E-06	8.765516E-04
6.309573E+03	4.768608E-02	-1.623686E+00	3.585815E-06	9.699496E-04
7.943282E+03	2.396089E-02	-1.379444E+00	3.122317E-06	8.386703E-04
1.000000E+03	1.148859E-02	-8.767534E-01	2.205375E-06	7.251592E-04
1.258925E+04	4.663466E-03	-7.220698E-01	1.958659E-06	6.270114E-04
1.584893E+04	1.599977E-03	-4.650747E-01	1.468000E-06	5.421476E-04
1.995262E+04	2.850033E-04	-3.005671E-01	1.144637E-06	4.687699E-04
2.511885E+04	0.	0.	0.	0.
3.162278E+04	0.	0.	0.	0.
3.981072E+04	0.	0.	0.	0.
5.011872E+04	0.	0.	0.	0.
6.309573E+04	0.	0.	0.	0.
7.943282E+04	0.	0.	0.	0.
1.000000E+05	0.	0.	0.	0.
1.258925E+05	0.	0.	0.	0.
1.584893E+05	0.	0.	0.	0.
1.995262E+05	0.	0.	0.	0.
2.511886E+05	0.	0.	0.	0.
3.162278E+05	0.	0.	0.	0.
3.981072E+05	0.	0.	0.	0.
5.011872E+05	0.	0.	0.	0.
6.309573E+05	0.	0.	0.	0.
7.943282E+05	0.	0.	0.	0.
1.000000E+06	0.	0.	0.	0.

Table 5. Modal parameters associated with diffusion for $n = 10^6$ cm^{-3} and neutral density = 10^{10} cm^{-3}. The diffusion coefficients and rates (DIFRTM) for this table are plotted in Figures 5 and 10. The frequency, k_z and k_y values of the mode with largest diffusion contribution for given ambient parameters are given as FREQM, KZM, and KYM, respectively. The corresponding modal growth rate (γ) is (DIFRTM) x $(L_\perp/\rho_i)$, with $\rho_i = 4.62 \times 10^2$ cm.

L	DIFRTM	FREQM	KZM	KYM
1.000000E+03	1.702275E+00	-1.037543E+01	1.121000E-05	1.175676E-03
1.258925E+03	7.903521E-01	-7.753612E+00	8.403553E-06	9.452586E-04
1.584893E+03	2.961617E-02	-5.481703E+00	6.299708E-06	7.600003E-04
1.995262E+03	7.100461E-02	-3.514090E+00	4.622389E-06	6.110503E-04
2.511886E+03	0.	0.	0.	0.
3.162278E+03	0.	0.	0.	0.
3.981072E+03	0.	0.	0.	0.
5.011872E+03	0.	0.	0.	0.
6.309573E+03	0.	0.	0.	0.
7.943282E+03	0.	0.	0.	0.
1.000000E+04	0.	0.	0.	0.
1.258925E+04	0.	0.	0.	0.
1.584893E+04	0.	0.	0.	0.
1.995262E+04	0.	0.	0.	0.
2.511886E+04	0.	0.	0.	0.
3.162278E+04	0.	0.	0.	0.
3.981072E+04	0.	0.	0.	0.
5.011872E+04	0.	0.	0.	0.
6.309573E+04	0.	0.	0.	0.
7.943282E+04	0.	0.	0.	0.
1.000000E+05	0.	0.	0.	0.
1.258925E+05	0.	0.	0.	0.
1.584893E+05	0.	0.	0.	0.
1.995262E+05	0.	0.	0.	0.
2.511886E+05	0.	0.	0.	0.
3.162278E+05	0.	0.	0.	0.
3.981072E+05	0.	0.	0.	0.
5.011872E+05	0.	0.	0.	0.
6.309573E+05	0.	0.	0.	0.
7.943282E+05	0.	0.	0.	0.
1.000000E+06	0.	0.	0.	0.

$$\gamma_1 = -\sqrt{2}\,\frac{\left[1 + T_i/T_e - I_o\, e^{-b_i}\right]^{3/2}}{(I_o - I_1)^{1/2}\, e^{-b_i/2}}\left(\frac{n_o}{n}\right)^{1/2}\frac{v_e}{v_{ti}}\,\omega' \qquad (12)$$

where ω' is the mode oscillatory frequency, n_o is the ambient ionized density outside of the striation $v_e = c|E_x|/B$, $b_i = (k_y\rho_i)^2$, and I_o and I_1 are the modified Bessel functions of zero and first order. (See Eq. (B-14) and the preceding argument in Appendix B for details.) This effect is due to convection of the mode out from a central region, i.e., the drift-dissipative eigenmode is treated non-locally in the x-direction, the direction of both the density gradient and the background electric field. The expression for the diffusion rate is assumed to be given by Eq. (7) with

$$k_x^{-2} = 8\left[\frac{(v_i^*)_{av}}{v_e}\right]\left(\frac{n}{n_o}\right)^{1/2}\rho_i \propto \frac{[I_o(b_i) - I_1(b_i)]^{1/2}\; e^{-b_i/2}}{[1 + T_i/T_e - I_o(b_i)]^{3/2}} \quad .$$

but the growth rate, which scales inversely as the gradient scale length at the location around which the mode is centered, is less by a factor of order $(v_i^*)_{av}/v_e$ even without the additional decrement of Eq. (12). (See Eq. B-12) in Appendix B and the proceeding argument for details.)

Hence diffusion and growth are inhibited whenever $(v_i^*)_{av}/v_e \ll 1$, with growth inhibited at least as rapidly as $(v_i^*)_{av}/v_e$, and with diffusion at least as rapidly as $[(v_i^*)_{av}/v_e]^2$.

6. CHARACTERIZATION OF THE DIFFUSION COEFFICIENT FROM DRIFT-DISSIPATIVE MODES IN COMPUTER SIMULATIONS

Values for D*, the anomalous diffusion coefficient in the absence of a background electric field parallel to the ionized density gradient, can be obtained from the graphs of Figures (3)-(7) and (13)-(16).

From Eqs. (B-12), (B-13) and (B-14) with $b_i \ll 1$ and

$$\omega' = \frac{C_s (v_i^*)_{av}\, \beta}{L_\perp v_e \alpha} \quad ,$$

the suggested form for the instability growth rate when

$$|v_e| > T_i/(m_i \omega_{ci} L_\perp)$$

is

$$\gamma \approx \frac{C_s}{L_\perp} \frac{\beta}{\alpha} \frac{(v_i^*)_{av}}{v_e} \left[.25 - \sqrt{2} \left(\frac{n_0}{n} \right)^{\frac{1}{2}} \frac{v_e}{v_i} - \nu_i \right] \quad . \tag{13}$$

Hence, a necessary condition of instability is then

$$\left(\frac{n_0}{n} \right)^{\frac{1}{2}} \frac{v_e}{v_{ti}} < 0.18 \quad .$$

Now define

$$\alpha_0 = \frac{c|E \cdot \nabla n|}{B|\nabla n|} \quad ,$$

$$\alpha_1 = \frac{T_i |\nabla n|}{m_i \omega_{ci} n} \quad .$$

In view of (13), as a lower bound on the anomalous diffusion coefficient D, we have

$$D = D^* \quad , \quad \alpha_0 < \alpha_1 \tag{14a}$$

$$D = 0 \quad , \quad \alpha_0 > \alpha_1 \quad . \tag{14b}$$

As un upper bound on D, we have

$$D = D^* \quad , \quad \alpha_0 < \alpha_1 \tag{15a}$$

$$D = D^*(\alpha_1/\alpha_0)^2 \quad , \quad \alpha_0 > \alpha_1 \tag{15b}$$

7. OBSERVATIONAL ASPECTS OF DRIFT-DISSIPATIVE MODES

7.1 ESTIMATION OF THE VARIANCE DUE TO DRIFT-DISSIPATIVE MODES

The variance is related to an integral over the power spectral density. The contribution to this integral from drift-dissipative modes is likely to be almost directly proportional to a second integral for the root mean square of the density gradient due to drift-dissipative modes. Since the second integral can be estimated by physical arguments, a plausible estimate is possible for the variance, even though the power spectral density is not known in detail.

We employ the definitions[13]

$$\phi_N(k_x,k_y) = \frac{1}{4\pi^2 XY} \left\langle \left| \int_0^x dx \int_0^y dy\, e^{ik_x x + ik_y y}\, N(x,y) \right|^2 \right\rangle$$

for the 2-D power spectral density and

$$\sigma_{ND}^2 = \int_{-\infty}^{\infty}\int_{-\infty}^{\infty} \phi_N(k_x,k_y)\, dk_x\, dk_y$$

for the variance.

First, represent the drift-dissipative mode as a single mode which varies harmonically in the y-direction. We have

$$N(x,y) = n_1(k_y')\, e^{-ik_y' y - K_x |x|} \quad . \tag{16}$$

Define

$$f = \int_0^x dx \int_0^y dy\, e^{ik_x x + ik_y y}\, N(x,y) \quad .$$

After some algebra, we have

$$|f|^2 = Y^2 |n_1(k_y')|^2 \frac{4K_x^2}{\left(K_x^2 + k_x^2\right)^2}\, \delta_{ky,ky'}$$

and

$$\phi_N(k_x,k_y) = |f|^2/(4\pi^2 XY) \quad .$$

This results in

$$\sigma_{ND}^2 = \frac{|n_1(k_y')|^2}{k_x X} \quad .$$

For purposes of estimates on using Eq. (5), we have

$$|n_1(k_y')| \simeq \frac{n_0}{k_x L_\perp}$$

where

$L_\perp$ = gradient scale length for region where mode is located,

and, as noted in Section 5,

$$K_x = (\rho_i L_\perp)^{-\frac{1}{2}} \quad .$$

Then,

$$\sigma_{ND}^2 = \frac{n_0^2}{K_x^2 L_\perp^2} \frac{1}{K_x X} = n_0^2 \frac{\rho_i^{3/2}}{L_\perp^{\frac{1}{2}} X} \quad .$$

If we identify X with an outer-scale length L_0 (possibly a rod radius, assuming striations to be rods of enhanced density in the plane $\perp\vec{B}$), a plausible limitation for $L_\perp$ is

$$4\rho_i < L_\perp < L_0 \quad .$$

Hence,

$$n_0^2 \frac{\rho_i^{3/2}}{L_0^{3/2}} < \sigma_{ND}^2 < \frac{n_0^2 \rho_i^{3/2}}{2\rho_i^{\frac{1}{2}} L_0} \quad .$$

As examples, for $L_0 = 4 \times 10^4$ cm, $\rho_i = 4 \times 10^2$ cm:

$$n_0^2\, 10^{-3} < \sigma_{ND}^2 < n_0^2\, 5 \times 10^{-3}$$

and for $L_0 = 2 \times 10^6$ cm, $\rho_i = 4 \times 10^2$ cm:

$$n_0^2\, 3 \times 10^{-6} < \sigma_{ND}^2 < n_0^2\, 10^{-4} \quad .$$

7.2 MODIFICATION FOR DRIFT WAVE REPRESENTATION AS A SERIES OF k_y MODES

We now let

$$N(x,y) = \sum_{k_y'} n_1(k_y')\, e^{-ik_y'y - K_x|x| + i\phi(k_y')} \quad .$$

Stabilization is expected when

$$\nabla N \simeq n_0/L_\perp \quad .$$

We estimate

$$\nabla N = \left(\left| \nabla \sum_{k_y'} n_1(k_y')\, e^{-ik_y'y - K_x|x| + i\phi(k_y')} \right|^2 \right)^{\frac{1}{2}} \quad .$$

If there is no correlation between the various $\phi(k_y')$, then at $|x| = 0$

$$\nabla N \simeq \left(\sum_{k_y'} |n_1(k_y')|^2\, K_x^2 \right)^{\frac{1}{2}} \quad .$$

If K_x does not vary significantly over k_y', as seems reasonable for drift-dissipative modes, then

$$\sum_{k_y'} |n_1(k_y')|^2 \simeq \frac{n_0^2}{L_\perp^2\, K_x^2} \quad .$$

In parallel with the single-mode calculation,

$$f = \sum_{k_y'} Y\, n_1(k_y')\, e^{-i\phi(k_y')}\, \frac{2K_x}{K_x^2 + k_x^2}\, \delta_{k_y, k_y'}$$

and

$$\sigma_N^2 = \frac{1}{K_X X} \sum_{k_y'} |n_1(k_y')|^2 \simeq \frac{1}{K_X X} \frac{n_0^2}{K_x^2 L_\perp^2} \quad .$$

This is the same expression as for the single-mode case, so that the same numerical estimates apply.

7.3 ESTIMATE OF THE MAXIMUM PSD

It is reasonable to assume that the maximum in the PSD due to drift waves is peaked at $k_{x,m}$ and $k_{y,m}$ corresponding to the modal parameters for the maximum linear growth rate, and that the variance can be calculated by assuming that the maximum is roughly constant over two regions of range $\Delta k_x \simeq 2k_{x,m}$, $\Delta k_y \simeq k_{y,m}$ with negligible contribution beyond.

Then,

$$\phi_N(k_{x,m},k_{y,m})\ 4k_{x,m}\ k_{y,m} \simeq \sigma_N^2$$

or using $k_{x,m} = k_x = (\rho_i L_\perp)^{-\frac{1}{2}}$, $k_{y,m} = .4/\rho_i$, results in

$$\phi_N\left[(\rho_i L_\perp)^{-\frac{1}{2}},\ .4/\rho_i\right] \simeq .6\ n_0^2\ \rho_i^3/X \quad . \tag{17}$$

This result can be compared against the two-dimensional form[14] of the isotropic power spectral density evaluated at $(k_{x,m},k_{y,m})$ for a spectrum which in one-dimension varies as k^{-2}:

$$\phi(k_x,k_y) = \frac{4\pi^{\frac{1}{2}}\ \overline{\Delta n^2}\ \Gamma(3/2)\ L^{-1}}{4\pi^2(L^{-2} + k_x^2 + k_y^2)^{3/2}} \quad . \tag{18}$$

(Here and below, we have used the results of Ref. (14) for ϕ, multiplied by an additional factor $(4\pi^2)^{-1}$ in order to preserve

$$\int\phi(k_x,k_y)\ dk_x\ dk_y = \overline{\Delta n^2} \quad .)$$

For $\rho_i/L_\perp \simeq .16$ and $\overline{\Delta n^2} = n_0^2/4$,

$$\phi(k_x,k_y) \simeq .22\ n_0^2\ \rho_i^3/L \quad . \tag{19}$$

For $\rho_i/L \ll .16$ and $\overline{\Delta n^2} = n_0^2/4$,

$$\phi(k_x,k_y) \simeq .6\, n_0^2\, \rho_i^3/L \quad . \tag{20}$$

By way of comparison, the contribution from a cylindrical rod of radius L in the limit $(k_x^2 + k_y^2)^{\frac{1}{2}} L \gg 1$, taking the average over rapidly varying phases, is about 0.72 of (18) in the same limit

7.4 OBSERVABILITY OF THE DRIFT WAVE PSD THROUGH IN-SITU MEASUREMENT

Comparison of (17) with (19) or (20) indicates the possibility of detection of drift waves against the 2-D equivalent of a 1-D k^{-2} background. One has

$$\frac{n_0^2}{4\overline{\Delta n^2}} \lesssim \frac{\phi_D(k_{x,m},k_{y,m})}{\phi_{\nu=2}(k_{x,m},k_{y,m})} \lesssim \frac{2.5\, n_0^2}{4\overline{\Delta n^2}} \tag{21}$$

where ϕ_D denotes the theoretically estimated PSD contribution from drift-dissipative modes and $\phi_{\nu=2}$ denotes the contribution from the 2-D counterpart of a 1-D k^{-2} PSD.

Comparison (21) is appropriate to the detectability of drift waves through in-situ measurement. To see this, assume a probe moving in the x_1-direction and no variation in the x_3-direction. The measured Fourier component is

$$\tilde{n}_1(k_{1,0}) = \frac{1}{X_2} \int n(x_1,x_2)\, e^{-ik_1x_1}\, dx_2\, dx_1 \tag{22}$$

(where we have averaged over the x_2-direction), and the spectral density is

$$\phi_{N1}(k_{1,0}) \propto |\tilde{n}_1(k_{1,0})|^2$$

where the subscript 1 refers to the x_1,x_2 coordinate axes. If the x_1 axis makes an angle θ with the x-axis of our previous analysis, then

$$\phi_{N1}(k_{1,0}) = \phi_N(k_1 \cos\theta, k_1 \sin\theta) \quad .$$

Hence, a peak in the 2-D PSD could be observable provided $k_{mx} \simeq k_1 \cos\theta$, $k_{my} \simeq k_1 \sin\theta$. There are three caveats:

1. For $k_{my} >> k_{mx}$, the range of θ with appreciable drift mode contributions will be small, if in addition the various (localized) regions with drift waves are not randomly oriented.

2. The quantity $\phi_{N1}(k1,0)$ or $\phi_N(k_{xm},k_{ym})$ is an average. A single rod of radius L can (within a factor of order unity) account for a 1-D PSD of form k^{-2} with outer-scale length L. If the drift waves are found only on the edges of a small number of large rods, one could have an observation pattern in which most measurements showed no contribution with an occasional very large contribution.

3. Even if $\phi_D(k_{xm},k_{ym})/\phi_{\nu=2} < 1$, the anomalous diffusion coefficient could still be much larger than the coulomb diffusion coefficient.

7.5 OBSERVABILITY OF THE DRIFT WAVE PSD THROUGH SCINTILLATION MEASUREMENT

We now consider the contribution of the theoretically derived drift-dissipative waves to scintillation, especially as a diagnostic of drift wave behavior for the correlation functions of the log amplitude and the phase fluctuations in the Rytov approximation.

Paraphrasing Ref. (2), one has respectively:

$$\overline{\chi(x_1)\,\chi(x_1+\rho)} = k^2 \int_{-\infty}^{\infty} \frac{dk_1}{2\pi} \int_0^{x_s} dz\, \sin^2\left[\frac{k_1^2}{2k}(x_{2s}+x_{2g}-x_2)\right]\phi_2(x_2,k_1)\,\exp(kl_1\rho) \tag{23}$$

$$\overline{\phi_s(x_1)\,\phi_s(x_1+\rho)} = k^2 \int_{-\infty}^{\infty} \frac{dk_1}{2} \int_0^{x_s} dz\, \cos^2\left[\frac{k_1^2}{2k}(x_{2s}+x_{2g}-x_2)\right]\phi_2(x_2,k_1)\,\exp(ik_1\rho) \tag{24}$$

where

k = rf wave number

x_2 = coordinate along propagation line of sight

x_1 = coordinate perpendicular to line of sight

x_{2s} = turbulent layer thickness

x_{2g} = distance from bottom of turbulent layer to receiver

The turbulent layer has no variation in the third direction (parallel to the magnetic field).

In Eqs. (23) and (24),

$$\phi_2(x_2,k_1) = \frac{|\Delta n_i(k_1,k_2 = 0)|^2}{X_1\ X_2} = 4\pi^2\ \phi(k_1,0)\ \alpha^2$$

where Δn_i is the deviation of the index of refraction from its mean, ϕ is the 2-D density PSD, and α^2 is the proportionality constant between density variation and index of refraction variation. For $\omega >> \omega_p$ (with ω_p the electron plasma frequency), $\alpha = 4\pi e^2/(m_e\omega^2)$.

For drift waves with $k_{ym} \gtrsim k_{xm}$, a necessary condition for scintillation contribution from a given in-situ $\vec{k}$, typified by (k_{xm},k_{ym}) is $e_2 \cdot \vec{k} = 0$, where e_2 is the unit vector in the x_2-direction. Therefore, drift waves contribute to scintillation only if the magnitude of the angle θ of rf-wave propagation with respect to the x-direction (i.e., the direction of the background density gradient projected perpendicular to the ambient magnetic field) is less than θ^* where $\theta^* = \tan^{-1}(k_{xm},k_{ym})$. The range in magnitude for contributing k_1 is k_{ym}. Hence, (with e_x, the unit vector in the x-direction) from Eqs. (17) and (25),

$$\phi_2(x_2,k_1) = \frac{.6\ n_0^2\ \rho_i^2}{X}\ 4\pi^2\alpha^2 \quad , \quad \frac{.2}{\rho_i} < k_1 < \frac{.6}{\rho_i} \quad , \tag{26}$$

$$\cos^{-1}(k_2\cdot e_x/|k_2|) < \tan^{-1}(k_{xm}/k_{ym}) \quad ,$$

$$\phi_2(x_2,k_1) = 0 \text{ otherwise.} \tag{27}$$

Denote drift wave contributions by the subscript D and power law contributions from a 2-D k^{-3} PSD by the subscript P. For

$$x_{2s} + x_{2g}/x^2 < k < (x_{2s} + x_{2g})(.08)/\rho_i^2 \tag{28}$$

from Eqs. (23) and (24), we have

$$\overline{X_D^2}(x_1)/\overline{X_p^2}(x_1) > \overline{\phi_D^2}(x_1)/\overline{\phi_p^2}(x_1) \quad .$$

Given Eqs. (23), (26), and (28),

$$\overline{\chi_D^2}(x_1) = 2.38 \times 10^2 \left(\frac{e^2}{mc^2}\right)^2 \frac{n_0^2 \rho_i^2 X_{2s}}{k^2 X} \quad .$$

From Eq. (24a) of Ref. (14) for $x_{2g} \gtrsim x_{2s}$,

$$\chi_p^2(x_1) \simeq 3.62 \times 10^1 \left(\frac{e^2}{mc^2}\right)^2 \overline{\Delta n^2} \frac{x_{2g} x_{2s}}{k^3 X} \quad .$$

Therefore, the condition for drift wave dominance is

$$k \geq k^* = \frac{x_{2g}}{6.57} \frac{\overline{\Delta n^2}}{n_0^2} \frac{1}{\rho_i^2} \quad . \tag{29}$$

The maximum value of $\overline{\chi_D^2}(x_1)$, with Eq. (29) satisfied, occurs with $k = k^*$. Then,

$$\chi_D^2(x_1) = 1.0 \times 10^4 \left(\frac{e^2}{mc^2}\right)^2 \frac{n_0^6}{(\overline{\Delta n^2})^2} \rho_i^6 \frac{X_{2s}}{X x_{2g}^2} \quad .$$

As an example, using the data of Ref. (15) (e.g., $n_0 = 6 \times 10^5$ cm^{-3}, $\overline{\Delta n^2} = 3.6 \times 10^9$ cm^{-6}, $\rho_i = 3.35 \times 10^2$ cm, $X_{2s} = 2 \times 10^7$ cm, $X_{2g} = 3 \times 10^7$ cm, $x = 2. \times 10^6$ cm), one has:

$$k^* = .41 \text{ cm}^{-1}$$

$$\overline{\chi_D^2}(x_1) = 4.6 \times 10^{-5} \quad .$$

Hence, there can be rather stringent conditions on the observability of drift waves by scintillation.

7.6 ESTIMATE OF DECAY OF THE PRIMARY (LARGE WAVELENGTH) VARIANCE IN TERMS OF THE DRIFT WAVE VARIANCE

It is clear that Eq. (8) applies for a diffusion coefficient $D_\perp$ due to drift-dissipative modes. On using Eqs. (5) and (7), Eq. (8) becomes

$$\frac{\partial}{\partial t} \int n^2 \, dV = -2 \int \left\langle \frac{\gamma}{k_x^2} \right\rangle k_x^2 n_1^2 \, dV \quad ,$$

where the right-hand side of the equation is due to drift wave contributions. On neglecting variations in k_x, we have

$$\frac{\partial \sigma_N^2}{\partial t} = -2 \langle \gamma \rangle \sigma_{ND}^2$$

where σ_N^2 is the larger wavelength, non-drift wave variance and σ_{ND}^2 is the drift wave variance. Hence, for a time scale Δt for decay of σ_N^2, we have

$$\Delta t \simeq \frac{1}{2} \frac{\sigma_N^2}{\sigma_{ND}^2} \frac{L_\perp(\text{cm})}{8.6 \times 10^3} \quad \text{sec} \quad .$$

Here, $L_\perp$ is the scale length for density variation in the region where drift waves are found.

We caution that Eq. (30) is equivalent to a time derivative evaluated at $t = 0$. Variations in σ_{ND}^2 and $\langle \gamma \rangle$ with increasing time will affect the time for σ_N^2 to decrease a given non-infinitessimal amount.

8. DISCUSSION OF EXPERIMENTAL DATA WITH RESPECT TO DRIFT WAVES AND DIFFUSION

8.1 BUARO

The BUARO barium plasma injection experiment conducted by Group J-10 of the Los Alamos Scientific Laboratory in June 1976 provides some data which may be directly relevant to drift mode diffusion of striations. Figure 6 of the Quick-Look Report,[16] (our Figure 25), ranges from about 250 km in altitude (bottom of photograph) to 400 km in altitude (top of photograph). The striations are oriented along the magnetic field lines which make an angle of about 45° with the vertical. It would appear that the cloud is optically thin especially at its higher altitudes. The photograph, taken at 810 seconds after the injection, indicates more diffuse structure at higher altitudes in that the gaps between striations at lower altitudes appear to fill in at higher altitudes. More quantitative measurements bear this out.[17]

We consider the possibility that the diffusion at higher altitudes is due to drift-dissipative modes which are not as strongly unstable at lower altitudes. Using a CIRA Model 2 atmosphere at 4 AM[18] the neutral number densities at 250 km and 400 km are approximately 10^9 cm^{-3} and 2×10^7 cm^{-3}. The barium ion column density has been estimated at about 8×10^{11} cm^{-2},[17] leading to a representative barium ion density of about 8×10^4 cm^{-3}. The column density of ambient ionization is roughly the same. We choose ion and electron temperatures of 0.1 and 0.2 eV, respectively. These values are somewhat arbitrary and will be discussed below. Since the barium photoelectrons are emitted with an energy of order 0.6 eV and since the barium ions can have an energy of order 1.5 eV it is reasonable to choose temperatures above the ambient neutral temperature of 0.07 eV.

Results for the diffusion coefficient as a function of L for barium are shown in Fig. (22) for $n = 10^5$ and n_n the neutral density, equal to 10^6 through 10^{10} with a scale length parallel to the magnetic field of 100 km.

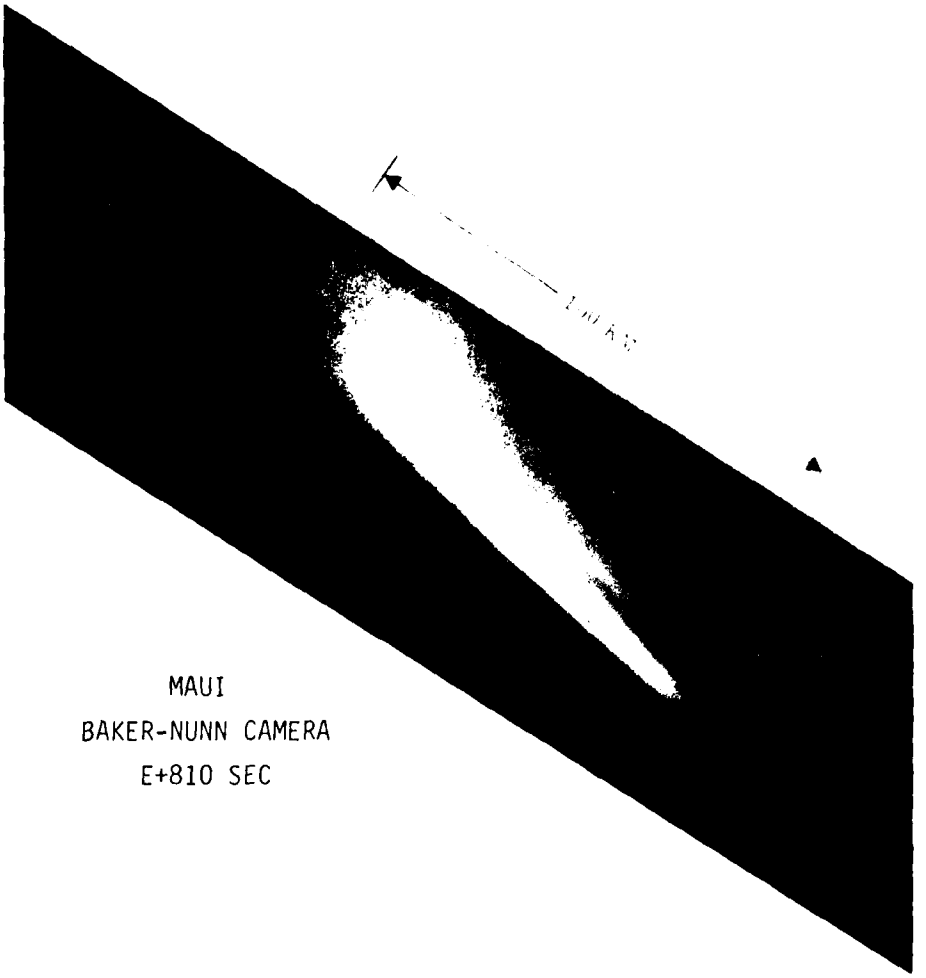

Figure 25. View of BUARO at 810 sec after release. The release extends in altitude from about 250 to 400 km.

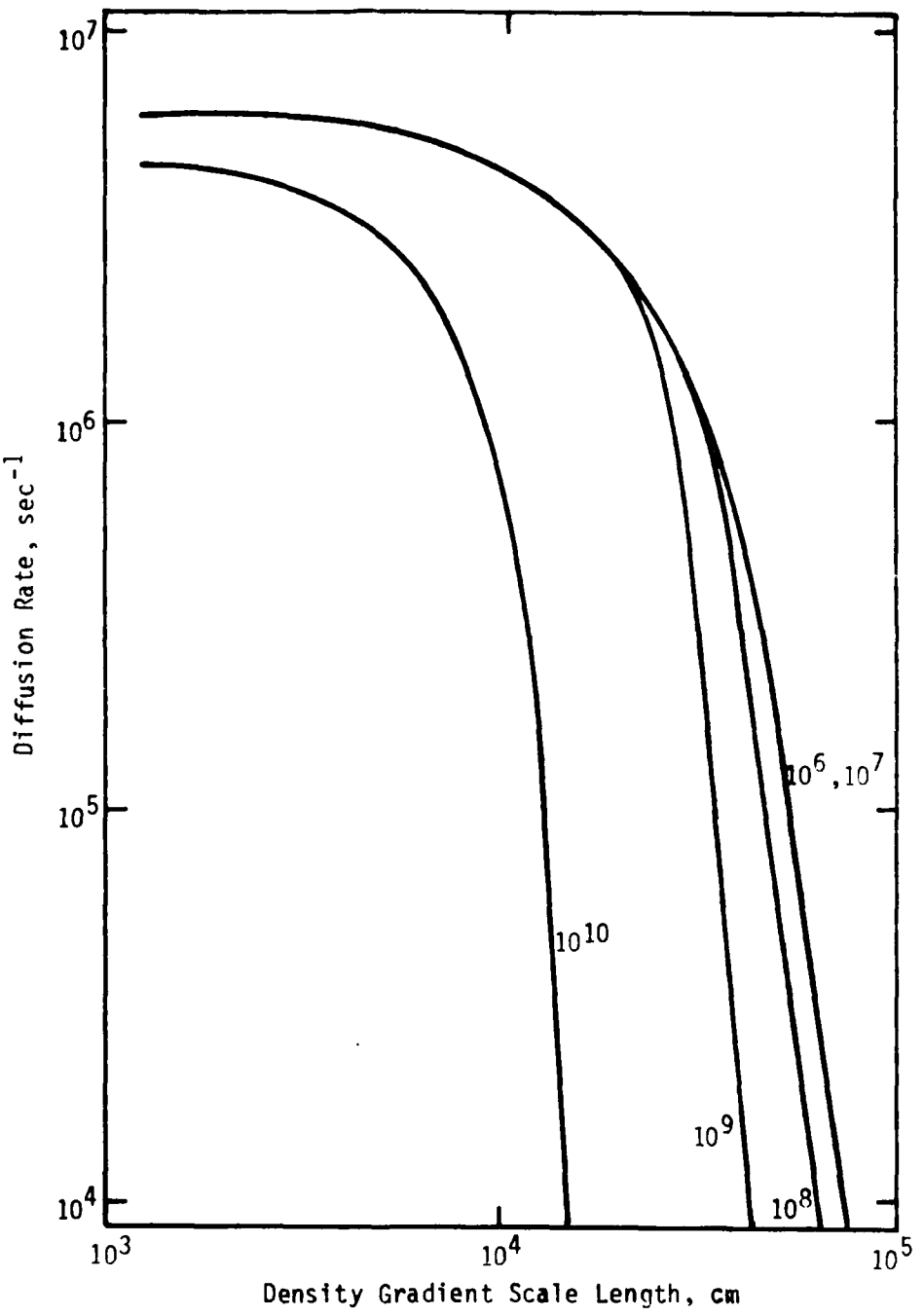

Figure 26. Plot of diffusion coefficient (in cm^2/sec) vs L_p (in cm) for single ionized barium ions. $n = 10^5\ cm^{-3}$, $T_i = 0.1$ eV, $L_z = 10^7$ cm, B = 0.35 gauss.

The suppression of diffusion for $n_n = 10^{10}$ and $L_\perp > 0.1$ km when compared to $n_n \leq 10^9$ is qualitatively in keeping with the possibility that drift dissipative modes are suppressed at lower altitudes for the BUARO release (although the actual densities at 250 km and 400 km in the release are 10^9 and 2×10^7 cm^{-3} respectively). For $n_n \leq 10^9$ cm^{-3}, the diffusion coefficients, $D_\perp$, as calculated are somewhat below 10^7 cm^2/sec and the region with $D_\perp > 10^6$ cm^2/sec extends up to $L_\perp = 0.3$ km. Thus for $n_n \leq 10^9$ cm^{-3} as contrasted to $n_n = 10^{10}$ cm^{-3}, over a time of 1000 seconds the calculations indicate significant diffusion for scale lengths in the 0.1 - 0.5 km range.

We note however that diffusion if it affects the barium cloud features is more likely to be in the 1.0 - 5.0 range.

The comparison is of course only semi-quantitative. An increase in the barium ion on neutral collision frequency of a factor of three would, roughly speaking, lower the neutral density appropriate to each contour by a factor of three. The values of the diffusion coefficient would be increased by larger temperatures and possibly by more accurate eigenmode calculations, especially of k_x. Since the ion dynamics of the modes is primarily in the perpendicular direction, any noise with wavelength primarily parallel to the magnetic field could act to increase the electron collision frequency without similarly increasing the ion collision frequency. With the background parameters we use this would encourage growth.

Further differentiation between growth at higher and lower altitudes would occur if there is significant barium ion temperature variation as a function of altitude. Barium ions can lose energy through collisions with atomic oxygen ions (time scale of 35 seconds with ionized oxygen density of 10^5 cm^{-3}). The oxygen ions can then engage in resonance charge exchange[17a] with oxygen atoms (time scale of about 5 sec at 300 km, and about 50 sec at 400 km). Hence assuming an e-folding time for barium temperature decay of 85 sec at 400 km altitude it would appear that barium ion temperatures of greater than 0.2 eV can exist there for a time of order several hundred seconds. The temperature loss process would be slower if any appreciable fraction of ambient oxygen ions recombined with explosion byproducts.

8.2 STRESS

Data from the rocket probe experiments for STRESS exhibits high frequency behavior, specifically a peak in $(\Delta n_{RMS}/n)$ as a function of frequency.

(Here Δn_{RMS} is the root mean square ionized density irregularity amplitude.) Together with other rocket parameters, data for the peak can be summarized as:

		Rocket Velocity	
Event	Frequency	Perpendicular to B	Parallel to B
Esther	$\approx 900\ sec^{-1}$	0.8 km/sec	1.04 km/sec
Fern	$\approx 1200\ sec^{-1}$	0.26 km/sec	1.34 km/sec

The peak is observed prior to entering the barium cloud (Case A) (our Fig. 27a, Fig. 6.1 of Ref. 19), and while in the barium cloud but not in the striated region (Case B) (our Fig. 27b, Fig. 6.3 of Ref. 19). For the barium cloud striated region there is a flat region of $(\Delta n_{RMS}/n)$ from about 10^2 Hz up to the frequency designating the peaks, then a sharp drop above the peak frequency (Case C) (our Fig. 27c, Fig. 6.7 of Ref. 19). The value of $(\Delta n_{RMS}/n)$ appears appreciably higher outside of the barium cloud than in the striated region of the barium cloud.

It is likely that the peak in $(\Delta n_{RMS}/n)$ represents density fluctuations parallel to the magnetic field. For fluctuations parallel to B the wavelength is given by

$$\frac{\text{rocket velocity parallel to B}}{\text{frequency}} .$$

For fluctuations perpendicular to B the wavelength is given by

$$\frac{\text{rocket velocity perpendicular to B}}{\text{frequency}} .$$

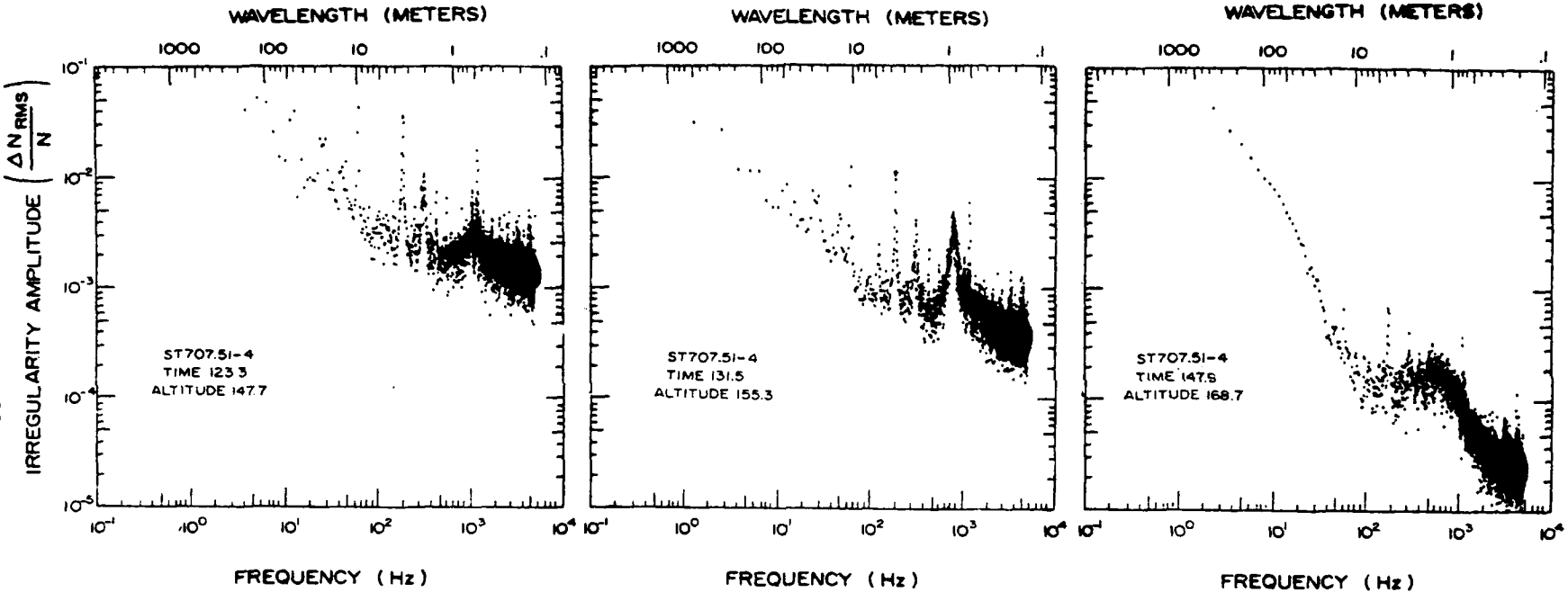

a. Prior to Entering the Barium Cloud

b. In an Unstriated Region of the Barium Cloud

c. In a Striated Region of the Barium Cloud

Figure 27. Irregularity Amplitude vs Frequency for the Esther Release of Project Stress as Measured by Probe Rocket at Release Plus 46 Minutes.

If the density fluctuation is parallel to B the wavelength is about 1.1 meter for both Esther and Fern. If the density fluctuation is perpendicular to B it is about 0.9 meter for Esther and 0.2 meter for Fern. Hence if the wave has the same wavelength in both cases it is parallel to B.

Further, the value of $(\Delta n_{RMS}/n)$ appears to decrease within the striated region compared to either of the other two regions. From Figure (5.3) of Ref. 9, it would not be surprising if Δn in the range of 10^2-10^3 Hz were roughly the same for Figures 27a and 27c. For modes dependent on density gradients, one would expect $(\Delta n_{RMS}/n)$, if anything, to increase the striated regions, since the density gradients are larger there. In addition, for the altitudes ($\simeq$ 170 km) and density ($n_e > 10^6$ cm^{-3}) of the Project Stress barium clouds, theoretically we do not expect short wavelength drift wave phenomena to be significant.

These considerations lead us to believe that the high frequency disturbances are not related to drift mode diffusion perpendicular to the magnetic field. The difference between Cases B and C is suggestive of nonlinear plasma behavior. The existence of density scale lengths of order 15 meters[19] is consistent with the absence of diffusive instabilities on the sides of striations as expected theoretically at these altitudes and densities.

8.3 THREE METER BACKSCATTER

Backscatter by 3 meter irregularities moving vertically with vertical k vector is frequently observed in Equatorial Spread F.[20] One possible explanation for this phenomenon is that the 3 meter disturbance is either an unstable drift-dissipative mode or is driven by somewhat larger wavelength unstable drift-dissipative modes. The proposed geometry is shown in Figure 28. Along the sides of the depleted region there may be a background electric field, E_x, in the direction of the density gradient.[21]

In this subsection we treat the connection between drift-dissipative modes at 3 meter wavelengths and the power spectral density at longer wavelengths, which would be expected to dominate the contributions to anomalous diffusion. A power law fall-off for the 1D PSD of the form $k^{-\nu}$, $\nu = 7$ would be required to link both the theoretically calculated PSD at $k_y = 0.4/\rho_i$ and the observed PSD at $k_y = 2.1 \times 10^{-2}$ cm.

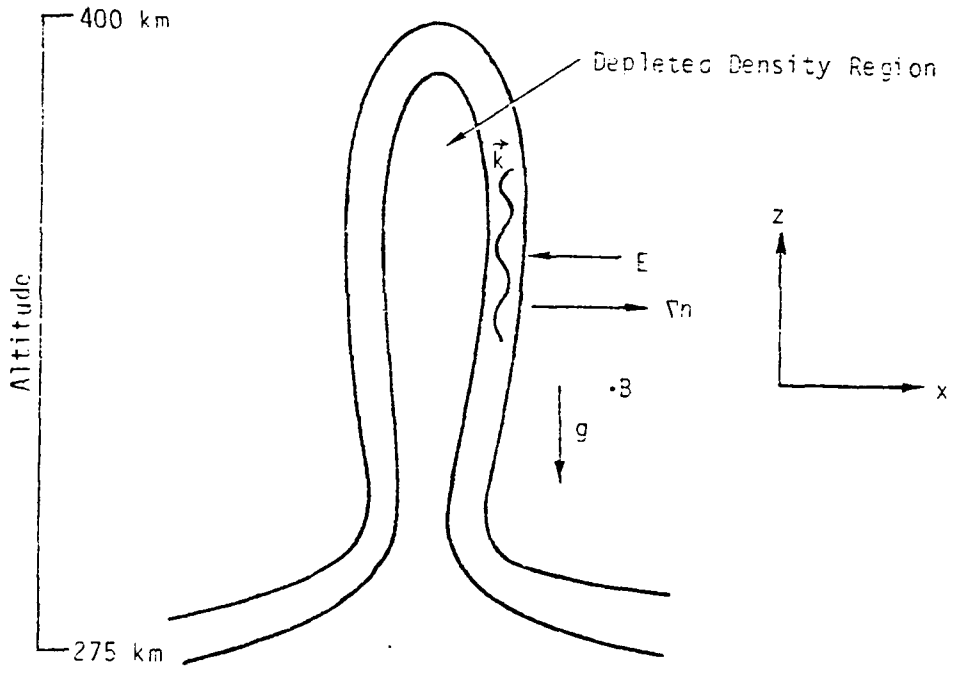

Figure 28. Schematic geometry for drift-dissipative explanation for 3 meter backscatter. (Wavelength of mode not to scale.)

We first present a detailed treatment of backscatter contributions from power law power spectral density, then determine the power law variation, and then present some discussion (based on other theoretical calculations) of factors which would work in the direction of a rapid fall-off of the PSD with increasing $\vec{k}$.

The formula for the Poynting flux from backscatter is:

$$\langle S(r)\rangle = \frac{c}{8\pi}\left(\frac{k^2}{4\pi}\right)^2 \mathrm{Re}\int_V\int_V n(r')|A_o(r')|^2 \sin^2\chi(r')\, B_\varepsilon(r',r'')$$

$$\times\{\exp ik[|r - r'| - |r - r''| + |R - r'| - |R - r''|]\}$$

All quantities are as defined in Tatarskii.[22] For our purposes it is sufficient to specify

$$B_\varepsilon(r',r'') = \varepsilon_1(r')\,\varepsilon_1(r'')$$

where ε_1 is the dielectric constant. Further for $\omega \geq 2\omega_{pe}$ (with ω_{pe} the electron plasma frequency)

$$\varepsilon_1(r') = (-)\frac{4\pi e^2}{\omega^2 m}\sum_i \delta(r' - r_i) \tag{31}$$

with i the sum over electrons. We note

$$\sum_i \delta(r' - r_i)\, d_3r = n(r')\, d_3r$$

with n the electron density

Using (31) we may write:

$$\varepsilon_1(r')\varepsilon_1(r'') = \left(\frac{4\pi e^2}{\omega^2 m}\right)^2\left[\sum_i\sum_{i'\neq i}\delta(r' - r_i)\delta(r'' - r_i') + \sum_i\sum_{i'\neq i}\delta(r' - r_i)\delta(r'' - r_i')\right]$$

The first double summation is the contribution from incoherent backscatter; the second double summation is the contribution from coherent backscatter. Hence the ratio of coherent backscatter to incoherent backscatter is $I_2(k)/I_1(k)$ where:

$$I_2(k) = \iint_V\int_V \sum_i\sum_{i'\neq i}\delta(r' - r_i)\delta(r'' - r_i)\exp\{ik[|r - r'| - |r - r''|$$

$$+ |R - r'| - |R - r''|]\} \, d_3r' \, d_3r'' \quad ,$$

$$I_1(k) = \iint_V \sum_i \delta(r' - r_i)\delta(r'' - r_i) \exp\{ik[|r - r'| - |r - r''|$$

$$+ |R - r'| - |R - r''|]\} \, d_3r' \, d_3r'' \quad .$$

to within about a factor of 2 accuracy:[23,24]

$$I_1(k) = n \int_V d_3r'$$

where V is the backscatter volume. For backscatter at $k_y = k_1$:

$$I_2 = \frac{1}{(2\pi)^2} \int\int |\tilde{n}(k_x - 2k_1, k_z)|^2 \, e^{ik_z x - ik_i x^2/r} \, e^{ik_z z - (ik_i/r)z^2} \, dk_x dx dk_z dz \tag{32}$$

with

$$\tilde{n}(\vec{k}) = \int_V n \, e^{-ik\cdot r} \, d_3r \quad .$$

[r is the distance from the scattering volume to the receiver (sender).]

For a power law, power spectral density with variance $\langle \delta n \rangle^2$ and 1D power spectral density varying as $k^{-\nu}$, we have[14]:

$$|\tilde{n}(k_x, k_y, k_z)|^2 = \frac{\Delta}{\varepsilon} \frac{1}{(L^{-2} + k_x^2 + k_y^2 + k_z^2/\varepsilon^2)^{\nu/2+1}} \tag{33}$$

with

$$\Delta = \frac{\langle \delta n \rangle^2 \, V \, 2\Gamma(\nu/2 + 1)(2\pi)^3}{4\pi \, L^{\nu-1} \, \Gamma(3/2) \, \Gamma[(\nu - 1)/2]} \quad . \tag{34}$$

(z is the direction of the magnetic field with anisotropy parameterized by ε.) The normalization for $|\tilde{n}|^2$ follows from the constraint

$$\int |\tilde{n}(\vec{k})|^2 \, d_3k = (2\pi)^3 \int n^2(\vec{r}) \, d_z\vec{r} = V(2\pi)^3 \langle \delta n \rangle^2 \quad .$$

We define z* to be the spatial extent of the scattering volume in the z-direction. Then three convenient limits obtain from Eqs. (32) and (33):

Case 1 $\quad z^* \ll \frac{1}{k_1 \varepsilon}$, $\sqrt{\frac{2k_1}{\pi r}}\, z^* \ll 1$;

$$I_2(k_1) = \frac{1}{2\pi}\,\Delta\,\frac{1}{[1/L^2 + (2k_1)^2]^{(\nu/2)+(1/2)}}\,\frac{1}{2}\,\frac{\Gamma(1/2)\,\Gamma[(\nu+1)/2]}{\Gamma[(\nu/2)+1]}\,2z^* \tag{35}$$

Case 2 $\quad z^* \ll \frac{1}{k_1 \varepsilon}$, $\sqrt{\frac{2k_1}{\pi r}}\, z^* \gg 1$;

$$I_2(k_1) = \frac{1}{2\pi}\,\Delta\,\frac{1}{[1/L^2 + (2k_1)^2]^{(\nu/2)+(1/2)}}\,\frac{1}{2}\,\frac{\Gamma(1/2)\,\Gamma[(\nu+1)/2]}{\Gamma[(\nu/2)+1]}\,\sqrt{\frac{\pi r}{2k_1}} \tag{36}$$

Case 3 $\quad z^* \gg \frac{1}{k_1 \varepsilon}$

$$I_2(k_1) = \frac{\Delta}{\varepsilon}\,\frac{1}{[1/L^2 + (2k_1)^2]^{(\nu/2)+1\ 2}}\ . \tag{37}$$

Woodman and Basu[15] have examined the compatibility of a one-dimensional power spectral density with $\nu = 2$ and the observed ratio:

$$\log \frac{I_2(k)}{I_1(k)} \simeq 40 \text{ db} \quad , \qquad k = 2k_1 = 2.09 \times 10^{-2} \text{ cm}^{-1} \ . \tag{38}$$

In the interest of clarity, we repeat the evaluation of $\log[I_2(k)/I_1(k)]$ using their experimentally determined values: $L = 2 \times 10^6$ cm, $\delta n = 6 \times 10^4$ cm^{-3}, $n = 6 \times 10^5$ cm^{-3}, $\rho_i = 3.35 \times 10^2$ cm.

If one associates the 3 meter behavior with drift-dissipative modes, by our numerical calculations the most unstable k_z at $k_y = 1.04 \times 10^{-2}$ cm, $n = 10^5$ cm^{-3}, $n_n = 10^8$ cm^{-3} is $k_z \simeq 10^{-5}$ cm^{-1}. One then has

$$\frac{1}{\varepsilon} \simeq \frac{k_y}{k_z} \simeq 10^3 \ .$$

Then from "Case 3" with $\nu = 2$ we obtain

$$\log\left(\frac{I_2}{I_1}\right) = 84 \text{ db} \ . \tag{39}$$

This compares with the previously estimated[15] value of 82 db. Thus is appears likely that the $\nu = 2$ spectrum does not persist down to backscatter wavelengths.

Alternately one can ask for the value of ν consistent with the theoretical drift-dissipative wave estimate of Eq. (17) at $k_y = 0.4/\rho_i$ and with the experimental observation of Eq. (39) at $k_y = 2k_1 = 2.1 \times 10^{-2}$ cm^{-1}.

Experimentally, using (37) and (38):

$$I_2(k_1) \simeq \frac{\Delta}{\varepsilon} \frac{1}{(2k_1)^{\nu+2}} = 10^4 \, n_o V \quad . \tag{40}$$

Let us assume that $\phi_N(k_{xm},k_{ym})$, as given by (17), and the three meter backscatter behavior are linked by the same power law.

On using (17), (33) and (34) we obtain:

$$\phi_N(k_{xm},k_{ym}) = \frac{\langle \delta n \rangle^2 \, (\nu - 1)}{4\pi \, L^{\nu-1}} \frac{1}{\left(L^{-2} + k_{xm}^2 + k_{ym}^2\right)^{(\nu/2)+(1/2)}} = 0.6 \, n_o^2 \rho_i^3 L^{-1} \quad . \tag{41}$$

On using (41) to eliminate $\langle \delta n \rangle^2 / L^{\nu-1}$ in Δ in (40) and taking $L^{-2} \ll k_{xm}^2 + k_{ym}^2$, we obtain for $k_{xm} = k_{ym} = 0.4/\rho_i$, $\nu \simeq 7.3$ and for $k_{xm} = 0$, $k_{ym} = 0.4/\rho_i$, $\nu \simeq 6.4$.

Hence the theoretically calculated PSD at k_{xm},k_{ym} is not necessarily inconsistent with the 3 meter observations but a very rapid fall-off with increasing k is required. Such behavior could occur if smaller values of n and/or L are required for instability to break out at short wavelengths.

Our numerical calculations with drift-dissipative modes tend to bear this out (although lower hybrid modes have not been examined in detail). The following observations are available for drift-dissipative modes (DDM):

1. At 3 meter wavelengths there is no instability from DDM for any $n \geq 10^4$ cm^{-3}, $10^6 \leq n_n \leq 10^{10}$ cm^{-3}, $L_\perp \geq 10^3$ cm for $T_e = T_i = 0.1$ eV, B = 0.35 g, $L_z = 10^7$ cm.

2. For wavelengths in the range 6-12 meters, there can be instability for $n \leq 10^5$ cm^{-3}, $n_n \leq 10^9$ cm^{-3}.

3. For the particular case of $n = 10^4$ cm^{-3}, $n_n = 10^8$ cm^{-3}: at 6 meters there is instability for $10^3 < L_\perp < 1.25 \times 10^4$, at 12 meters there is instability for $10^3 < L_\perp < 4.0 \times 10^4$ cm.

4. For the case of $n = 10^5$ cm^{-3}, $n_n = 10^8$ cm^{-3}: at 6 meters there is

stability, at 12 meters there is instability for $10^3 < L_\perp < 5.0 \times 10^3$ cm.

5. On the other hand, for DDM including all wavelengths with $k_y L_\perp > 1$, from Figures 3-7, one has for:

$n = 10^4$, $n_n = 10^8$, instability for $10^3 \leq L_\perp \leq 4.0 \times 10^4$

$n = 10^5$, $n_n = 10^8$, instability for $10^3 \leq L_\perp \leq 8.0 \times 10^4$

$n = 10^6$, $n_n = 10^8$, instability for $10^3 \leq L_\perp \leq 10^5$

On the basis of these calculations, it appears possible that stable DDM disturbances at 3 meters could be driven nonlinearly by unstable DDM at 6 meters, and that it would not be unreasonable for this to happen preferentially at lower background plasma densities (of order 10^4 cm^{-3} rather than 10^5 cm^{-3} or 10^6 cm^{-3}). Hence the very low PSD at 3 meters would result from the combination of factors:

1. The mode at 3 meters is stable.

2. The ambient density of the localized region in which the nonlinear driving takes place may be relatively low compared to the average ambient density (10^4 cm^{-3} vs 10^5-10^6).

3. If the ambient density is not relatively low compared to the average ambient density, then the volume occupied by regions of the then requisite high density gradients could be very small or non-existent.

As an additional aside we note that the presence of a range of excited k_y at the same altitude and time should result in Frequency Spread F.

9. CONCLUDING REMARKS

1. It appears possible that plasma turbulence involving modes other than the gradient drift, E × B mode[6] can contribute significantly to striation dynamics at high altitudes. The BUARO barium plasma release at 450 km altitude has a diffusion pattern which is qualitatively similar to that expected from drift-dissipative mode turbulence. Three meter backscatter in Equatorial Spread F can be explained as due to drift-dissipative modes [e.g., stable modes being driven by nearly (in $\vec{k}$ space) unstable modes]. In both cases other explanations are possible; however, the explanations involving drift dissipative modes have been followed through in some detail and within current observational and theoretical uncertainties appear to be consistent with the phenomena.

2. There are several aspects to the role of drift dissipative modes in diffusion and the power density spectrum.

At striation tips the outbreak of drift modes can effectively transfer fluctuations over a range in length scale typically from 0.5 km to 0.05 km. Drift-dissipative waves should furnish small scale diffusion of large scale density gradients and inhibit bifurcation, provided the maximum length scale of the modes producing diffusion is much smaller than the bifurcation wavelength, e.g., Eq. (10) is satisfied, and provided the resulting diffusion is sufficiently large to satisfy a criterion of the form of Eq. (9a) [or perhaps Eq. (9b)]. Since drift-dissipative wave diffusion itself is a sensitive function of $L_\perp$, bifurcation, in practice, will be limited by the smaller of the value of $L_\perp$ satisfying condition (11) or the value of $L_\perp$ (characteristically of order 0.5 km) for which D becomes sufficiently large to satisfy (9a). (This, of course, is based on the assumption $\nu_{in} >> \tau^{-1}$ where ν_{in} is the ion-neutral collision frequency and τ is the time scale for plasma velocity change.) The suppression of bifurcation does not necessarily prevent the outer scale length of a striation (= ℓ_0) from subsequently decreasing from additional plasma convective behavior but it appears likely to be a controlling influence on ℓ_0 in many cases of interest. The value of 0.5 km for ℓ_0 is consistent with data for outer scale lengths in Equatorial Spread F.[25]

The disposition of the drift dissipative modes can probably occur through nonlinear processes such as the production of long wavelength vortex modes[26] as well as through linear diffusion processes.

Either direct nonlinear estimates[5] or wave-particle diffusion in drift-dissipative turbulence[11] result in estimates for the power density spectrum

$$\frac{n_1(\vec{k})^2}{n} = \frac{\rho_i}{L} \quad ,$$

where $n_1(\vec{k})$ is the modal amplitude for density as a function of $\vec{k}$. This spectrum is flat as a function of $\vec{k}$, therefore looking different from the frequently measured k^{-2} power density spectrum. The occurrence of the spectrum at striation tips which occupy a relatively small fraction of the perimeter of a striation does not contradict the existence of drift-dissipative modes at striation tips.

Along the sides of striations drift-dissipative modes can act to diffuse plasma and presumably alter the power density spectrum. Except at its tip, a single striation can be taken to be elongated in the y-direction with density $n(x)$ and $E_x(x)$ related by the condition of continuity of the Pedersen current in the x-direction. This is valid provided the ion-neutral collision frequency is larger than the reciprocal of the time scale associated with plasma inertial effects.

It is shown in Appendix B and Section 5 that drift-dissipative waves are inhibited whenever

$$\varkappa >> \rho_i[v_{ti}/(cE_x/B)] \quad . \tag{42}$$

(Here $\varkappa$ is a typical scale length for the x-directed density gradient.) Therefore drift-dissipative wave effects are most likely in regions across the thin (x) dimension of a striation where $\varkappa$ is small. If the inner scale length for the power density spectrum corresponds to a real region in coordinate space, drift-dissipative wave turbulence will tend to develop in this region and we would expect 3 meter backscatter to originate from such regions. The observation of inner scale lengths of order tens of meters in Equatorial Spread F[25] is consistent with (42) if one takes $\rho_i \approx 3$ meters and $[v_{ti}/(cE_x/B] \approx 10$.

Drift-dissipative waves in such a case would not have to alter a k^{-2} power density spectrum except by affecting the inner scale length and spatial

frequencies above the spatial frequency corresponding to the inner scale length. The effect on diffusion and scintillation decay would depend strongly on the nonlinear behavior and coupling of the modes.

3. Calculation of drift-dissipative growth rates under model HANE conditions as exemplified in Figures 3-7 indicates that diffusion peaks at $n \leq 10^6$ cm^{-3} for the parameters chosen. At higher ionized densities the ion-ion collision frequency becomes so large that long wavelength, low frequency modes are the only ones possible. Electron-ion collisions and the resulting ambipolar diffusion further dampen the waves. Increasing neutral density acts monotonically to inhibit the waves.

Results for a model of a "heaved" plasma are shown in Figures 13-20. Here, too, at higher altitudes, lower magnetic field values and larger gradient scale lengths parallel to the ambient magnetic field, turbulent diffusion can be significant.

4. On the basis of this report we suggest a number of experimental and observational approaches with theoretical interaction for examining striation decay, scintillation behavior and the occurrence of drift modes:

(a) In-situ measurement is likely to be the key to direct observation of drift-modes at the relatively long wavelengths (≈ 60 meters, for an O^+ plasma with B = 0.35 gauss) expected to be primarily responsible for anomalous diffusion. The contribution of drift modes to scintillation appears to be weak in comparison to a k^{-2} one-dimensional power spectral density.

(b) For drift-dissipative waves (or even gradient-drift waves) the flux due to turbulent diffusion can be approximated as

$$\left\langle \frac{n_1 \; c \; \vec{E}_1 \times \vec{B}}{B^2} \right\rangle \tag{43}$$

where n_1 and $\vec{E}_1$ are respectively the density and electric field associated with a plasma mode, and the brackets, $\langle\rangle$, denote a suitable space and time average. Hence in situ electric field measurements and determination of (43), which depends on the correlation between n_1 and E_1, would be desirable. Expression (43) is a vector expression; ideally

one would want to know its direction relative to the background (zero order) plasma density gradient. (If E_1 is parallel to the background density gradient, no diffusion results.)

(c) It is possible that barium cloud releases in the 200-300 km altitude range, for which some drift dissipative wave turbulence is expected (see Figs. 21-24) could exhibit drift-dissipative wave phenomena. Since barium cloud density gradients can be determined rather reliably optically, it would seem that one could obtain a good idea of the direction of expression (43) with respect to the zero-order plasma density gradient.

(d) Computer simulations of the type performed by NRL,[8] using diffusion coefficients as defined in Section 6 would be useful in determining and/or verifying observational consequences of formation due to anomalous diffusion. (This would apply to structure at length scales typically greater than or equal to the drift wave length scales.) Such simulations would also be appropriate for assessing observational differences between barium cloud striation behavvior in the 200-300 km range and that of releases at lower altitudes.

(e) Rocket probe measurements of density alone as a function of wave number in Equatorial Spread F could aim at establishing correlations between plasma turbulence and the decay of Spread F both along the elongated sides of Spread F density structures and at their tips. Additionally if drift mode turbulence is present at striation tips we would expect the horizontal widths (or outer scale lengths) of ionization structures (similar to individual striations in barium clouds) to have a minimum size of order 0.5 km, and it would appear relatively simple to determine this with rocket probes. (Similar measurements could be done for Mid-Latitude Spread F.)

(f) Backscatter measurements can determine the power spectral density at wavelengths short compared to the expected maximum drift-dissipative contribution at about 60 meters. If measurements could be made at in-situ wavelengths greater than three meters, some extrapolation up to the 60 meter wavelength range might be possible. The three meter disturbances if they are drift waves are not as significant for diffusion as longer wavelength drift modes. Larger wavelength drift waves are limited less by ion-ion diffusion and hence

should occur earlier in time. The measurements could also be correlated with scintillation decay.

A range of vertical wave vectors, k_y, at the same altitude and time should result in frequency Spread F.

(g) Usage of a mid-latitude-shape charge release aimed vertically upwards at an altitude sufficiently high that the mean free path is greater than the scale height with particle velocities of order 5 km/sec would serve to create striations under conditions more likely to be characteristic of HANE conditions, with ionized density greater than the ambient at altitudes substantially greater than 200 km. We expect drift-dissipative turbulence to be prominent under these conditions (see Figs. 13-20).

REFERENCES

1. Spitzer, Jr., L., Physics of Fully Ionized Gases, Second Edition, <publisher>, p. 158 (1962).

2. Goldman, S. R., L. Baker, S. L. Ossakow and A. J. Scannapieco, "Striation Formation Associated with Barium Clouds in an Inhomogeneous Ionosphere," J. Geophys. Res. 81, 5097 (1976).

3. Lee, W. W. and H. Okuda, "Anomalous Transport and Stabilization of Collisionless Drift Wave Instabilities," Phys. Rev. Letts. 36, 870 (1976).

3a. Johnson, T. H., "Drift Waves, the Universal Instability and Anomalous Diffusion in Ionospheric Striations," AFWL report, January 1977.

4. Costa, E. and M. C. Kelly, "Calculations of Equatorial Scintillations at VHF and Gigahertz Frequencies Based on a New Model of the Disturbed Equatorial Ionosphere," Geophys. Res. Lett. 3, 677 (1976).

5. Kadomtsev, B. B., Plasma Turbulence, Academic Press, N.Y., Ch. IV (1965).

6. Linson, L. M. and J. B. Workman, "Formation of Striations in Ionospheric Plasma Clouds," J. Geophys. Res. 75, 3211 (1970).

7. Kilb, R. W., Mission Research Corporation, private communication (1978).

8. McDonald, B. E., S. L. Ossakow, S. T. Zalesak, and N. J. Zabusky, "Determination of Minimum Scale Size in Plasma Cloud Striations," in "Proceedings of the 2nd Symposium on the Effect of the Ionosphere on Space Systems and Communications," Naval Research Laboratory, January 24-26, 1978.

9. McDonald, B. E., private communication (1978).

10. Goldman, S. R., "Plasma Physics Mechanisms Relevant to Striation Structuring and Decay," DNA 4245T (1977).

11. Dupree, T. H., "Nonlinear Theory of Low Frequency Instabilities," Phys. Fluids 11, 2680 (1968).

12. Weinstock, J. and R. H. Williams, "Nonlinear Theory of Macroinstabilities and Enhanced Transport in Plasmas," Phys. Fluids 14, 1472 (1971).

13. Wortman, W. R. and R. W. Kilb, "The Relation between PSDs and Striation Properties," Mission Research Corporation, (Unpublished).

14. Wittwer, L., "The Propagation of Satellite Signals Through Turbulent Media," AFWL-TR-77-183, Air Force Weapons Lab, Kirtland AFB, New Mexico, 1978.

15. Woodman, R. F. and S. Basu, "Comparison Between In-Situ Spectral Measurements of F Region Irregularities and Backscatter at 3 m Wavelength," Geophys. Res. Letters 5, 869 (1978).

16. Pongratz, M. B. and R. A. Jeffries, "A BUARO Quick-Look Report: Instrument Performance and Preliminary Data Analysis," Los Alamos Scientific Laboratory Report No. J-10-4227, August 18, 1976.

17. Pongratz, M. B., private communication, 1978.

17a. Banks, P. M. and G. Kockarts, Aeronomy Part A, p. 224, Academic Press, New York (1973).

18. CIRA 1965, Committee on Space Research, International Council of Scientific Unions, North Holland Publishing Company, Amsterdam, 1965.

19. Baker, k. D., J. C. Ulwick, M. C. Kelley, L. C. Howlett, G. D. Allred, D. Debrey and N. Grossbard, "Electron Density Structure in Barium Clouds - Measurements and Interpretation," First Report (preliminary draft) - Project STRESS, Utah State University, November 1977.

20. Kelley, M. C. et al., "Evidence for a Raleigh-Taylor Type Instability and Upwelling of Depleted Density Regions During Equatorial Spread F," Geophys. Res. Lett. 3, 448 (1976).

21. Scannapieco, A. J. and S. L. Ossakow, "Nonlinear Equatorial Spread F," Geophys. Res. Lett. 3, 451 (1976).

22. Tatarkii, V. I., "The Effects of the Turbulent Atmosphere on Wave Propagation," National Technical Information Service, Springfield, VA, p. 111 (date?)

23. Chesnut, W. G., "Gradient Scattering Theory Demonstrates that VHF, Spread F Radar Backscatter Reveals Streaming Instabilities," Technical Report 2 for DNA, Stanford Research Institute, Menlo Park, CA, Nov. 1968, and private communication.

24. Salpeter, E. E., "Density Fluctuations in a Nonequilibrium Plasma," JGR 68, 1321 (1963).

25. Basu, S. and M. C. Kelley, "Review of Scintillation Phenomena in Light of Recent Developments in the Theory and Measurement of Equatorial Irregularities," to be published in J.A.T.P. (1978).

26. Cheng, C. Z. and H. Okuda, "Formation of Convective Cells, Anomalous Diffusion and Strong Plasma Turbulence Due to Drift Instabilities," Phys. Rev. Lett. 38, 708 (1977).

27. Fried, B. D. and S. D. Conte, "The Plasma Dispersion Function," Academic Press, New York, 1961.

28. Morse, P. M. and H. Feshbach, Methods of Theoretical Physics, McGraw-Hill, New York, 1953, p. 1565.

29 Pearlstein, L. D. and H. L. Berk, "Universal Eigenmode in a Strongly Sheared Magnetic Field," Phys. Rev. Lett. 23, 220 (1969).

30. Sperling, J. L. and F. W. Perkins, "Ion-Cyclotron Waves in Nonuniform Plasmas and Parametric Instabilities," Phys. Fluids 19, 281 (1976).

31. Braginskii, S. I., in Reviews of Plasma Physics I, edited by M. A. Leontovich, Consultants Bureau, New York, p. 205 (1965).

32. Dougherty, J. P., "Model Fokker-Placek Equation for a Plasma and its Solution," Phys. Fluids 7, 1788 (1971).

33. Allen, W., and J. J. Sanderson, "Collisional Destruction of the Bernstein Modes in the High-Frequency Regime," J. Plasma Phys. 15, 41 (1976).

34. Huba, J. D., P. K. Chaturvedi, S. L. Ossakow, and D. M. Towle, "High-Frequency Drift Waves with Wavelengths Below the Ion Gyroradius in Equatorial Spread F," Geophys. Res. Lett. 5, 695 (1978).

APPENDIX A

PHYSICAL MECHANISM FOR THE GROWTH OF THE DRIFT DISSIPATIVE MODE

The growth of the drift dissipative mode requires that the wave frequency have a smaller magnitude than the diamagnetic drift frequency, i.e.,

$$\omega < \omega_{DE} \quad . \tag{A-1}$$

Provided the full electron and ion dynamics permit Eq. (A-1) to be satisfied, we show in this appendix, using simple physical arguments, that electron collisions destabilize the drift dissipative mode.

The electron dynamics of the drift dissipative mode are described by the following set of fluid equations

$$0 = -i\omega n_1 + \partial(nv_{x1})/\partial x + \partial(nv_{z1})\partial z \tag{A-2a}$$

$$v_{x1} = -ick_y\phi_1/B \tag{A-2b}$$

$$v_{z1} = \frac{ik_z}{m_e\nu_e n}\,(qn\phi_1 - n_1T_e) \tag{A-2c}$$

with first order variables denoted by the subscript "one." Equation (A-2a) states that the rate of change of the perturbed electron density per unit time is balanced by the flux of electrons in the ambient gradient direction, $\hat{x}$, and the magnetic field direction, $\hat{z}$. The velocity associated with the x-directed flux is the E x B velocity in the mode (Eq. (A-2b)). The velocity in the z-direction is a consequence of the balance of electron collisions with the wave electric field and pressure (Eq. (A-2b)).

Substituting Eqs. (A-2b) and (A-2c) into Eq. (A-2a) results in the expression for the perturbed electron density previously calculated[10]

$$\frac{n_1}{n} = \frac{q\phi_1}{T_e}\left(\frac{i\omega_{DE} - \delta}{i\omega - \delta}\right) \tag{A-3}$$

(Note that in this paper temperature is multiplied by Boltzmann's constant.)

By using Eq. (A-3), Eq. (A-2c) can be rewritten in the following way:

$$v_{z1} = \frac{ik_z}{m_e \nu_e n} (qn\phi_1) \frac{(\omega - k_y v_{DE})(\omega - i\delta)}{\omega^2 + \delta^2} \quad . \tag{A-4}$$

The work done by the wave is then equal to

$$\frac{1}{2} (j_{z1}^* E_{z1} + j_{z1} E_{z1}^*) = \frac{\delta q^2 n}{T_e} |\phi_1|^2 \frac{\omega(\omega - k_y v_{DE})}{\omega^2 + \delta^2} \quad . \tag{A-5}$$

Hence, if Eq. (A-1) is satisfied, work is done by the plasma on the mode and the drift dissipative mode becomes unstable. A qualitative understanding of the instability can be obtained by recognizing that if Eq. (A-1) is satisfied and the growth rate is sufficiently small one has:

$$|n_1/n| > q\phi_1/T_e \quad . \tag{A-6}$$

Then along the magnetic field lines the electron flow from diffusion is larger than the electron flow from mobility, and the electrons tend to flow in a direction opposite to the electric force on them. In this case the electrons lose energy to the wave and the wave grows.

APPENDIX B

ELECTRIC FIELD LIMITATION OF DRIFT DISSIPATIVE MODE DIFFUSION

The purpose of this calculation is to evaluate the effect of an electric field $E_x(x)$ on drift dissipative mode growth rates and diffusion. We assume that the background density gradient is in the x-direction and that the mode is harmonic in y and z.

The motivation for this study is the observation that striations perpendicular to the magnetic field tend to be elongated in the direction of the E × B drift. Hence around most of the perimeter of a striation the electric field should be parallel (or anti-parallel) to the density gradient. [$E_x(x) \neq 0$.] [With $E_x(x) = 0$ previous work shows that drift mode growth rates are likely to be large enough to lead to diffusion of density profiles in the 0.1-1.0 km range.

For collisionless ions and electrons with no ambient electric field the drift wave equation has the form[26]

$$\frac{d^2\tilde{\phi}}{d^2} + Q(x,\omega)\,\tilde{\phi} = 0 \quad . \tag{B-1}$$

where

$$Q = \Sigma_\alpha \left\{1 + [\omega_\alpha + \omega_d^*(x)]\, X_{0\alpha}\right\}/T_\alpha \quad . \tag{B-2}$$

with

$$\Delta = \Sigma_\alpha \rho_\alpha^2 [\omega + \omega_\alpha^*(x)]\,(X_{0\alpha} - X_{1\alpha})/T_\alpha \quad .$$

Here α denotes the species, $v_{ta} = (T_\alpha/m_\alpha)^{1/2}$, $\rho_\alpha = v_{t\alpha}/\omega_{c\alpha}$, $\omega^* = k_y T_e K/m_i\omega_{ci}$, $\omega_e^* = -\omega^*$, $\omega_i^* = \omega^* T_i/T_e$, $K = -(dn/dx)/n$, and $L_\perp = 1/|K|$ is the density scale length at $x = 0$, the point around which the mode is centered. Further:

$$X_{\ell\alpha} = I_\ell(b_\alpha)\exp(-b_\alpha)\, Z(\omega/\sqrt{2}\, k_z v_{t\alpha})/\sqrt{2}\, k_z v_{t\alpha} \,, \tag{B-3}$$

with $b_\alpha = k_y^2 \rho_\alpha^2$ and Z the plasma dispersion function.[27] We note for $\xi >> 1$

$$Z(\xi) = i\,\pi^{1/2}\,\sigma\,e^{-\xi^2} - \xi^{-1}\,(1 + 0.5\,\xi^{-2}) \qquad \text{(B-4)}$$

with $\sigma = 0$, Im $\xi > 0$; $\sigma = 1$, Im $\xi = 0$; $\sigma = 2$, Im $\xi < 0$.

We now modify Eq. (B-1) to account for drift-dissipative modes in the presence of the electric field, $E_x(x)$:

(a) In the limit, $k_y v_{t\alpha}/\omega_{ce} \ll 1$, the contribution from

$$\left\{1 + [\omega_e + \omega_e^*(x)]x_{oe}\right\}/T_e$$

is equal to:[5]

$$\frac{n_1}{q\tilde{\phi}n} \quad ,$$

as calculated for electrons of charge -q. The corresponding quantity in the limit $\nu_e \gg \omega$, $k_z v_{te}$ is[10]

$$\left(\frac{ik_y v_{DE} - \delta}{i\omega - \delta}\right)\frac{1}{T_e} \quad .$$

with $\delta = k_z^2 T_e/m_e\nu_e$ and $v_{DE} = (+c/qB)T_e K$.

(b) The summation over α in Δ involves finite Larmor radius contributions. Since we expect finite electron Larmor radius effects to be small we take

$$\Delta = \Delta_i \equiv \rho_i^2[\omega + \omega_i^*(x)](X_{oi} - X_{1i})/T_i \quad .$$

(c) Further we assume that the sole effect of the electric field $E_x(x)$ is to introduce a Doppler shift so that the wave frequency ω is replaced by $\omega + k_y cE_x/B$ ($\equiv \omega'$) wherever it occurs. Defining $v_e = c|E_x|/B$ we neglect differences in the gyrofrequency and gyroradius of order $(v_e/v_{ti})(\rho_i/L_\perp)$ and corrections to the ion orbits at frequency $2\omega_{ci}$ of order $(v_e/v_{ti})(\rho_i/L_\perp)^2$ with respect to the gyroradius.

With these assumptions, Eq. (B-1) can be approximated:

$$\frac{d^2\tilde{\phi}}{dx^2} + \frac{\bar{Q}(x,\omega')\tilde{\phi}}{\Delta_i} = 0 \qquad \text{(B-5)}$$

with

$$\bar{Q}(x,\omega') = \left\{1 + \omega' + \omega_i^*(x)]X_{oi}\right\}/T_i + (ik_y v_{DE} - \delta)/(i\omega - \delta)T_e \qquad \text{(B-6)}$$

To illustrate the effect of the electric field it appears sufficient to consider drift modes in the limit $\delta >> kv_{DE}$, $\omega = kv_{DE}$. Then around an arbitrarily chosen origin one may expand

$$Q(x) = Q(o) + xQ'(o) + \frac{x^2}{2} Q''(o) \quad . \qquad \text{(B-7)}$$

The local theory[10] corresponds to setting $(d^2\phi/dx^2) = 0$ and choosing the origin so that $Q'(o) = 0$. If the degree of localization,

$$\ell = 2(2)^{1/2} \, |Q''(o)|^{-1/4} \quad , \qquad \text{(B-8)}$$

is much larger than the wavelength in the y direction, i.e., $\ell >> \lambda_y$, the local theory can be expected to be approximately satisfied. Of course, the nonlocal theory to be discussed subsequently gives an even more accurate description of the mode.

Using Eqs. (B-3) and (B-6) one obtains

$$Q = \frac{1}{T_i \Delta_i \omega'}\left\{\omega'\left[1 + \frac{T_i}{T_e} - I_o(b_i)\, e^{-b_i}\right] - \omega_i^*\, I_o(b_i)\, e^{-b_i}\right\} \quad . \qquad \text{(B-9)}$$

Letting $a = 1 + T_i/T_e - I_o(b_i)e^{-bi}$, $b = -I_o(b_i)e^{-bi}$, since $Q \approx 0$, one has

$$\frac{dQ}{dx} = \frac{1}{T_i \Delta_i \omega'}\left(a \frac{d\omega'}{dx} + b \frac{d\omega_i^*}{dx}\right) \quad . \qquad \text{(B-9a)}$$

The condition $dQ/dx = 0$ results in

$$\frac{d^2Q}{dx^2} = \frac{1}{T_i \Delta_i \omega'}\left(a \frac{d^2\omega'}{dx^2} + b \frac{d^2\omega_i^*}{dx^2}\right) \quad .$$

We have:

$$\omega_i^* = \frac{k_y T_e}{m_i \omega_{ci}} \left(-\frac{1}{n}\right) \frac{dn}{dx} \frac{T_i}{T_e}$$

$$\omega' = \omega + k_y \frac{cE_x}{B}$$

The ion momentum equation has the form:

$$0 = \frac{q\vec{v}_i \times B}{m_i c} - \nu_i \vec{v}_i + \frac{q\vec{E}}{m_i} - \frac{T_i}{m_i n} \nabla n$$

from which to lowest order in ν_i/ω_{ci}:

$$v_{ix} = \left(\frac{qE_x}{m_i} - \frac{T_i}{m_i n} \frac{dn}{dx}\right) \frac{\nu_i}{\omega_{ci}^2} \quad .$$

In the limit $\nu_e/\omega_{ce} << \nu_i/\omega_{ci}$ the condition of quasi-neutrality results in

$$\frac{\partial}{\partial x} (n v_{ix}) = 0$$

from which

$$\omega' + \omega_i^* = \omega + k_y \frac{cE_{xo}}{B} \frac{n_o}{n} \quad . \tag{B-10}$$

Hence

$$\frac{d\omega'}{dx} = -\frac{d\omega_i^*}{dx} + k_y \frac{cE_{xo}}{B} \frac{(-n_o)}{n^2} \frac{dn}{dx}$$

$$\frac{d^2\omega'}{dx^2} = -\frac{d^2\omega_i^*}{dx^2} - k_y \frac{cE_{xo} n_o}{B} \frac{d}{dx}\left(\frac{1}{n^2} \frac{dn}{dx}\right)$$

and

$$\frac{dQ}{dx} = \frac{1}{T_i \Delta_i \omega'}\left[-(1 + T_i/T_e)\frac{d\omega_i^*}{dx} - a\, k_y \frac{cE_{xo}}{B} \frac{n_o}{n} \frac{1}{n} \frac{dn}{dx}\right]$$

as well as

$$\frac{d^2Q}{dx^2} = \frac{1}{T_i \Delta_i \omega'}\left[-(1 + T_i/T_e) \frac{d^2\omega_i^*}{dx} - a\, k_y \frac{cE_{xo}}{B} n_o \frac{d}{dx}\left(\frac{1}{n^2} \frac{dn}{dx}\right)\right] \quad . \tag{B-11}$$

For $E_{xo} = 0$, $dQ/dx = 0$ is equivalent to $d\omega_i^*/dx = 0$ and the mode is centered around an extremum of $1/n(dn/dx)$. This is the situation conventionally analyzed. For $E_{xo} \neq 0$, from $dQ/dx = 0$ and $Q \approx 0$, one has:

$$\left(\frac{1}{n}\frac{dn}{dx}\right)^2\left[\frac{T_i}{m_i\omega_{ci}}\left(1+\frac{T_i}{T_e}\right)+\frac{aT_i}{m_iT_{ci}}\right]-\left(\frac{1}{n}\frac{dn}{dx}\right)av_e-\frac{T_i}{m_i\omega_{ci}}\frac{1}{n}\frac{d^2n}{dx^2}=0$$

The first term in the equation is of order $v_i^*(1/n)(dn/dx)$ for a and T_i/T_e of order unity. (We note $v_i^* = \omega_i^*/k_y$.)

If $v_e >> v_i^*$ one has

$$\frac{1}{n}\frac{dn}{dx} = -\frac{T_i}{m_i\omega_{ci}}\frac{1}{n}\frac{d^2n}{dx^2}\frac{1}{av_e}$$

If

$$\left(\frac{1}{n}\frac{d^2n}{dx^2}\right)^{1/2} \approx \frac{1}{n}\frac{dn}{dx} \ ,$$

the condition for mode localization is not met. Hence we anticipate the mode to be located where the value $1/n(d^2n/dx^2)^{1/2}$ is of order the average value found over the entire region of non-zero density gradient. If $\mathscr{L}$ is the typical scale length for the region one has:

$$\frac{1}{n}\frac{d^2n}{dx^2} = \frac{\beta}{\mathscr{L}^2}$$

with β of order unity and:

$$\frac{1}{n}\frac{dn}{dx} = -\frac{T_i}{m_i\omega_{ci}}\frac{\beta}{\mathscr{L}^2}\frac{1}{av_e} \ .$$

This is the same as:

$$\frac{1}{n}\frac{dn}{dx} = \frac{1}{\mathscr{L}}\frac{(v_i^*)_{av}}{v_e}\frac{B}{a} \ .$$

with

$$(v_i^*)_{av} = \frac{-T_i}{m_i \omega_{ci} \mathscr{L}} \quad ,$$

an average value for the ion-diamagnetic drift velocity in the region of density gradient one has

$$\frac{1}{L_\perp} = \frac{1}{\mathscr{L}} \frac{(v_i^*)_{av}}{v_e} \frac{\beta}{a} \quad . \tag{B-12}$$

Hence the mode is located where the density gradient ($L_\perp^{-1}$) is appreciably less [by a factor of $(v_i^*)_{av}/v_e$] than the mean ($=\mathscr{L}^{-1}$) and its growth rate, proportional to $L_\perp^{-1}$ is correspondingly decreased.

For $v_e \approx v_i^*$, we expect $L_\perp^{-1} \approx \mathscr{L}^{-1}$.

On the basis of previous work[10] instability for the drift-dissipative mode is characterized by

$$\frac{C_s}{L_\perp \nu_i} > 4 \tag{B-13}$$

where c_s is the ion sound speed $= (T_e/m_i)^{1/2}$ and $\nu_i = \nu_{in} + 0.3\ \nu_{ii}(k_y \rho_i)^2$, with ν_{in} the ion-neutral collision frequency, ν_{ii} the ion-ion collision frequency and the deviation of T_e/T_i from unity is neglected. For $v_e >> (v_i^*)_{av}$ a necessary condition for instability becomes

$$\frac{C_s}{\mathscr{L}\nu_i} > \frac{4v_e}{(v_i^*)_{av}} \frac{a}{\beta}$$

or equivalently:

$$\mathscr{L} < \frac{C_s}{4\nu_i} \frac{\beta}{a} \left[\sqrt{\frac{T_i}{T_e + T_i}}\ \frac{a}{\beta} \left(\frac{4\nu_i}{\omega_{ci}} \frac{v_{ti}}{v_e} \right) \right]^{1/2} < \frac{C_s}{4\nu_i} \quad .$$

The effect on the diffusion coefficient $D_\perp$ can be estimated through the formula

$$D_\perp = \frac{\gamma}{k_x^2}$$

with $1/k_x^2 \approx 2\sqrt{2}\ |[Q''(o)]^{1/2}|^{-1}$. For $v_e \lesssim v_i^*$, there is no significant modification in the previous results for $Q''(o)$[10] which yields $k_x \alpha (\mathscr{L} \rho_i)^{-1/2}$. For $v_e >> v_i^*$ one has - given that

$$\frac{1}{n^2}\frac{d^2n}{dx^2} >> \left[\frac{1}{n}\left(\frac{dn}{dx}\right)\right]^2 \quad ,$$

and using Eqs. (B-3), (B-4), (B-6) with Q = 0, (B-9a) with dQ/dx = 0, and (B-11):

$$\frac{d^2Q}{dx^2} \simeq \frac{\left[1 + \frac{T_i}{T_e} - I_o(b_i)\, e^{-b_i}\right]^3}{[I_o(b_i) - I_1(b_i)]\, e^{-b_i}} \frac{n_o}{n}\left[\frac{v_e}{(v_i^*)_{av}}\right]^2 \frac{1}{\rho_i^2 \ell^2} \quad . \tag{B-14}$$

We now discuss the effect of non-localness of the mode.

From the forms of Eqs. (B-5), (B-7) and (B-14) it is apparent that the mode has a nonlocal mode structure about x = 0. As shown in Figure 29 an analogous quantum mechanical picture, that the mode is centered a the top of a potential hill, can also be made. The precise solution of Eq. (B-5) can be written in terms of $D_p(z)$, the parabolic cylinder functions[28] of order p, where

$$0 = \left(\frac{d^2}{dz^2} + \frac{1}{2} + p - \frac{z^2}{4}\right) D_p(z)$$

For

$$z = x/\ell$$

$$Q(o) = \left(\frac{1}{2} + p\right) \ell^{-2}$$

$$Q''(o) = -\frac{1}{2}\ell^{-4}$$

and a boundary condition corresponding to the outward propagation of energy, the appropriate eigenmode solution to Eq. (B-5) is

$$\phi(x) = \phi_o\, D_p\left[\exp(-i\pi/4)\ |2Q''(o)|^{1/4}\ x\right]$$

or for $|x| \to \infty$

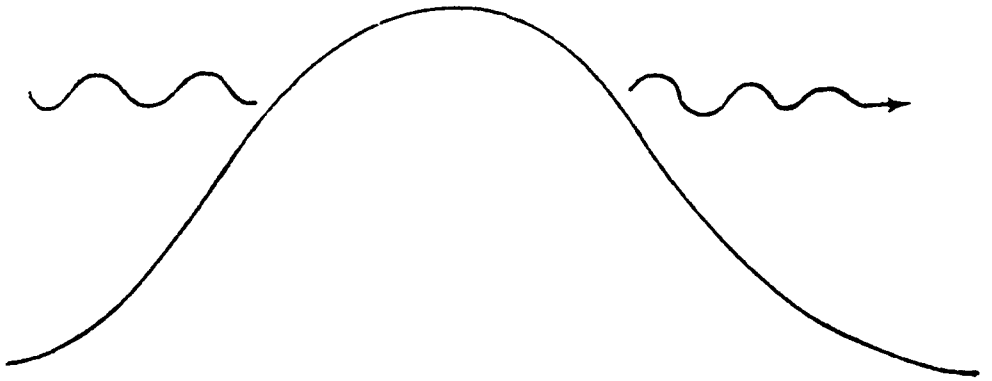

Figure 29. The nonlocal propagation for the solution of Eq. (B-5) is analogous to the quantum mechanical picture of a particle in the presence of a potential hill.

$$\phi(x) = \phi_0 \exp(-ip\pi/4)\ |Q''(o)|^{p/4}\ x^p \times \exp\left| i\left(\frac{|Q''(o)|^{1/2}}{(2)^{3/2}}\right)x^2 \right|$$

where ϕ_0 is a constant. Eigenvalues are given by the relation

$$Q(o) = -\ i(2)^{1/2}\left(\frac{1}{2} + p\right)\ |Q''(o)|^{1/2}$$

$$p = 0,\ 1,\ 2,\ \ldots$$

Assuming the damping rate, γ, is much smaller than the wave frequency, then from Eqs. (B-9) and (B-14)

$$\gamma = -\ (1 + 2p)\ \sqrt{2}\ \frac{\left[1 + T_i/T_e - I_o\ e^{-b_i}\right]^{3/2}}{(I_o - I_1)^{1/2}\ e^{-b_i/2}}\left(\frac{n_o}{n}\right)^{1/2}\ \frac{v_e}{v_{ti}}\ \omega' \qquad \text{(B-15)}$$

From the form of Eq. (B-13) it is evident that the minimum value of the damping rate occurs for $p = 0$. It also appears that electric field gradients act like magnetic shear to stabilize drift modes by convective damping.[29] Electrostatic ion-cyclotron ,waves propagating in the ion diamagnetic drift direction also tend to be damped by wave convection in the x-direction.[30]

The physical mechanism leading to the damping decrement given by the expression, Eq. (B-15), is the convection of wave energy away from $x = 0$. Roughly then the damping decrement must scale as the group velocity in the x-direction divided by the scale length in the x-direction, ℓ:

$$\gamma \simeq -\left(\frac{\partial \omega}{\partial k_x}\right)\frac{1}{\ell}\ .$$

Then using the replacement

$$\frac{\partial \phi(x)}{\partial x} \simeq i\ k_x \phi(x)$$

in Eq. (B-5) results in an expression for the damping rate which is in agreement with Eq. (B-15) to within a constant and so verifies the convective explanation for the damping.

APPENDIX C

DERIVATION OF MODAL GROWTH RATES TAKING INTO ACCOUNT FINITE ION LARMOR RADIUS AND ELECTRON-ION COLLISIONAL EFFECTS

Drift modes with frequencies below the ion-cyclotron frequency (i.e., $\omega < \Omega_i$) can be driven unstable in an inhomogeneous plasma if the wave frequency is smaller than the diamagnetic drift frequency, ω_D,[5] e.g.,

$$\omega < \omega_D = \frac{k_y v_i^2}{\Omega_i L_n} \tag{C-1}$$

where

$$v_i^2 = T_i/m_i \quad , \quad \Omega_i = e B_0/m_i c \quad . \tag{C-2}$$

In Eqs. (C-1) and (C-2), the quantities e, c, k_y, and L_n are the magnitude of the electron charge, the speed of light, the y-directed wavenumber, and the density gradient scale length, respectively.

In a collisionless plasma, the mechanism responsible for the instability is inverse electron Landau damping[5]. Electron diffusion parallel to the magnetic field drives the instability in a collisional plasma. In either case, it is apparent from Eq. (C-1) that low-frequency drift instabilities may exist in plasmas with

$$k_y \rho_i << 1 \quad , \quad \rho_i/L_n << 1 \tag{C-3}$$

where

$$\rho_i = v_i/\Omega_i \tag{C-4}$$

is the ion Larmor radius.

The dispersion relation for the low-frequency can be derived using the linearized kinetic equation, Eq. (IV.100), in Ref. 5.

$$(\nu_s - i\omega + ik_z v_z - \Omega_s \frac{\partial}{\partial\theta}) f_{1s}(\vec{v}) = i \frac{g_s}{m_s} \vec{k} \cdot \frac{\partial f_{0s}(\vec{r},\vec{v})}{\partial \vec{v}} + \nu_s \frac{n_{1s}}{n_{0s}} f_{0s}(\vec{r},\vec{v}) \tag{C-5}$$

where

$$f_{0s}(\vec{r},\vec{v}) = n_{0s}\left(2\pi v_s^2\right)^{-3/2} \exp\left(-v^2/v_s^2\right)\left[1 + \frac{(x + v_y/\Omega_s)}{L_n}\right] \qquad \text{(C-6a)}$$

$$f_{1s}(\vec{r},\vec{v},t) = f_{1s}(\vec{v}) \exp[i(k_y y + k_z z - \omega t)] \qquad \text{(C-6b)}$$

$$\phi_1(\vec{r},t) = \phi_1 \exp[i(k_y y + k_z z - \omega t)] \qquad \text{(C-6c)}$$

$$n_{1s}(\vec{r},t) = n_{1s} \exp[i(k_y y + k_z z - \omega t)] \qquad \text{(C-6d)}$$

$$\phi = \cos\left(\frac{\vec{k}_y \cdot \vec{v}}{|\vec{k}_y||\vec{v}_y|}\right) \quad . \qquad \text{(C-6e)}$$

In Eqs. (C-5) and (C-6), subscript "0", subscript "1", and subscript "s" denote the ambient quantities, perturbed quantities, and arbitrary species designations. Also, ϕ_1 is the perturbed potential. The symbol ν_s represents the effective collision frequency, x, for species s.

A straightforward approach to the solution of Eq. (C-5) is based on a Fourier-Bessel analysis. We write

$$f_{1s}(\vec{v}) = \exp\left[i \frac{k_\perp v_\perp}{\Omega_s} \sin(\theta)\right] \sum_{p=0}^{\infty} J_p\left(\frac{k_\perp v_\perp}{\Omega_s}\right) \exp(-ip\theta) f_{1s}^p(v_\perp, v_{11}) \qquad \text{(C-7)}$$

and the inverse transformation

$$f_{1s}^p(v_\perp, v_{11}) = \left[J_p\left(\frac{k_\perp v_\perp}{\Omega_s}\right)\right]^{-1} \int_0^{2\pi} \frac{d\theta}{2\pi} \exp\left[ip\theta - i \frac{k_\perp v_\perp}{\Omega_s} \sin(\theta)\right] f_{1s}(\vec{v}) \quad . \qquad \text{(C-8)}$$

Here, J_p is the Bessel function of the first kind of order p. One finds

$$f_{1s}^p = -\frac{q_s n_{0s}}{m_s v_s^2} (k_z v_z + p\Omega_s - \omega + i\nu_s)^{-1} \left[(p\Omega_s + k_z v_z)\left(1 + \frac{p}{k_y L_n}\right) - \omega_{Ds}\right]$$
$$\left(2\pi v_s^2\right)^{-3/2} \exp\left(-v^2/v_s^2\right) + i\nu\, n_{1s}(k_z v_z + p\Omega_s - \omega + i\nu_s)^{-1}$$
$$\left(2\pi v_s^2\right)^{-3/2} \exp\left(-v^2/v_s^2\right) \quad . \qquad \text{(C-9)}$$

Taking the density moment of the perturbed distribution function and substituting into Poisson's Equation,

$$k^2\phi_1 = -4\pi e(n_{1e} - n_{1i}) \quad , \tag{C-10}$$

results in the following dispersion relation for electrostatic modes,

$$0 = 1 + \sum_s \frac{1}{k^2 \lambda_{Ds}^2} \left\{ \sum_{p=\infty}^{\infty} \left[1 + \frac{\omega + i\nu_s - \omega_{Ds}}{(2)^{\frac{1}{2}} k_{\parallel} v_s} Z\left(\frac{\omega + i\nu_s - p\Omega_s}{(2)^{\frac{1}{2}} k_z v_s} \right) I_p(\lambda_s) \exp(-\lambda_s) \right] \right\}$$

$$\left\{ \sum_{p=\infty} \left[1 + \frac{i\nu_s}{(2)^{\frac{1}{2}} k_{\parallel} v_s} Z\left(\frac{\omega + i\nu_s - p\Omega_s}{(2)^{\frac{1}{2}} k_{\parallel} v_s} \right) \right] I_p(\lambda_s) \exp(-\lambda_s) \right\}^{-1} \tag{C-11}$$

where

$$\lambda_{Ds}^2 = \frac{T_s}{4\pi n_s e^2} \quad , \quad \lambda_s = \frac{k_y^2 v_s^2}{\Omega_s^2} \quad ,$$

$$Z(x) = -2 \exp(-x^2) \int_0^x dt \exp(t^2) + i\pi^{\frac{1}{2}} \exp(-x^2) \; . \tag{C-12}$$

In Eq. (C-12), I_p is the modified Bessel function of the first kind and order p.

The incorporation of electron collisions with ions in determination of n_{1e} and of ion collisions with electrons in determination of n_{1i} poses a special problem in that each species has a velocity which oscillates as part of the wave. Hence, the collisional contributions for each species on the righ hand of Eq. (C-5) should depend on the wave fluid velocity of the other species. However, the collisional model of Eq. (C-5) does not include this behavior.

The effect of interspecies coulomb collisions on drift-dissipative modes can be estimated from the ions and electron fluid equations in the limit $k_y\rho_i << 1$. For simplicity, we take the zero-order (background) ion and electron velocities to be zero. Define the first-order velocities [varying as $\exp(ik_y y + ik_z z - i\omega t)$] as v_+ and v_- for ions and electrons, respectively. The first-order fluid velocity equations are

$$\frac{\partial v_\pm}{\partial t} = v_\pm \times \omega_{c_\pm} - \nu_{n_\pm} v_\pm - \nu_{c_\pm}(v_\pm - v_\mp) + \frac{q_\pm E}{m_\pm} - \frac{\nabla p_\pm}{m_\pm n} \tag{C-13}$$

where ν_{c_+} denotes the collision frequency for ions on electrons, and ν_{c_-} denotes the frequency for electrons on ions. Now expand

$$v_{\pm} = v_{\pm}^0 + v_{\pm}^1$$

where

$$v_{\pm}^0 \times \vec{\omega}_{c\pm} = -\frac{q_{\pm} E_1}{m_{\pm}} + \frac{\nabla p_{\pm}}{m_{\pm} n}$$

$$v_{\pm}^1 \times \vec{\omega}_{c\pm} = \nu_{n\pm}\left(v_{\pm}^0 \times \omega_{c\pm}\right) + \nu_{c\pm}\left(v_{\pm}^0 - v_{\mp}^0\right) \times \omega_{c\pm} + \frac{\partial v_{\pm}^0}{\partial t} \times \omega_{c\pm} \quad .$$

(Effectively, a series in inverse powers of B is generated for $v_{\pm\perp}$, the component of wave fluid velocity perpendicular to B.) We note

$$\vec{\omega}_{c+} = |\omega_{c+}|\vec{B}/|\vec{B}|\vec{\omega}_c = -|\vec{\omega}_{c-}|\vec{B}/|\vec{B}| \quad .$$

After some algebra, one obtains for electrons

$$v_{1\perp} = \frac{q_+}{m_+}\frac{E_1 \times \hat{k}}{\omega_{c\pm}} - \frac{\nabla p_- \times \hat{k}}{m_+ n\omega_{c-}} - \frac{\nu_{c_-}}{|\omega_{c-}|^2}\left(\frac{\nabla p_-}{m_- n} + \frac{\nabla p_+}{m_- n}\right)$$

$$v_{1z} = -\frac{k_b T_e\, ik_z\, n_1}{m_e\, n_0\, \nu_e} + \frac{q\, ik_z\, \phi_1}{m_e\, \nu_e}$$

and for ions

$$v_{1\perp} = \frac{q_+}{m_+} E_1 \times k - \frac{\nabla p_+ \times \hat{k}}{m_+ n\omega_c} - \frac{\nu_{n_+}}{\omega_c^2}\left[-\frac{q_+ E_1}{m_+} + \frac{\nabla p_+}{m_+ n}\right] - \nu_{c+}\left(\frac{\nabla p_+}{m_+ n\omega_{c+}^2} + \frac{\nabla p_-}{m_+ n\omega_{c+}^2}\right)$$

$$- \frac{\partial}{\partial t}\left(-\frac{q_+ E_1}{m_+ \omega_{c+}^2} + \frac{\nabla p_+}{m_+ n\omega_{c+}^2}\right) \quad .$$

Here, $\hat{k} \equiv \vec{B}/|\vec{B}|$. On neglecting ion velocity || B and using the first-order electron and ion continuity equations,

$$\frac{\partial n_{\pm}}{\partial t} + \nabla \cdot (n_{\pm} \vec{v}_{\pm}) = 0 \quad ,$$

one obtains for electrons

$$\frac{n_{1e}}{n_0} = \frac{q\phi_1}{k_b T_e} \frac{(\omega_{De}^* + i\delta)}{(\omega + i\delta + iD_\perp k_y^2} \tag{C-14}$$

and for ions

$$\frac{n_{1i}}{n_0} = \frac{q\phi_1}{k_b T_e} \frac{(\omega_{De}^* - \omega k_y^2 \rho_i^2 \frac{T_e}{T_i} - i\nu_{n_+} k_y^2 \rho_i^2 \frac{T_e}{T_i})}{(\omega + i\nu_{n_+} k_y^2 \rho_i^2 + iD_\perp k_y^2)} \tag{C-15}$$

Here,

$$\omega_{De}^* = +\frac{k_y}{m_e} \frac{\partial n_0}{\Omega_e \partial x} \frac{k_b T_e}{n_0} ,$$

$$D_\perp = \frac{\nu_{c_+}}{|\omega_{c_+}|} \frac{k_b(T_i + T_e)}{m_+ |\omega_{c_+}|} = \frac{\nu_{c_-}}{|\omega_{c_-}|} \frac{k_b(T_i + T_e)}{m |\omega_{c_-}|} = \nu_{ie} \rho_i^2 (1 + T_e/T_i)$$

$$\Omega_e = \frac{q_e B}{m_e c}$$

$$\delta = \frac{k_b T_e k_z^2}{m_- \nu_-} .$$

We further note

$$\nu_- = \nu_{en} + \nu_{ei} \tag{C-15a}$$

$$\nu_{en} = 3.5 \times 10^{-9} n_n \tag{C-15b}$$

$$\nu_{n_+} = \nu_{in} + .3 \nu_{ii} k_y^2 \rho_i^2 \tag{C-15c}$$

$$\nu_{in} = 8.3 \times 10^{-10} n_n \tag{C-15d}$$

$$\nu_{ei} = \frac{n_e[23.4 - 1.15 \log_{10} n_e + 3.45 \log_{10} T_e]}{3 \cdot 5 \times 10^5 T_e^{3/2}} \tag{C-15e}$$

$$\nu_{ie} \simeq \nu_{ei} \left(\frac{T_e}{T_i}\right)^{3/2} \frac{m_e}{m_i} \tag{C-15f}$$

$$\nu_{ii} = \frac{n_e (m_p/m_i)^{\frac{1}{2}} [23.4 - 1.15 \log_{10} n_e + 3.45 \log_{10} T_e]}{2.12 \times 10^7 \, T_i^{3/2}} \tag{C-15g}$$

The ratio of proton to ion mass is written as m_p/m_i. The quantities ν_{en}, ν_{in}, ν_{ie}, ν_{ei}, and ν_{ii} denote the electron-neutral, ion-neutral, ion-electron, electron-ion, and ion-ion collision frequencies, respectively. In formulas (C-15a) through (C-15c), all quantities are in cgs units, except for the temperature, which is in units of electron volts. The formulas (C-15a) through (C-15c) are taken from Ref. 10, while formulas (C-15d) through (C-15g) are taken from Ref. 31.

Kinetically from Eqs. (C-10) and (C-11) on taking p = 0 contributions,

$$\frac{n_{1i}}{n_0} = -\frac{e\phi_1}{k_b T_i} \frac{\left[1 + \frac{\omega + i\nu_i - \omega_{Di}}{2^{\frac{1}{2}} k_z v_i} Z\left(\frac{\omega + i\nu_i}{2^{\frac{1}{2}} k_z v_i}\right) I_0(\lambda_i) e^{-\lambda_i}\right]}{\left[1 + \frac{i\nu_i}{2^{\frac{1}{2}} k_z v_i} Z\left(\frac{\omega + i\nu_i}{2^{\frac{1}{2}} k_z v_i}\right) I_0(\lambda_i) e^{-\lambda_i}\right]} .$$

In the limit $(\omega + i\nu_i)/(2^{\frac{1}{2}} k_z v_i) \gg 1$ on neglecting non-dominant terms in λ_i, this becomes

$$\frac{n_{1i}}{n_0} = -\frac{e\phi_1}{k_b T_i} \frac{\left[1 + \frac{(\omega + i\nu_i - \omega_{pi})(-)}{\omega + i\nu_i} I_0(\lambda_i) e^{-\lambda_i}\right]}{\left[1 + \frac{i\nu_i (-)}{\omega + i\nu_i} I_0(\lambda_i) e^{-\lambda_i}\right]} \tag{C-16}$$

$$= \frac{e\phi_1}{k_b T_i} \left[-\frac{(\omega + i\nu_i)\left[1 - I_0(\lambda_i) e^{-\lambda_i}\right] - \omega_{pi} I_0(\lambda_i) e^{-\lambda_i}}{\omega + i\nu_i \left(1 - I_0 e^{-\lambda_i}\right)}\right] .$$

If one identifies $\nu_i = \nu_{n+}$, expands to first order in λ_i, and notes $\omega_{De} = \omega_{Di}/R_T$, Eqs. (C-15) and (C-16) differ only in the term in $D_\perp k_y^2$ in the denominator of (C-15). Therefore, we modify the kinetic result (C-16) with

$\omega \to \omega + i_{D_\perp} k_y^2$ in the denominator, so that

$$\frac{n_{1i}}{n_0} = \frac{e\phi_1}{k_b T_i}\left[-\frac{(\omega + i\nu_i)\left[1 - I_0(\lambda_i)e^{-\lambda_i}\right] - \omega_{Di}\, I_0(\lambda_i)e^{-\lambda_i}}{\omega + i\nu_i\left(1 - I_0(\lambda_i)e^{-\lambda_i}\right) + iD_\perp k_y^2}\right] \quad \cdot \text{(C-17)}$$

We note

$$r = \frac{\nu_i\left(1 - I_0(\lambda_i)e^{-\lambda_i}\right)}{D_\perp k_y^2} \gtrsim \frac{.3\,\nu_{ii}(k_y\rho_i)^2(k_y\rho_i)^2}{\nu_{ie}(k_y\rho_i)^2(1 + T_i/T_e)} \gtrsim \frac{.15(3.5 \times 10^5)}{(2.12 \times 10^7)}\left(\frac{m_e}{m_i}\right)^{\frac{1}{2}}\left(\frac{m_i}{m_e}\right)(k_y\rho_i)^2 \,.$$

Using $m_p = 16$,

$$r \gtrsim 18(k_y\rho_i)^2 \quad . \qquad \text{(C-18)}$$

Hence, the additional term is non-dominant for $k_y\rho_i > .24$, and it appears reasonable to use Eq. (C-17) for all $k_y\rho_i < 1$.

Taking quasi-neutrality ($n_{ie} = n_{1i}$) and using Eqs. (C-14) and (C-17), with $\alpha = I_0(\lambda_i)\exp(-\lambda_i)$ results in the equation

$$\left(\frac{\omega'}{\nu_i}\right)^2 + (b_r + ib_i)\left(\frac{\omega'}{\nu_i}\right) + c_r + ic_i = 0 \qquad \text{(C-19)}$$

where

$$\omega' = \omega + iD\ k_y^2 \qquad \text{(C-20)}$$

$$b_r = + \frac{\omega_{De}}{\nu_i} R_T$$

$$b_i = 1 + \frac{\delta}{\nu_i}\left(1 + \frac{R_T}{1-\alpha}\right) - \frac{D_\perp k_y^2}{\nu_i}$$

$$c_r = -\frac{\delta}{\nu_i}(1 + R_T) + \frac{D_\perp k_y^2}{\nu_i}\frac{\delta}{\nu_i}$$

$$c_i = \frac{\omega_{De}}{\nu_i} R_T\left(+1 - \frac{\alpha}{1-\alpha}\frac{\delta}{\nu_i}\right) \quad .$$

This equation can be solved by the standard quadratic formula to yield two values for ω', which by Eq. (C-20) determine values for ω. Our computer program calculates the root with largest algebraic imaginary part ($=\gamma$). If $\gamma > 0$, a diffusion coefficient $D_\perp = \gamma/k_x^2$ with $k_x^2 = (\rho_i\ L_\perp)$; if $\gamma < 0$, no diffusion is anticipated.

For a given set of background physical parameters (e.g., ambient magnetic field, ion species, ion temperature, electron temperature, electron density, neutral density, background plasma scale length parallel to the ambient magnetic field, plasma gradient scale length perpendicular to the ambient magnetic field), values of k_y are scanned in geometric increments over the range

$$\frac{\omega_{ci}}{v_{ti}} > k_y > \frac{1}{L_\perp} \quad ,$$

and values of k_z are scanned in geometric increments over the range

$$\min\left(\frac{\nu_e}{v_{te}} \ , \ \frac{\omega_D}{v_{ti}}\right) > k_z > \frac{2\pi}{L_z} \quad .$$

Further, it is necessary to check $\nu_e > \omega$.

The larges value of γ for a pair of k_y, k_z over the permissible range of k_y, k_z parameter space is taken to determine the diffusion coefficient.

Some further insight into the effect of interspecies coulomb interactions is provided by consideration of the limit $k_y \rho_i >> 1 >> k_y \rho_e$. Then one expects from finite ion Larmor radius effects that $|v_+| << |v_-|$ and $\nu_e = \nu_{ei} + \nu_{en}$ in Eq. (C-13). Also, the ion behavior should be predominantly independent of ν_{ie} because of the dominance of ion-ion viscosity over ion-electron collisions (see Eq. (C-18)).

On using Eq. (C-13) for the electrons, we have

$$\frac{n_{1e}}{n_0} = \frac{q\phi_1}{k_b T_e}\left[\frac{\omega_{De}^* + i\delta + i(\nu_{n-} + \nu_{c-})(k_y \rho_e)^2}{\omega + i\delta + i(\nu_{n-} + \nu_{c-})(k_y \rho_e)^2}\right] \quad , \qquad \text{(C-21)}$$

while for the ions, we have Eq. (C-16).

On taking quasi-neutrality and using Eqs. (C-16) and (C-21), the solution equation is again of the form of Eq. (C-19) with δ replaced by $\delta + (\nu_{n-} + \nu_{c-})(k_y \rho_e)^2$ and $D_\perp$ replaced by 0 in Eq. (C-20).

In this case, electron-ion collisional effects are neither inherently stabilizing nor destabilizing. For k_z such that $k_z^2 k_b T_e/m_e \nu_e << |\omega_{De}^*|$, the effects are destabilizing; for k_z such that $k_z^2 k_b T_e/m_e \nu_e >> |\omega_{De}^*|$, the effects are stabilizing.

APPENDIX D

SURVEY OF OTHER DENSITY-GRADIENT INSTABILITIES POSSIBLY RELEVANT TO ANOMALOUS DIFFUSION UNDER HANE CONDITIONS

Anomalous diffusion in plasmas is not a priori limited to diffusive behavior driven by any particular plasma mode. Hence it is relevant to consider modes in addition to the drift-dissipative mode[1,2] as possible sources of wave turbulence and diffusion.

Our purpose here is to survey the various types of linear wave instabilities (besides the drift-dissipative mode) which could be driven unstable as a result of the free energy associated with an ambient density gradient and with both an ambient density gradient and an ambient electric field for lower-hybrid waves. We consider ionospheric situations with the following parameters relevant to long-time striation behavior and scintillations:

$$n_e = n_i = 10^6 \text{ cm}^{-3}, \quad T_e = T_i = 0.1 \text{ ev},$$

$$B = 0.3 \text{ gauss} . \tag{D-1}$$

In Equation (D-1) the quantities n, T, and B denote the density, temperature, and ambient magnetic fields, respectively. The subscripts "e" and "i" represent electrons and ions, respectively, a quasineutral plasma made up of singly ionized oxygen is also assumed. Given the parameters of Equation (D-1) the ratio of plasma to magnetic field pressure, β, is

$$\beta \approx 9 \times 10^{-5} \tag{D-2}$$

which is comparable to the ratio of electron to oxygen masses,

$$\frac{m_e}{m_i} = 3.4 \times 10^{-5} . \tag{D-3}$$

Consequently, except for some possible modes (to be discussed subsequently) with wavelengths parallel to the magnetic field of the order of several tens or hundreds of kilometers, the relevant modes from the standpoint of anomalous transport will primarily be electrostatic.

We assume a z-directed magnetic field of strength, B, an x-directed density gradient and uniform plasma properties in the y-direction. This slab like plasma model most closely approximates the true ionospheric plasma if the wavelengths of modes are much smaller than the inhomogeneity scale lengths. This geometry is shown in Figure 30.

In the following subsections we analyze the linear stability of drift instabilities associated with cyclotron, acoustic, lower-hybrid and electromagnetic behavior. The calculations support the conclusion that the drift-dissipative mode is the dominant wave turbulence factor in anomalous diffusion under HANE conditions.

A. ANALYSIS OF MODES

1. Ion-Cyclotron Drift Modes

Drift instabilities with frequencies comparable to the fundamental or harmonics of the ion-cyclotron frequency can be driven unstable if

$$p\Omega_i < |\omega_D| \tag{D-4}$$

where "p" is equal to a nonnegative integer, ω_D is the diamagnetic drift frequency, e.g.,

$$\omega_D = k_y v_i^2/\Omega_i L_n$$

with $v_i^2 = T_i/m_i$, $\Omega_i = eB/m_i c$.

An equivalent condition to Equation (D-4) is[5]

$$p < (k_y \rho_i) \frac{\rho_i}{L_n} \tag{D-5}$$

Hence, for situations with weak density gradients such that

$$\rho_i << L_n \tag{D-6}$$

we require

$$k_y \rho_i >> 1 \tag{D-7}$$

for instability.

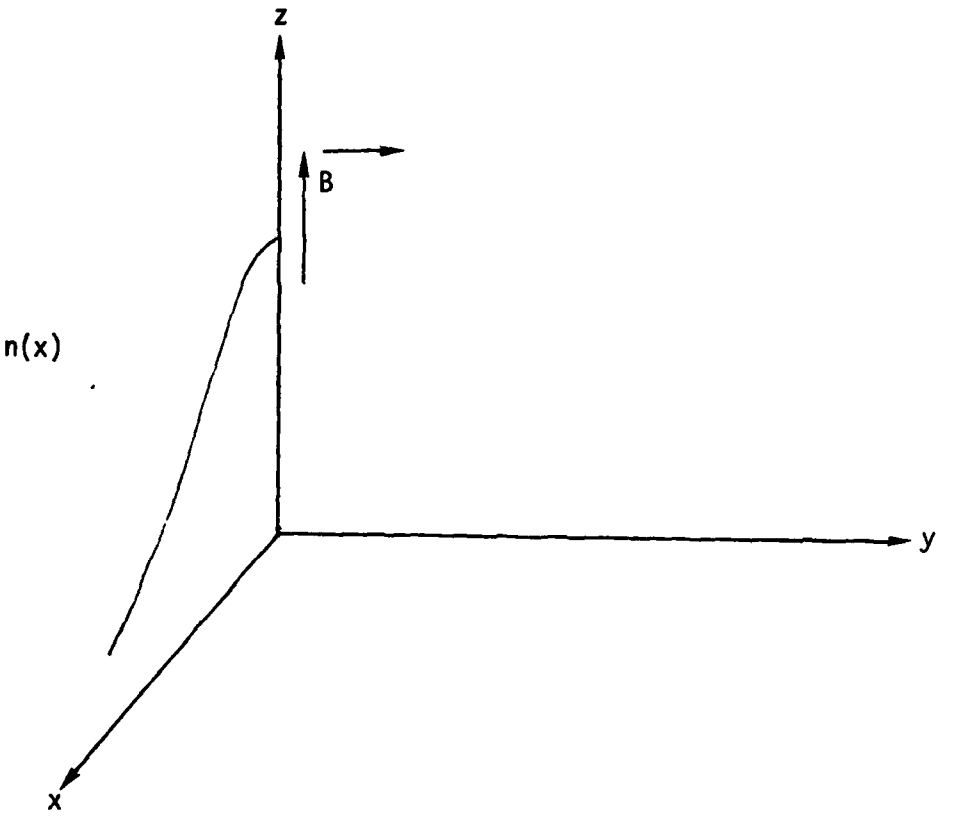

Figure 30: The plasma model used in the calculations of Appendix D. There is a uniform z-directed magnetic field, an x-directed density gradient, and uniform plasma properties in the y-direction.

A factor which can severely limit the destabilization of ion-cyclotron modes is ion-ion and ion-neutral collisions. In particular if[32,33]

$$\Omega_i \ll \nu_i \equiv \nu_{in} + .3\, k_2^2\, \rho_i^2\, \nu_{ii} \tag{D-8}$$

ion-cyclotron modes are no longer effective in the plasma dynamics. In Equation (D-8) we have inserted the .3 in the ion-ion contribution to the effective collision frequency as a reflection of the results of a detailed calculation using the Fokker-Planck operator in the $k_2\rho_i \ll 1$ limit.[11]

Using Equations (D-5) and (D-8) for singly ionized oxygen ions with

$$n_n = 10^8\ \text{cm}^{-3}\ ,\quad n_e = 10^6\ \text{cm}^{-3}\ ,\quad T_e = .1\ \text{ev}\ ,$$

$$B = .3\ \text{G} \tag{D-9}$$

it is apparent that

$$k_\perp \rho_i < 10\ ,\quad \rho_i/L_n > .1 \tag{D-10}$$

is necessary for the existence of ion-cyclotron modes. Hence, the ion-cyclotron drift instabilities require rather sharp density gradients.

The conditions given by Equation (D-10) represent necessary criteria for the existence of the ion-cyclotron instabilities. However, even when inequality (D-8) is not satisfied, ion collisions can still stabilize ion-cyclotron modes. Using the general dispersion relation for electrostatic modes given by Eq. (C-11) in Appendix C and assuming short perpendicular wavelength perturbations such that

$$k_\perp \rho_i \gg 1 \tag{D-11}$$

we can rewrite the dispersion relation as

$$0 = \chi_e \left[1 - \frac{i\nu_i}{\omega + i\nu_i - p\Omega i} \; \frac{1}{(2\pi)^{\frac{1}{2}}\, k_\perp \rho_i} \right] + \frac{1}{k^2 \lambda_{Di}^2} \left[1 - \frac{\omega + \omega_{Di} + i\nu_i}{\omega + i\nu_i - p\Omega_i} \; \frac{1}{(2\pi)^{\frac{1}{2}}\, k_\perp \rho_i} \right] \tag{D-12}$$

where $p\Omega_i$ is the harmonic of the ion-cyclotron frequency to which w is most closely approximated (e.g., $|\omega - p\Omega_i| \ll \Omega_i$) and χ_e is the electron susceptibility. From Equation (D-12) the expression for the frequency is given by

$$\omega = p\Omega_i + \frac{\omega_{Di} + p\Omega_i}{(2\pi)^{\frac{1}{2}}\, k_\perp \rho_i} \frac{\chi_{er} + \frac{1}{k^2\lambda_{Di}^2} - i\chi_{ei}}{\left[\left(\chi_{er} + \frac{1}{k^2\lambda_{Di}^2}\right)^2 + \chi_{ei}^2\right] k^2\lambda_{Di}^2 - i\omega_i} \qquad \text{(D-13)}$$

where

$$\chi_{er} = \mathrm{Re}\,(\chi_e) \quad , \quad \chi_{ei} = \mathrm{Im}\,(\chi_e) \quad .$$

Ion collisions tend to stabilize the ion cyclotron. For situations when instability can occur,

$$|\omega_{Di}| > |p\Omega_i| \quad . \qquad \text{(D-14)}$$

Stability is assured if

$$.3k_\perp^2 \rho_i^2 \nu_{ii} > \left| \frac{2\omega_{Di}}{(2\pi)^{\frac{1}{2}}\, k_\perp \rho_i} \right| = \left(\frac{2}{\pi}\right)^{\frac{1}{2}} \Omega_i \frac{\rho_i}{L_n} \quad . \qquad \text{(D-15)}$$

Using Equation (D-3) and assuming the parameters given by Equation (D-9) as well as

$$\rho_i / L_n = .1 \qquad \text{(D-16)}$$

we see that

$$k_\perp \rho_i > 3 \qquad \text{(D-17)}$$

for stabilization by ions. Even for electron densities as low as 10^5 cm^{-3} the requirement that

$$k\, \rho_i > 9 \qquad \text{(D-18)}$$

for stability shows that, unless density gradients are very sharp or densities are very low, ion-cyclotron drift modes are not likely to be driven unstable in the ionosphere solely by density gradients.

2. Acoustic Modes ($\omega > \Omega_i$)

Acoustic waves with frequencies above the ion-cyclotron frequency satisfy the following expression for

$$\nu_e >> k_z v_e: \tag{D-19}$$

$$0 = \frac{T_i}{T_e} \frac{\omega_{De} + i\delta}{\omega + i\delta} - \left[\frac{\omega_{Di}}{\omega} + \frac{k_z^2 v_i^2}{\omega^2}\right]\left[1 - \frac{i\nu_i}{\omega}\right]^{-1} \tag{D-20}$$

The criterion for the derivation of Equation (D-20) from Equation (C-11) is that

$$k_\perp \rho_i < p \tag{D-21}$$

where

$$\omega \approx p\Omega_i \quad . \tag{D-22}$$

In the ionosphere the electron and ion temperatures are comparable and we require

$$\rho_i > L_n \tag{D-23}$$

for instability. It then follows that the ion Larmor radius must be larger than the density gradient scale length,

$$\omega_D > \omega \tag{D-24}$$

for a gradient driven acoustic instability. Hence, the acoustic instability will occur only for situations where the density gradient is extreme. Since only ion dynamics have been used to establish Equation (D-24), our arguments also apply to the case when Equation (D-19) is not satisfied and the electrons are collisionless.

3. Lower-Hybrid Waves

In the collisionless limit the dispersion relation for lower-hybrid waves satisfying Equations (D-21) and (D-22) is

$$0 = 1 + \frac{k_\perp^2}{k^2} \frac{\rho_e^2}{\lambda_{De}^2} - \frac{k_z^2}{k^2} \frac{\omega_{pe}^2}{\omega^2} - \frac{\omega_{pi}^2}{\omega^2} - \frac{\omega_{Di}}{\omega}$$

$$+ i \frac{(\pi/2)^{1/2}}{k^2 \lambda_{De}^2} \frac{\omega - \omega_{De}}{|k_z| \nu_e} \exp\left(- \frac{\omega^2}{k_z^2 \nu_e^2}\right) \qquad \text{(D-25)}$$

Again, as for the case of acoustic modes, we require that

$$\rho_i > L_n \qquad \text{(D-26)}$$

be satisfied for instability. Hence, as in the case of acoustic modes, collisionless lower-hybrid waves driven solely by the density gradient and satisfying Equations (D-21) and (D-22) are not likely to be present in the ionosphere.

The case of a background electric field has recently been raised by Huba et al.[34] in connection with the interpretation of enhanced backscatter from Equatorial Spread F by the ALTAIR radar on Kwajalein. The calculation was done assuming that the inequality represented by Equation (D-21) was reversed (i.e., $k_\perp \rho_i > p$ for $\omega \approx p\Omega_i$). Under such circumstances the quantity ρ_i/L_n can be less than one for a lower-hybrid instability. However, the stabilizing influence of electron collisions discussed here are not included in Reference (1) and so the examples used in the reference to explain the backscatter are inappropriate.

The plasma model of Reference 34 assumes a uniform z-directed magnetic field of strength B, uniform plasma properties in the y-direction, and an x-directed density profile of the form

$$n_0(x) = n_0(1-x/L_n) \quad . \qquad \text{(D-27)}$$

The ions are assumed to be in local thermodynamic equilibrium with an ambient electric field of strength, $E_0(x)$ and potential $\phi_0(x)$:

$$\frac{T_i}{e} \nabla \ln (n_0(x)) = E_0(x) = - \nabla \phi_0(x) \qquad \text{(D-28)}$$

where T_i is the ion temperature in electron volts.

To lowest order, the ion dynamics can be treated as being straight-line and unmagnetized if the ion-ion collisional viscosity decorrelates the ion gyromotion over a scale length on the order of an inverse y-directed wave number, k_y^{-1}. Quantitatively for the ions to be unmagnetized,

$$.3(\nu_{ii}/\Omega_i)\ k_y^2 \rho_i^2 >> 1 \qquad \text{(D-29)}$$

where

$$\nu_{ii} = \frac{4}{3}\left(\frac{\pi}{m_i}\right)^{\frac{1}{2}} \frac{e^4 n_o}{T_i^{3/2}} [23.4 - 1.15 \log_{10}(n_o) + 3.45 \log_{10}(T_e)] ,$$

$$\Omega_i = \frac{eB}{m_i c} ,$$

$$\rho_i = \frac{\nu_i}{i} ,$$

$$\nu_i = \left(\frac{T_i}{m_i}\right)^{\frac{1}{2}} , \qquad \text{(D-30)}$$

are the ion-ion collision frequency, ion gyrofrequency, ion gyroradius, and ion thermal speed, respectively. In the definitions of Equation (D-30), the ions have been assumed to be singly ionized.

Contrary to the ion motion, the gyration of the electrons in the ambient magnetic field is crucial to the development of a lower-hybrid instability and is necessarily included in all treatments of lower-hybrid waves. What are not included in the treatment of Reference 34 are the electron-electron and electron-ion collisions which obviously must be considered in a self-consistent collisional treatment of lower-hybrid waves in the ionosphere if ion-ion collisions are included. The electron-electron and electron-ion collision frequencies (ν_{ee} and ν_{ei}, respectively) have the form

$$\nu_{ee} = \nu_{ei} = \left(\frac{2T_i^3}{T_e^3}\frac{m_i}{m_e}\right)^{\frac{1}{2}} \nu_{ii} . \qquad \text{(D-31)}$$

For situations where Equation (D-29) is satisfied and the ion-ion mean free path is much larger than the inverse y-wavenumber,

$$\nu_i/\nu_{ii} >> k_y^{-1} \quad , \tag{D-32}$$

the ion dynamics in the lower-hybrid wave are collisionless and are described by the linearlized and unmagnetized Vlasov equation

$$\left(\frac{\partial}{\partial t} + \vec{v} \cdot \frac{\partial}{\partial \vec{r}}\right) f_{1i}(\vec{r},\vec{v},t) = - \frac{e \vec{E}_1}{m_i} \cdot \frac{\partial}{\partial \vec{v}} f_{0i}(\vec{r},\vec{v}) \quad . \tag{D-33}$$

In Equation (D-33), wave and background quantities are represented by subscript "1" and "0", respectively, and

$$f_{1i}(\vec{r},\vec{v},t) = f_{1i}(\vec{v}) \exp[k_y y - \omega t)] \tag{D-34}$$

$$f_{0}i(\vec{r},\vec{v}) = (2\pi\ T_i/m_i)^{-3/2} \exp\left[\left(\frac{mv^2}{2} - e\phi\right)/T_i\right]$$

$$\vec{E}_1 = -\hat{y}\ i\ k_y \phi \exp[i(k_y y - \omega t)] \quad .$$

The electron dynamics in the wave are magnetized and collisional. For lower-hybrid waves, the electron collisions with ions can be assumed to be Lorentz-like, and the effect of electron-electron viscosity can be assumed to be additive to the electron-ion collision frequency in the following way:

$$\nu_e = \nu_{ei} + .3\nu_{ee} (k_y \rho_e)^2 \tag{D-35}$$

where

$$\rho_e = -\left(\frac{T_e}{m_e}\right)^{\frac{1}{2}} \frac{m_e c}{e B} \quad . \tag{D-36}$$

In Equation (D-35), the effective electron collision frequency is defined by ν_e. An appropriate linearized kinetic equation for the electrons is

$$\left[\frac{\partial}{\partial t} + \vec{v} \cdot \frac{\partial}{\partial \vec{v}} - \frac{e}{m}\left(\vec{E}_0 + \frac{\vec{v} \times \vec{B}}{c}\right) + \nu_e\right] f_{1e}(\vec{r},\vec{v},t) \tag{D-37}$$

$$= \nu_e \frac{n_{1e}(\vec{r},t)}{n_{0e}(x)} f_{0e}(\vec{r},\vec{v}) + \frac{e}{m_e} \vec{E} \cdot \frac{\partial}{\partial \vec{v}} [f_{0e}(\vec{r},\vec{v},)] \quad .$$

Here,

$$n_{1e}(\vec{r},t) = n_{1e} \exp[i(k_y y - \omega t)] \tag{D-38}$$

$$f_{1e}(\vec{r},\vec{v},t) = f_{1e}(\vec{v}) \exp[i(k_y y - \omega t)]$$

$$f_{0e}(\vec{r},\vec{v}) = (2\pi\, T_e/m_e)^{3/2} \exp\left(-\frac{m_e v^2}{2 T_e}\right) n_0\left(1 - \frac{x + v_y/\Omega_e}{L_n}\right) \quad .$$

In the ionosphere, the relation

$$\frac{\omega_{pe}^2}{\Omega_e^2} = \frac{4\pi n_0 e^2/m_e}{(e B/m_e c)^2} = \frac{4\pi n_0 c^2 m_e}{B^2} >> 1 \quad ,$$

is satisfied. Since for the lower-hybrid mode one also has

$$|\Omega_e| >> \omega \quad ,$$

the mode can be assumed to be quasi-neutral.

Using standard techniques, the dispersion relation for the lower-hybrid modes can be written, using Equations (D-32) and (D-37), as

$$0 = [1 + yZ(y)] + \left[1 - \frac{\omega - \omega_{De} + i\nu_e}{\omega + i\nu_e}\ \Gamma_0(\lambda_e)\right] \tag{D-40}$$

$$\left[1 - \frac{i\nu_e}{\omega + i_e}\ \Gamma_0(\lambda_e)\right]^{-1} \quad .$$

Here,

$$Z(y) = -2 \exp(-y^2) \int_0^y dt \exp(t^2) + i(\pi)^{\frac{1}{2}} \exp(-y^2)$$

$$y = \frac{\omega - \omega_{Di}}{(2)^{\frac{1}{2}} k_y v_i}$$

$$\omega_{Di} = k_y \frac{T_i}{m_i \Omega_i L_n} \quad , \omega_{De} = k_y \frac{T_e}{m_e \Omega_e L_n}$$

$$\Gamma_0 = I_0(\lambda_e)\exp(-\lambda_e) \quad , \quad \lambda_e = k_y^2 \rho_e^2 \quad , \tag{D-41}$$

and I_0 is the modified Bessel function of the first kind and zero order. In writing Equation (D-40), Eq. (D-28) and a frame of reference moving with the ExB velocity have been used.

Assuming all the ions with the exception of resonant ions are in local thermodynamic equilibrium with the wave,

$$|\omega - \omega_{Di}| << (2)^{\frac{1}{2}} k v_i \quad , \tag{D-42}$$

the dispersion relation, Equation (D-40), can be rewritten as

$$0 = \omega(2 - \Gamma_0) - \omega_{Di} + i(\tfrac{\pi}{2})^{\frac{1}{2}} \omega \frac{\omega - \omega_{Di}}{k_y v_i} + 2i \nu_e(1 - \chi_0) \quad . \tag{D-43}$$

If in addition the effective electron collision frequency and the growth rate, γ, are much smaller that the real part of the frequency, ω,

$$|\gamma, \nu_e(1-\Gamma_0)| << |\omega| \quad , \tag{D-44}$$

then

$$\omega = \frac{\omega_{Di}\,\Gamma_0}{2 - \Gamma_0} + i(2\pi)^{\frac{1}{2}} \frac{\omega_{Di}^2}{k v_i} \frac{\Gamma_0(1 - \Gamma_0)}{(2 - \Gamma_0)^3} - i2\nu_e \frac{1 - \Gamma_0}{2 - \Gamma_0} \quad . \tag{D-45}$$

The last term on the right-hand side of Equation (D-45) represents the stabilizing influence of electron collisions on the lower-hybrid drift wave and was not included in the treatment of Reference 34. Hence, unlike the case of Reference 34, the consistent treatment of collisions results in a threshold criterion for the density gradient scale length necessary for instability. This criterion is

$$\frac{\rho_i}{L_n} > (\frac{\nu_e}{\Omega_i})^{\frac{1}{2}} (\frac{2\, m_e}{\pi m_i})^{\frac{1}{4}} \frac{2 - \Gamma_0}{(|k\rho_e|\Gamma_0)^{\frac{1}{2}}} \quad . \tag{D-46}$$

Example

As an example, consider an ionospheric plasma with

$$B = .3G \quad , \quad \frac{m_e}{m_i} = 3.4 \times 10^{-5} \quad , \quad n_0 = 10^6\ cm^{-3} \quad ,$$

$$\nu_{ee} = 1180\ Hz \quad , \quad T_e = T_i = .1\ eV \ .$$

The criterion of Equation (D-46) implies that:

$$\frac{\rho_i}{L_n} > 0.56 \quad \text{for} \quad |k_y \rho_e| = .1 \ ,$$

$$\frac{\rho_i}{L_n} > 0.37 \quad \text{for} \quad |k_y \rho_e| = .7 \ ,$$

$$\frac{\rho_i}{L_n} > 0.44 \quad \text{for} \quad |k_y \rho_e| = 1.0 \ . \tag{D-48}$$

The values of the y-wavenumber such that $|k_y \rho_e| = .1$ and .7 are appropriate to radar backscatter at 100 MHz and 50 MHz, respectively.

From the criterion of Equation (D-40), it is apparent that the examples of Reference 34 with the same parameters as those used here but with $\rho_i/L_n = 0.026$ actually correspond to a stable lower-hybrid drift wave. Based on Equation (D-46), it is clear that for the lower-hybrid drift instability to be driven unstable, the plasma density would have to be reduced to $\sim 10^4$ cm^{-3} if other plasma parameters were unchanged. For such densities, Equation (D-29) would still be satisfied as long as

$$|k_y \rho_e| \gg 0.1 \ . \tag{D-49}$$

Hence, it appears that lower-hybrid drift modes are not likely to be sources of anomalous diffusion under HANE conditions ($n_0 \gg 10^4$ cm^{-3}), unless gradient scale lengths are of the order of 10 m or less.

4. Electron-Cyclotron Modes

Electron-cyclotron waves have frequencies comparable to the fundamental or a harmonic of the electron-cyclotron frequency. Analogous to the treatment for ion-cyclotron drift instabilities, we require that

$$k_\perp \rho_e^2 / L_n > p \tag{D-50}$$

for instability. In Equation (D-50), the quantity p is the electron-cyclotron harmonic number to which the wave frequency is most closely approximated. Again, as in the case of ion-cyclotron modes, we require

$$.3 \, k_\perp^2 \rho_e^2 \nu_{ee} \ll |\Omega_e| \tag{D-51}$$

for the existence of electro-cyclotron modes. In terms of ion quantities, and using Equation (D-50), we find that a necessary condition for the destabilization of electron-cyclotron drift waves is

$$.3\, k_\perp^2\, \rho_i^2\, \nu_{ii} < \Omega_i (m_e/2m_i)^{\frac{1}{2}} \quad . \tag{D-52}$$

Hence, the density constraints for the existence of electron-cyclotron drift instabilities are more stringent than those for ion-cyclotron instabilities by the ratio $(m_e/2m_i)^{\frac{1}{2}}$.

5. Electron-Acoustic Modes

The destabilization of electron-acoustic modes with frequencies well above the electron-cyclotron frequency would require

$$|k_\perp \rho_e| << p \tag{D-53}$$

where p is an integer such that

$$\omega \simeq p\Omega_e \quad . \tag{D-54}$$

Hence, following the arguments used for ion-acoustic modes, it follows that

$$|\rho_e| > L_n \quad , \tag{D-55}$$

which corresponds to a very extreme condition on the density gradient. Hence, electron-acoustic modes driven unstable by density gradients should not exist in the atmosphere.

6. Electromagnetic Drift Modes

As the plasma energy becomes larger in a plasma configuration with a fixed magnetic field strength, it becomes easier for the plasma to modify the ambient magnetic field. Under such circumstances, instabilities in a plasma can have electromagnetic properties.

We have shown that electrostatic modes driven unstable solely by density gradients in the ionosphere are generally expected to have frequencies which are less than the ion-cyclotron frequency. Similarly, because the wave frequency must be smaller than the diamagnetic drift frequency for instability,

any possible electromagnetic modes driven by density gradients in the ionosphere should also have frequencies below the ion-cyclotron frequency.

Electromagnetic modes with frequencies below the ion-cyclotron frequency and driven unstable by a density gradient have the property that[5]

$$k_{\parallel} < \frac{\omega_D}{v_A} \simeq \left(\frac{\beta_i}{2}\right)^{\frac{1}{2}} \frac{k_\perp \rho_i}{L_n} \tag{D-56}$$

where

$$\beta_s = \frac{8\pi\, n_{0s}\, T_e}{B^2} \quad , \quad v_A = \frac{B}{(4\pi\, n_0\, m_i)^{\frac{1}{2}}} \tag{D-57}$$

are the ratio of the species s pressure to magnetic field pressure and the Alfyen speed, respectively. The quantity β is ubiquitous in discussions of low-frequency electromagnetic instabilities. The low-frequency electromagnetic instabilities also have the property that

$$|\varepsilon_{\parallel,\parallel}| \sim \frac{k_\perp^2\, c^2}{\omega^2} \tag{D-58}$$

where $\varepsilon_{\parallel,\parallel}$ is derived in Appendix E and the speed of light is written as c. Using Equation (E.4), we can verify Equation (D-58) if

$$|\varepsilon_{\parallel,\parallel}| > \frac{\omega_{pe}}{\nu_{ei}\omega} \gtrsim \frac{k_\perp^2\, c^2}{\omega^2} \quad . \tag{D-59}$$

Substituting the diamagnetic drift frequency for the frequency in Equation (D-59) and using Equation (D-56) allows for a criterion on the parallel current to be written for the electromagnetic modes to be written

$$\lambda_{\parallel} > 2\pi \frac{\nu_{ei}}{\omega_{pe}^2} \frac{c^2\, L_n^2}{\rho_i^2\, v_i} \left(\frac{2}{\beta_i}\right)^{\frac{1}{2}} \quad . \tag{D-60}$$

For the parameters

$$B = .3G \quad , \quad n_{0e} = n_{0i} = 10^6\ cm^{-3} \quad , \quad T_{0e} = T_{0i} = .1\ eV \tag{D-61}$$

in the ionosphere with singly ionized oxygen,

$$\lambda_{\parallel} > \left(\frac{L_n}{\rho_i}\right)^2 \text{ km} . \tag{D-62}$$

Unless the quantity, L_n/ρ_i, is much smaller than 10, the necessary requirement on the parallel wavelength for electromagnetic instabilities seems prohibitive. Even for the ion and electron densities of 10^8 cm^{-3}, we require the seemingly difficult inequality

$$\lambda_{\parallel} > 4.7\left(\frac{L_n}{\rho_i}\right)^2 \text{ km} \tag{D-63}$$

to be satisfied.

However, it is interesting to note that for plasma parameters such as

$$B \approx .03G , \quad n_{0e} \; n_{0i} = 10^8 \text{ cm}^{-3} , \quad T_{0e} = T_{0i} = .1 \text{ eV} ,$$

$$\beta_e \approx \beta_i ,$$

there is the possibility that electromagnetic modes will be driven unstable by the density gradient. Necessary conditions for instability are

$$\beta_e \approx \beta_i \approx .45 , \quad \lambda_{\parallel} > .47\left(\frac{L_n}{\rho_i}\right)^2 \text{ km} . \tag{D-65}$$

In this case, the total plasma energy is only slightly smaller than the magnetic field energy:

$$\beta = \beta_e + \beta_i \approx .90 . \tag{D-66}$$

B. SUMMARY

It is possible that lower-hybrid and/or electromagnetic drift modes can be driven unstable under ionospheric conditions. However, in both cases there appear to be rather stringent limitations on the parametric range of instability.

APPENDIX E

DERIVATION OF THE CURRENT PRODUCED IN A WAVE WITH $\omega << \Omega_i$ IN THE DIRECTION OF THE AMBIENT MAGNETIC FIELD

In this appendix, we derive the current produced by a low-frequency wave (i.e., $\omega << \Omega_i$) in the direction of the ambient magnetic field (which is taken to be the z-direction). We assume a collisional plasma (i.e., $\nu_{ei} >> \omega$) and use the fluid equations.

$$0 = -ik_z T_0 n_1 - e n_0 E_{z1} - m_e \nu_e n_0 v_{z1} \quad , \tag{E-1a}$$

$$0 = -i \omega n_1 + \frac{cE_{y1}}{B_0} \frac{\partial n_0}{\partial x} + ik_z n_0 v_{z1} \quad . \tag{E-1b}$$

Here,

$$\nu_e = \nu_{en} + \nu_{ei} \tag{E-2}$$

solving for the perturbed velocity parallel to the magnetic field, we obtain

$$v_{z1} = -\frac{1}{m_e \nu_{ei}} \left[e E_{z1} + ik_z T_0 \left(\frac{cE_{y1}}{B_0 L_n} - ik_z \frac{}{m_e \nu_{ei}} \right) \left(i\omega - \frac{k_z^2 v_e^2}{\nu_{ei}} \right)^{-1} \right] . \tag{E-3}$$

The parallel-parallel component of the dielectric tensor can then be written as

$$\varepsilon_{\parallel,\parallel} = \frac{4\pi i}{\omega} e n_0 v_{z1} = i \frac{\omega_{pe}^2}{\nu_e(\omega + i\delta)} \quad . \tag{E-4}$$

In Eq. (E-4),

$$\omega_{pe}^2 = \frac{4\pi n_0 e^2}{m_e} \quad , \quad \delta = \frac{k_\parallel^2 v_e^2}{\nu_e} \tag{E-5}$$

DISTRIBUTION LIST

DEPARTMENT OF DEFENSE

Assistant to the Secretary of Defense
Atomic Energy
ATTN: Executive Assistant

Defense Nuclear Agency
ATTN: STVL
3 cy ATTN: RAAE
4 cy ATTN: TITL

Defense Technical Information Center
12 cy ATTN: DD

Field Command
Defense Nuclear Agency
ATTN: FCPR

Field Command
Defense Nuclear Agency
Livermore Division
ATTN: FCPRL

Undersecretary of Defense for Rsch. & Engrg.
ATTN: Strategic & Space Systems (OS)

DEPARTMENT OF THE ARMY

BMD Advanced Technology Center
Department of the Army
ATTN: ATC-O, W. Davies
ATTN: ATC-R, D. Russ
ATTN: ATC-T, M. Capps

Harry Diamond Laboratories
Department of the Army
ATTN: DELHD-N-P

DEPARTMENT OF THE NAVY

Naval Research Laboratory
ATTN: Code 6700, T. Coffey
ATTN: Code 7500, B. Wald
ATTN: Code 7550, J. Davis
ATTN: Code 6780, S. Ossakow

Naval Surface Weapons Center
ATTN: Code F31

DEPARTMENT OF THE AIR FORCE

Air Force Geophysics Laboratory
ATTN: PHP, J. Aarons

Air Force Weapons Laboratory
Air Force Systems Command
ATTN: SUL
ATTN: DYC

DEPARTMENT OF ENERGY CONTRACTOR

Los Alamos Scientific Laboratory
ATTN: Document Control for D. Simons

DEPARTMENT OF DEFENSE CONTRACTORS

Berkeley Research Associates, Inc.
ATTN: J. Workman

ESL, Inc.
ATTN: J. Marshall

General Electric Company—TEMPO
ATTN: W. Knapp
ATTN: T. Stevens
ATTN: DASIAC

General Research Corp.
ATTN: J. Ise, Jr.
ATTN: J. Garbarino

University of Illinois
ATTN: Security Supervisor for K. Yeh

Mission Research Corp.
ATTN: R. Kilb

R & D Associates
ATTN: C. MacDonald

JAYCOR
ATTN: S. Goldman